VERSLAGEN EN VERHANDELINGEN

REPORTS AND TRANSACTIONS

NATIONAAL LUCHT- EN RUIMTEVAART-LABORATORIUM

NATIONAL AERO- AND ASTRONAUTICAL RESEARCH INSTITUTE

AMSTERDAM

XXIX - 1964

TECHNICAL REPORT M. 2122

ANALYSIS OF THE FATIGUE PHENOMENON IN ALUMINIUM ALLOYS

BY

J. SCHIJVE

PREFACE

The report published in this Volume of "Verslagen en Verhandelingen" ('Reports and Transactions') of the 'Nationaal Lucht- en Ruimtevaartlaboratorium', N.L.R. ('National Aero- and Astronautical Research Institute') served the author as a thesis for the degree of doctor in the Technical Sciences at the Technical University of Delft.

The greater part of the investigation was performed under contract with the 'Nederlands Instituut voor Vliegtuigontwikkeling' (N.I.V.) ('Netherlands Aircraft Development Board'). The permission for publication is herewith acknowledged.

A. J. Marx

July 1964

Director of the
'Nationaal Lucht- en Ruimtevaart-
Laboratorium'

Amsterdam

Summary

The fatigue phenomenon in aluminium alloys is analysed on the basis of empirical evidence derived from the literature and results of some recent NLR test series. Main emphasis is on the aluminium-copper alloys (2024-type). It has been attempted to develop a dislocation model which could explain crack nucleation and propagation. The following questions were studied: (1) does crack propagation occur along crystal planes, (2) does it occur in all load cycles, (3) is high-level fatigue fundamentally different from low-level fatigue, (4) how does cyclic strain-hardening occur and (5) what are the variables controlling the crack propagation? The discussion includes simple dislocation concepts, interactions of slip and precipitated zones and calculations on shear stress distributions around cracks. The model developed for the fatigue phenomenon is still qualitative. First steps to make it quantitative and difficulties involved are pointed out. New results from microscopic studies on the crystallographic orientation of cracks and the rate of propagation of micro-cracks are presented.

Contents

1 Introduction

The high degree of utilization of to-day's aircraft and the use of high strength aluminium alloys have made the fatigue problem one of major concern in aircraft design. Unfortunately accurate methods for calculating fatigue properties of an aircraft structure or structural components are not yet available. Difficulties involved are the insufficient knowledge of the fatigue process on one hand and the large number of factors which can affect the fatigue phenomenon on the other hand. The influence of many factors, although known from numerous empirical studies reported in the literature, cannot be quantitatively accounted for. However, qualitatively several trends observed can be understood and this understanding, which is steadily improving, can be very helpful for practical problems. Continued research efforts on the fatigue phenomenon, recognizing the fact that physically exact laws or accurate engineering rules will be extremely difficult to obtain, are therefore warranted.

Our present knowledge of the fatigue process is mainly based on microscopic studies. The problem received a revived interest by the impact from the rapid development of the dislocation theory in the last decades. In this study an attempt is made to analyse phenomenological evidence of fatigue based on simple dislocation concepts. The study is made for aluminium alloys of the duralumin type, the main aim being an improvement of the understanding of the fatigue process in these alloys. The study was initiated by the results obtained in some recent microscopic investigations, carried out at the NLR (National Aeronautical and Astronautical Research Institute), Amsterdam.

2 Scope of the present study

Microscopic studies on the fatigue of metals complemented by other experimental investigations have revealed two important features:

1. Fatigue requires cyclic *plastic* deformations.
2. Microcracks are nucleated early in the fatigue life.

This information, limited though it is, has been helpful already in explaining the influence of several factors on the fatigue behaviour under engineering conditions. On the other hand the two features are prompting several additional questions, of which the following are thought to be pertinent.

(a) How does crack nucleation occur?
(b) Is there a fundamental difference between crack nucleation and crack propagation? Which part of the fatigue life is covered by crack propagation?
(c) Does crack propagation occur along crystal planes?
(d) Does crack extension occur in every load cycle and what are the orders of magnitude of the crack length and the crack rate to be considered?
(e) What is the effect of the stress amplitude on the propagation mechanism? Is there a fundamental difference between low-amplitude and high-amplitude fatigue, as is sometimes postulated in the literature?
(f) How is the stress-strain behaviour of aluminium alloys under cyclic loading? The interaction of dislocation movements and the precipitation is a major aspect of this question.

An analysis of these questions forms the main part of this thesis. The first question is dealt with in chapter 5, in which existing theories are discussed and a simple dislocation model is conceived. In chapter 6, question (b) is considered together with the problem of how this model should be extended or modified to account for crack propagation. In chapters 7 to 10 questions (c) to (f) are discussed, including a presentation and analysis of experimental data relevant to the dislocation model developed in the two preceding chapters. In chapter 11 the first steps for a quantitative evaluation of the dislocation model are considered. Comments on future prospects are presented in chapter 12.

The fatigue mechanism is not necessarily the same for different metals. Even a generalization for alloys of the same metal may be incorrect. The present study is confined to aluminium-copper alloys. The selection of this type of material is explained in chapter 3. The major part of the information referred to in the discussion was drawn from tests on axially loaded sheet specimens and strictly speaking the discussion applies to these conditions.

Recent microscopic studies carried out at the NLR have some bearing on the present problem. One investigation on the crack rate in unnotched and notched aluminium alloy specimens is not yet fully completed and will be published in due course as a separate NLR report. A summary of the results is given in section 4.1. A second investigation of an exploratory nature, which will not be published separately is presented in sections 4.3, 4.4 and 4.5. Fatigue cracks were studied in pure aluminium sheet specimens, in the aluminium cladding of aluminium alloy sheet material and in unclad aluminium alloy sheet specimens. Section 4.2 gives some fractographical observations.

The aim of this report, being the evaluation of a model for crack nucleation and propagation in aluminium alloys, is certainly ambitious. Any theory on fatigue at the present time has to include certain elements of speculation. Proposals being made are therefore tentative. It was felt, however, that new experimental evidence and certain simple dislocation concepts did justify renewed efforts to reduce the degree of speculation and to arrive at a dislocation model, which should allow a better understanding of the hitherto rather obscure conception of "fatigue damage".

3 The aluminium alloy selected for the present study

A large variety of studies on deformation and fracture of metallic materials have shown that the behaviour of all materials is not uniform. In several cases differences can be correlated with certain specific properties of the structure of the metal or the alloy concerned. Diverging properties for different materials may then be illuminating. They also imply that a theory applying to one material is not necessarily true for another material. Aluminium alloys have some special features which are mentioned hereafter. These imply that one should be very careful in interpreting results of other materials for the fatigue behaviour of aluminium alloys.

The choice of aluminium alloys for fatigue investigations is an obvious one at an aeronautical laboratory, since these alloys are the main structural materials used for current aircraft construction. Al Cu Mg alloys and Al Zn Mg Cu alloys are employed, typical compositions and mechanical properties of which are given in the table below.

Usually the first alloy is naturally aged whereas the second one is artificially aged. In this study the alloys will be indicated by the designation of the American Society for Metals, 2024 and 7075 respectively.

The following special features apply to the above mentioned Al alloys:

Alloy	American designation	Chemical composition (%)			Typical properties		
		Cu	Zn	Mg	$S_{0,2}$ (kg/mm²)	S_u	δ (%)
Al Cu Mg	2024	4.5	—	1.5	32	45	18
Al Zn Mg Cu	7075	1.5	5.5	1.5	45	55	11

(1) From an elastic point of view the Al alloys are, contrary to most other metallic materials, almost isotropic. For aluminium the maximum and the minimum value of the elastic modulus have a ratio $E_{<111>}/E_{<100>} = 1.20$ (ref. 1). Since the elastic modulus is a structure-insensitive property the low elastic anisotropy will also apply to aluminium-rich alloys.

(2) The Al alloys have a face-centered cubic structure. Although this seems not to be a very peculiar feature it is still important to note that cleavage fracture is observed in metals with a body-centered cubic or a closepacked hexagonal structure, but not in metals with a face-centered cubic structure (ref. 2).

(3) A third peculiarity is the easy occurrence of cross-slip in aluminium, due to the high stacking-fault energy. Very little seems to be known about the stacking-fault energy in aluminium alloys. In a study on cold worked aluminium and aluminium alloys by an X-ray diffraction method Seemann and Stavenow (ref. 3) were unable to detect stacking faults in aluminium and in an Al Cu alloy. Stacking faults were indicated in Al Mg, Al Zn and Al Mg Zn alloys. It could thus be assumed that cross slip would be easy in the 2024-alloy, but not necessarily so in the 7075-alloy. This indicates that a generalization even amongst aluminium alloys is not a priori allowed.

(4) The Al alloys are precipitation hardened. The heat treatment gives the alloys a high hardness. The precipitated particles are still largely coherent with the matrix. In the 2024-alloy the hardening seems to be mainly due to coherency strain, whereas in the 7075-alloy the hardening effect is more a real dispersion hardening (see chapter 10). So here is another difference between the two alloys. The precipitation is undoubtedly a tremendously complicating factor.

Other differences between the two alloys may be added. The 7075-alloy is more fatigue notch-sensitive than the 2024-alloy and it is also more sensitive to stress corrosion and intergranular corrosion. The 2024-alloy is most widely used in aircraft structures if fatigue is a design consideration. In the present study the main interest is focused on this material. There are other practical reasons for doing so. Fatigue studies reported in the literature are more abundant for the 2024-alloy. Secondly many physical investigations were performed on the binary Al-4%-Cu alloy and there are some reasons to believe that its behaviour is similar to that of the 2024-alloy (see chapter 10).

4 Recent NLR studies on crack nucleation and propagation

The purpose of the tests described in this chapter is twofold:

(1) A determination of the orders of magnitude of the rate of crack growth in aluminium alloy specimens.

(2) An exploration of the crystallographic nature of fatigue cracks in aluminium and an aluminium alloy.

Recently the NLR completed some test series on unnotched and notched sheet specimens of an Al Cu Mg-alloy. The prime purpose of these tests was to study the notch effect and the size effect. The crack growth was observed during the fatigue tests since it was thought that such information might be useful for the evaluation of both effects. Data on the rate of crack growth are presented in section 4.1.

The crystallographic nature of crack growth was studied in aluminium, in the aluminium cladding of Al Cu Mg sheet material and the core of the same material*. The results obtained are discussed in sections 4.3 to 4.5 respectively. Section 4.2 gives some fractographical observations.

4.1 *The rate of crack growth in unnotched and notched sheet specimens of an Al Cu Mg—alloy*

The main purpose of the test programme was to study the notch effect and the size effect. A full account will be given in ref. 4. In this section the data on the rate of crack growth are summarized.

Fatigue tests were carried out on unnotched and simply notched specimens shown in the left top corner of figs 1 and 2 respectively. The specimens were axially loaded with zero minimum stress and

* Al Cu Mg sheet material for aircraft structures is usually provided with thin integral surface layers (cladding) of pure aluminium for protection against corrosion.

various values for the maximum stress. The fatigue machine was an Amsler High Frequency Pulsator, the test frequency being 70 cycles per second. Crack propagation was observed during the fatigue tests by means of two binocular microscopes with a low magnification, viz. 30 ×, employing stroboscopic light. In general cracks started from the edges of the cross section (unnotched specimens) or the edges of the hole (notched specimens), see for instance fig. 6, discussed in section 4.2. The smallest cracks observed had a length of about 0.1 mm. After detection of the crack a full record of its propagation was made. From the crack propagation curves the crack rate per cycle, $\mathrm{d}l/\mathrm{d}n$, was deduced as a function of the crack length l. A survey of the results is shown in figs 1 and 2. Figs 3 and 4 show the percentages of the fatigue life involved in certain amounts of cracking as a function of the applied stress.

For $l < 1$ mm the results indicated a linear relationship between $\mathrm{d}l/\mathrm{d}n$ and l, when plotted on a double-logarithmic scale (see figs 1 and 2) or

$$\frac{\mathrm{d}l}{\mathrm{d}n} = Cl^{\alpha} \tag{4.1}$$

If this relation is extrapolated to low values of l and $\mathrm{d}l/\mathrm{d}n$ their values at the beginning of the tests can be calculated by integration of eq. (4.1). The result

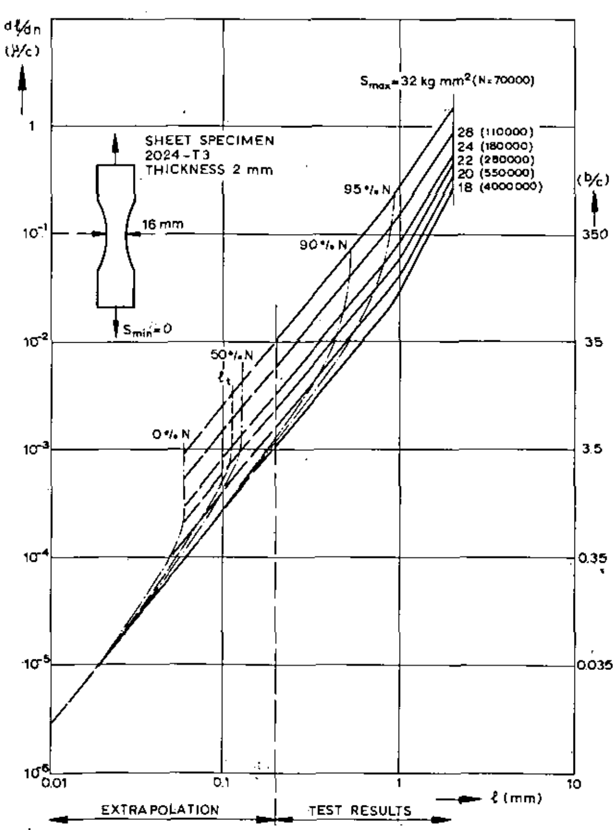

Fig. 1 Crack rate data of fatigue tests (R = 0) on unnotched specimens for various values of the applied stress (data from ref. 4). l is measured from the edge of the specimen along the sheet surface.

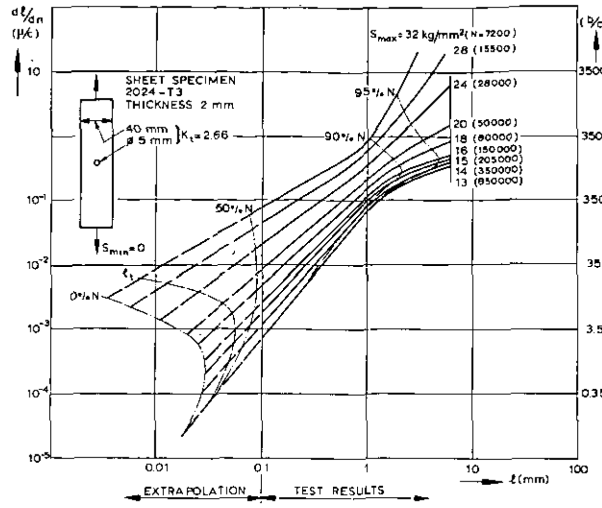

Fig. 2 Crack rate data of fatigue tests ($R = 0$) on notched specimens for various values of the applied stress (data from ref. 4). l is measured from the edge of the hole along the sheet surface.

is shown in figs 1 and 2 by the lines 0% N. Of course the linear extrapolation may be incorrect, but apart from this it is not accepted that crack nuclei of a finite length are present in a virgin specimen, this length moreover being dependent on the applied stress. Disregarding cracks emanating from inclusions it is thought that cracks start with a zero length as described in chapter 5. Relevant results were recently obtained by de Lange (ref. 5) in fatigue tests to explore the possibilities of a new replica method. He performed some tests on unnotched specimens of the 2024-alloy and found cracks of a length as small as 2.5 μ. His results show that micro-cracks were present after a few per cent of the fatigue life had elapsed. An evaluation of his crack growth data (see also ref. 4) gave the impression that crack growth started with an approximately constant crack rate over a certain period, after which it accelerated.

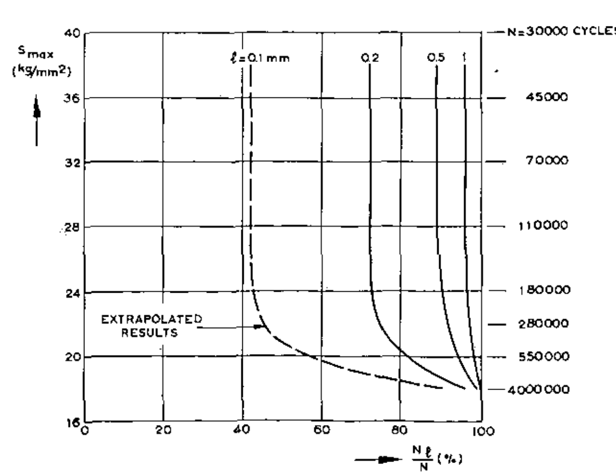

Fig. 3 Percentage fatigue life covered by crack propagation in unnotched specimens of 2024-T3 material. (Data from ref. 4).

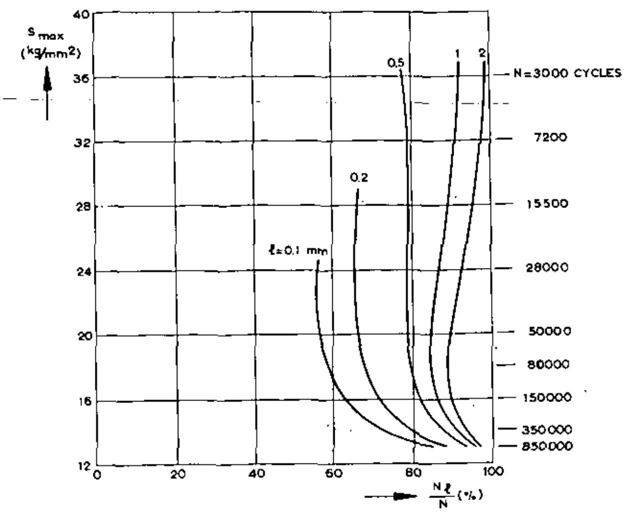

Fig. 4 Percentage fatigue life covered by crack propagation in notched specimens of 2024-T3 material. (Data from ref. 4).

The acceleration was in accordance with eq. (4.1). It is not so strange that the crack growth is not accelerating right from the beginning of the test. If a micro-crack is nucleated and growing, the stress concentration will increase with increasing crack length. However, the crack penetrating into the material away from the free surface, will meet with an increasing flow restraint at the tip of the crack, since the effect of the free surface is vanishing. In other words, there is a gradual transition from a biaxial to a triaxial state of stress. This is opposing the increasing stress concentration and the constant rate would suggest a certain balancing of the two effects. Based on the assumption that a constant crack rate in the beginning of the test also applies to the NLR-tests, this constant crack rate (which is also the minimum crack rate) can be calculated by integration. The results of these calculations are also shown in figs 1 and 2 by the line indicated as l_t. For $l < l_t$ the crack rate is assumed to be constant, for $l > l_t$ the crack rate is assumed to increase in accordance with the curves of the figures. The minimum crack rates obtained in this way are certainly not free from speculation. Nevertheless, it is thought that they are acceptable for an indication of the orders of magnitude of the minimum crack rates to be considered by a fatigue theory. The orders of magnitude are compiled in table 1, which also gives maximum values of the crack rate. These maximum values are associated with the crack rates at approximately 95% of the fatigue life. Table 1 gives values for "low" and "high" stress amplitudes. No exact definition of what is low and what is high will be given here. Qualitatively low and high stress amplitudes may be associated with fatigue lives below and beyond 100 000 cycles respectively. Since the sole purpose of table 1 is to arrive at orders of magnitude this vagueness of definitions is not an objection.

The results of table 1 have been obtained from tests performed at a zero stress ratio ($S_{\min} = 0 \rightarrow R = 0$) or $S_m = S_a$. For other values of the mean stress, but the same fatigue lives, other values of S_a would apply. It may well be assumed that this will not have a great effect on the shape of the crack propagation curves if positive mean stresses are considered. Consequently table 1 will still be applicable. A small effect of the mean stress on the shape of crack propagation curves was found for macro-cracks in a recent NLR-investigation (ref. 6).

In spite of its qualitative character table 1 clearly illustrates the large variation in crack rates for low and high stress amplitudes and for the beginning and the end of a fatigue test.

4.2 *Some fractographical observations*

One of the most characteristic features of low-level fatigue fractures in aluminium alloys (and in fact in most materials) is a macroscopic flatness of the fracture in a plane perpendicular to the maximum principal stress.

The NLR recently performed several test series to study the propagation of macro-cracks in sheet specimens with small artificial crack starters (refs 7, 8 and 6). The crack propagation initially pro-

TABLE 1

Orders of magnitude of the crack rate in unnotched and in notched specimens of 2024-T3 material in the beginning of fatigue tests and towards the end of fatigue tests (appr. 95% N), based on results of Schijve and Jacobs (ref. 4).

Type of specimen	Stress amplitude	Order of magnitude of dl/dn					
		(μ/c)		(Å/c)		(b/c)[1]	
		Min.	Max.	Min.	Max.	Min.	Max.
Unnotched	Low S_a	$3 \cdot 10^{-5}$	10^{-2}	0.3	100	0.1	30
	High S_a	$3 \cdot 10^{-3}$	1	30	10,000	10	3000
Notched	Low S_a	10^{-4}	10^{-1}	1	1,000	0.3	300
	High S_a	$3 \cdot 10^{-3}$	3	30	30,000	10	10,000

[1]) b = size of Burgers vector = 2.86 Å for the slip systems {111} <110> in aluminium.

ceeded in a plane perpendicular to the loading direction, i.e. in the characteristic fatigue mode. This type of fracture will be referred to as the 90°-mode. In a constant-load-amplitude test the crack rate increased and after some time a transition occurred as shown in fig. 5. The crack then continued propagating in a plane at an angle of 45° to the loading direction (and also at an angle of 45° to the sheet surface). This type of fracture will be indicated as the 45°-mode. Fig. 5 illustrates that the transition developed gradually, starting with small shear lips at the two surfaces of the sheet. In an investigation on the effect of mean stress and stress amplitude on macro-crack propagation (ref. 6) the impression was obtained that the transition to the 45°-mode was completed in all tests at approximately the same value of the crack rate. This value was in the order of 0.25 μ/c for the 2024-T3 alloy and 1.5 μ/c for the 7075-T6 alloy, or 1000 and 5000 b/c respectively.

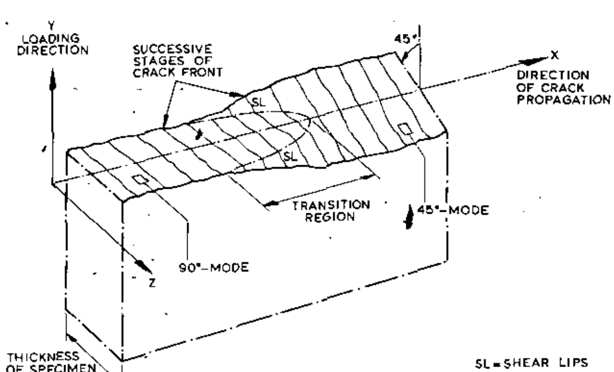

Fig. 5 The surface of a fatigue fracture in sheet material during the transition from the 90°-mode to the 45°-mode.

The transition was also observed in the tests on the small unnotched and notched specimens, discussed in the previous section. Examples are shown in fig. 6. The characteristic fatigue part of the fracture (i.e. the 90°-mode) is easily recognized, as well as the transition to the 45°-mode. It is sometimes suggested that the former part is the real part of the fracture and that the 45°-part is formed in the last cycle of the test, thus being a quasi-static failure. This is not correct since a considerable amount of fatigue crack growth remains after the transition has occurred. The orders of magnitude of the crack rate corresponding to the crack length at which the transition is completed are 6000 b/c and 2500 b/c for the unnotched and the notched specimens respectively, which are the same orders of magnitude mentioned for macro-cracking.

In fig. 5 both shear lips are deviating from the XZ-plane in the same direction. In some cases this occurs in opposite directions. At the end of the transition region one of the shear lips then rotates to the plane of the other shear lip, again forming a single shear fracture with the other shear lip. Sometimes this rotation does not occur and a double shear fracture is the result.

Fig. 6 reveals some other interesting features. It clearly shows that the characteristic fatigue part is becoming smaller for higher stress levels. This part has practically vanished for specimens 3A35 and 1A12. This suggests a gradual transition from a typical fatigue fracture to a static shear fracture when the maximum stress in the fatigue test is increased. The cracks start at a corner of the cross section and the shear lips develop at both the long edge and the short edge of the cross section. Very small shear lips at the short edge are visible in fig. 6, specimens 3B36 and 1A35. It is estimated that small shear lips were present at crack rates as low as 0.02 μ/c or 70 b/c. The presence of the shear lips is typically associated with the free surface and not with large crack rates.

The transition from the 90°-mode to the 45°-mode is further considered in chapters 7 and 9.

4.3 *Crack propagation in pure aluminium sheet specimens*

Six sheet specimens of technically pure aluminium were axially loaded in alternating tension to study whether crack propagation at very low stress amplitudes occurred along crystal planes. There were some indications for aluminium alloys, discussed in chapter 7, that the propagation occurs along such planes if the rate of propagation is very low. Since the complication of a precipitation is absent in pure aluminium some systematic tests on this material were considered worthwhile.

The specimens had a low thickness and were recrystallized to obtain a grain size considerably larger than the thickness. This allows the crack front to move forward in one crystal at a time. Restraint of neighbouring grains on the activation of slip systems and the path of crack propagation is practically absent then.

Specimens were cut to a width of 70 mm from aluminium foil with thicknesses of 0.2, 0.4 and 0.6 mm. The following recrystallization procedure was applied. (1) Annealing at 350°C for 3 hours. (2) Stretching in tension to 6% plastic strain. (3) Heating for recrystallization at 550°C for 24 hours. Impurities most probably necessitated the high recrystallization temperature. The tensile strength after the above treatment was 6.3 kg/mm². The specimens were provided with sharp notches to initiate cracks. Two types of notches were employed, viz. two edge cuts at both side edges of the specimen, and a central slit. The depth of the cuts was 2 mm and the width of the slit was 6 mm. The

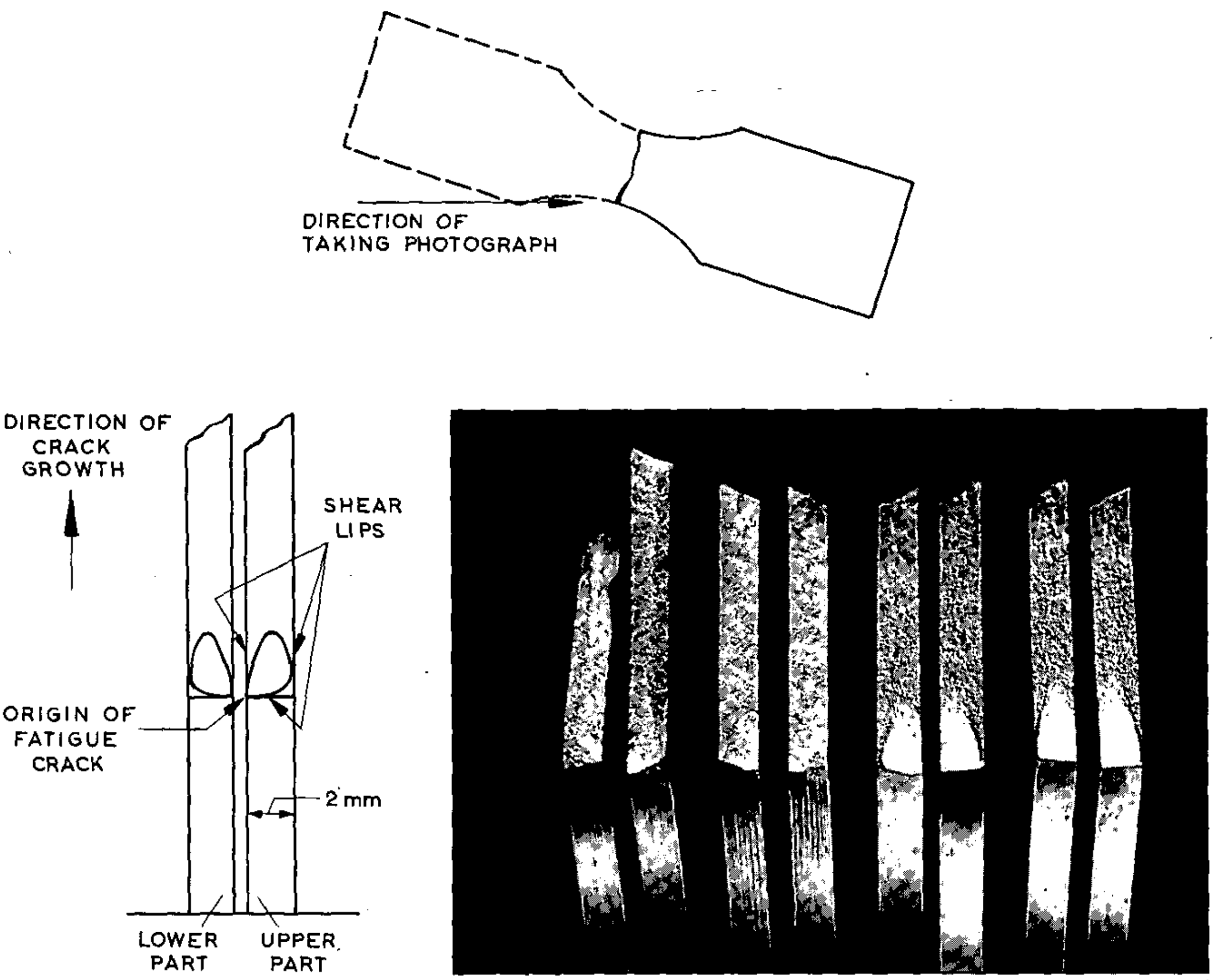

Specimen nr	3A35	1A12	3B36	1A35
S_{max} (kg/mm^2)	45.5	47	24	18
N (cycles)	13500	5500	141000	662000

Fig. 6 Upper and lower fracture surfaces of four unnotched specimens, tested at different stress levels (ref. 4).

specimens were etched with hydrofluoric acid and aqua regia before fatigue testing to reveal the grains. In view of the surface roughening by the latter agent it was not used in all cases. Hydrofluoric acid also reveals the grain boundaries, although less distinctly.

The tests were carried out on a 2 tons Amsler fatigue machine Vibraphore, which is an electrodynamic high-frequency pulsator. The machine was equipped with a 500 kg dynamometer. The test frequency was approximately 100 cycles per second. In view of buckling the specimens were loaded in tension only. Macrocreep occurred in all specimens, mainly in the beginning of the test. It was not easy to maintain the load at a constant value, the more since the loads were extremely low for the machine.

A survey of test data is given in table 2 including the grain size of the specimens. During the tests the crack propagation was observed, but no precise measurements of the crack length as a function of time were made. At the end of the test, when the total crack length was about half the specimen width, an average crack rate was calculated. In some tests the load was decreased during the test to avoid acceleration of crack growth. Values of the crack rate and the stress amplitudes have been collected in table 3. These data indicate the order of magnitude, but they do not have a high quantitative accuracy. This is not an objection in view of the qualitative character of the tests.

Macrographs and micrographs of the fatigue cracks are shown in figures 7 to 12. Examination of the specimens revealed that a tendency towards

TABLE 2

Data on the tests on the aluminium foil specimens

Specimen No.	Width (mm)	Thickness (mm)	Notches	Etching	Grain size[1] (mm)	Load (kg) Min. – Max.
4	70	0.2			3	3–42
5	70	0.2		HF + aqua regia	2	2–37,6–32,10–28,14–24
6	70	0.2	Two edge cuts		3	4–26, 2–16
7	70	0.2		HF and a short time in aqua regia	2.5	6–28, 6–20, 6–16
A	70	0.6	Central	HF	1.5	4–70
B	70	0.4	slit		20	4–48

[1]) Estimated mean value

TABLE 3

Results of the tests on the aluminium foil specimens

Specimen No.	S_a[1]) (kg/mm²)	Crack propagation rate dl/dn[1])		
		μ/c	Å/cycle	b/cycle[2])
4	1.4	0.03	300	100
5	0.7	0.02	200	70
6	0.5	0.01	100	35
7	0.4	0.005	50	20
A	0.7	0.003	30	10
B	0.7	0.005	50	20

[1]) Values in table are not very accurate and should be regarded as indicating the order of magnitude.
[2]) b = size of Burgers vector = 2.86 Å for the slip systems $\{111\}$ $\langle 110\rangle$ in aluminium.

crack growth along straight lines was more pronounced at lower crack rates than at higher crack rates (compare figs 11 and 12). This also applies to changes in the direction of growth after crossing a grain boundary. A striking example of this latter was shown by specimen B (see fig. 7). This specimen consisted of a few grains only. Changes of the direction of growth within one grain are not necessarily rare at low crack rates, which is also illustrated by specimen B (see fig. 8). Fig. 9 shows an enlarged detail of fig. 8. The left-hand flanks of the teeth are parallel to visible slip lines. The association with slip lines is also illustrated by fig. 10. However, it was not exceptional that a grain exhibiting crack growth along a straight line showed slip lines, which were not parallel to the crack but under a certain angle, see for instance the right-hand flank of the tooth in fig. 9.

Examination of the fracture surface showed this surface to be relatively flat if the crack was straight. It was more rumpled if the crack followed a fairly irregular path. Exceptions were also found, for instance the fracture surface of the crack in the large grain at the left-hand side of specimen B, see fig. 7, was not relatively flat.

Originally it was thought that a fracture surface, which was relatively flat might have an orientation parallel to a crystal plane, viz. a $\{111\}$ plane. This was checked by making Laue transmission photographs of five suitable grains. The Laue photographs were made and analysed at the Laboratory for Metallurgy of the Technological University at Delft. The geometrical orientations of the fracture surfaces were determined with the aid of a microscope. Four of the five grains did not show a correlation between the orientation of the fracture surface and orientations of crystallographic planes. In these four grains, slip lines, if observed, were not parallel to the fracture surface. The fifth grain showed the sawtooth character, see fig. 8 and 9. Each saw-tooth was a three-sided pyramid on the fracture surface, one side being the sheet surface. Of the two other sides, one was parallel to slip lines, see fig. 7. Within the accuracy of the measurements this side was parallel to a $\{111\}$ plane, which did not apply to the other side.

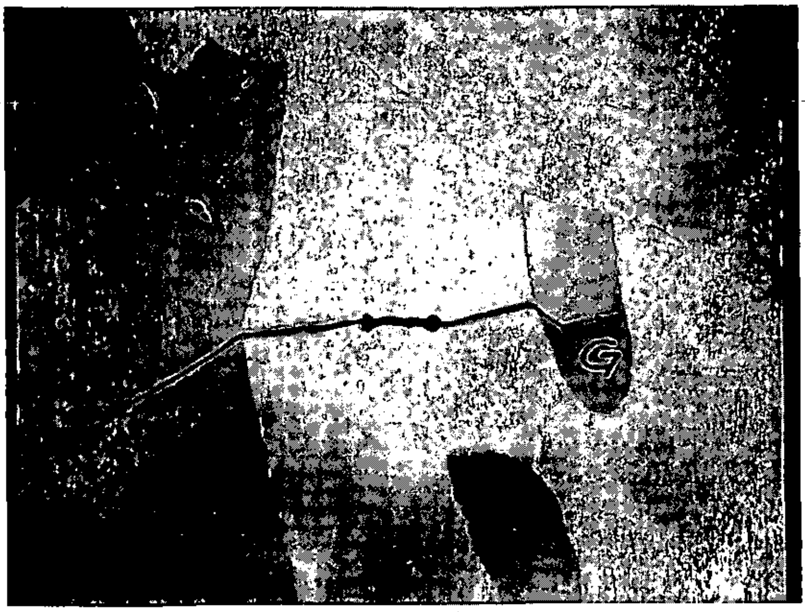

Material: pure aluminium

Fig. 7 Macrograph (1.5 ×) of specimen B, full width of specimen being shown. Cracks started at both edges of the central slit.

← direction of crack growth

Fig. 8 Macrograph (14 ×) of the central grain of specimen B (reverse side of fig. 7) showing a saw-tooth crack.

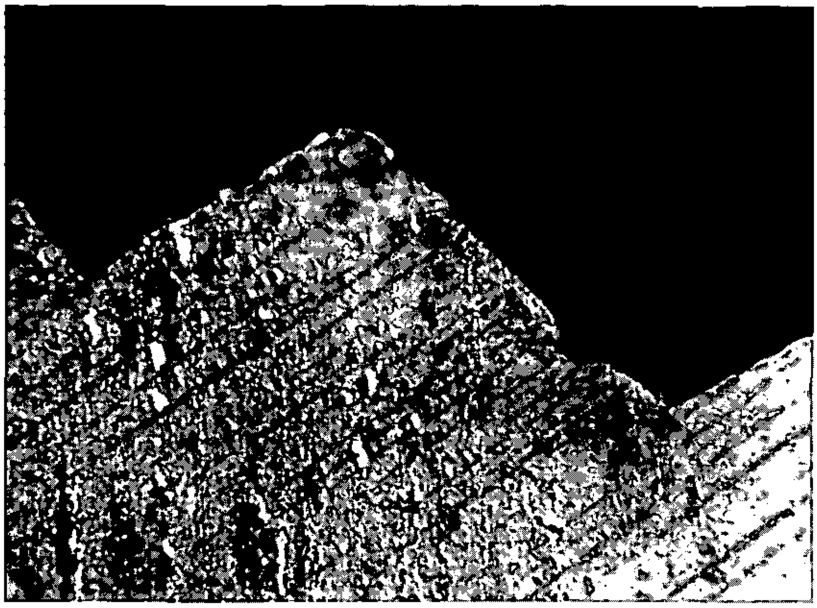

Fig. 9 Micrograph (220 ×, dark-field illumination) of one of the teeth of fig. 8.

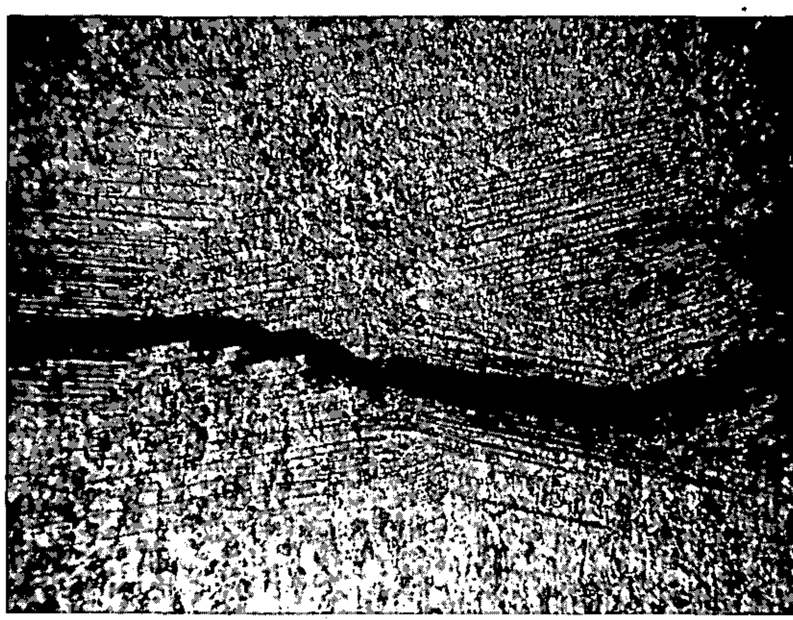

Material: pure aluminium

Fig. 10 Micrograph (50 ×, dark-field illumination) of specimen A.

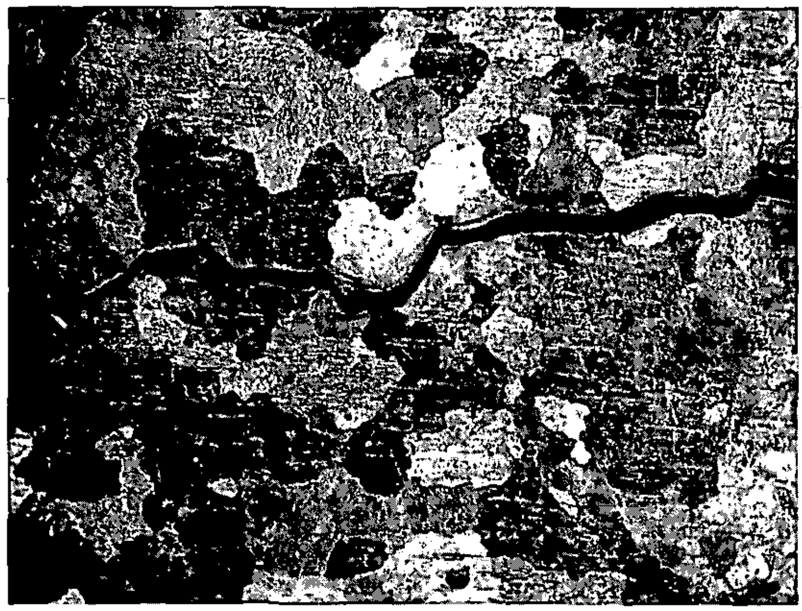

← *direction of crack growth*

Material: pure aluminium

Fig. 11 Macrograph (5 ×) of specimen 7, crack rate appr. 50 Å/c.

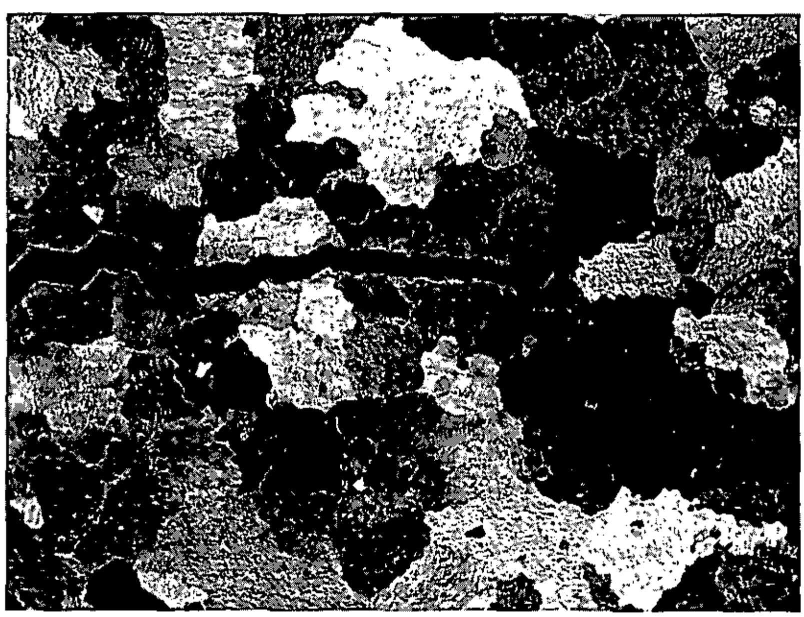

→ direction of crack growth

Material: pure aluminium

Fig. 12 Macrograph (4 ×) of specimen 4, crack rate appr. 300 Å/c.

In summary it may be said that the tests have shown that crack growth along straight lines was promoted by low stress amplitudes involving low rates of crack growth. The X-ray diffraction results give no conclusive evidence that crack extension occurs along crystallographic planes. A discussion of these results and a comparison with other investigations is given in chapter 7.

4.4 *Crack nucleation in the cladding of aluminium alloy sheet specimens*

The sheet material with the designation 2024-T3 Alclad consists of a strong core (90% of the thickness) of a precipitation hardened Al Cu Mg alloy and two surface layers (5% of the thickness each) of pure aluminium, referred to as the cladding. Such a sandwich material allows an interesting approach to the study of crack nucleation. The yield stresses for the core and the cladding differ greatly, viz. in the order of 32 and 5 kg/mm² respectively. If an unnotched specimen is cyclically loaded between, say $S_{min} = 1$ kg/mm² and $S_{max} = 20$ kg/mm² the straining of the core will be almost perfectly elastic. However, the thin cladding will be subjected to cyclic plastic strain with an approximately constant amplitude. As a consequence of the plastic strain, plastic shake-down of the stress in the cladding will occur and the mean stress will tend to zero. A difference with constant-strain amplitude tests on specimens of a single material, reported in the literature arises when a crack has been nucleated. The conventional constant-strain amplitude test is in fact a test with a constant amplitude for the total deformation of the specimen. If then a crack is nucleated it will introduce a severe concentration of plastic strain. This does not apply to the cladding, at least not to the same extent, in view of the presence of the elastic core. In other words, for a crack in the cladding there will be much more restraint on opening of the crack than for a crack which is not backed up by an elastic surrounding with a much higher yield stress.

Tests were carried out on unnotched sheet specimens, width 20 mm and sheet thickness 2 mm. The nominal thickness of the cladding was 0.1 mm = 100 μ. Before fatigue testing the surface was electrolytically polished and subsequently etched to reveal the grain boundaries. The specimens were tested in a vertical Schenck pulsator at a frequency of approximately 40 cycles per second. After a certain number of load cycles had been applied, the specimens were removed from the fatigue machine for a microscopic examination. The tests were carried out with $S_{min} = 1$ kg/mm² and with $S_{max} = 18, 20, 24, 28$ and 35 kg/mm² respectively, the number of cycles applied varying from 5000 to 20,000. All stresses quoted are nominal values. In view of the low yield stress of the cladding the stresses in the core were slightly higher and the stresses in the cladding much lower. Due to plastic shake-down the mean stress in the cladding was zero. The strain ranges in the cladding were approximately $(S_{max} - S_{min})/E$ where E is the elastic modulus, i.e. they ranged from 0.24% to 0.48%.

The microscopic results were qualitatively the same for all specimens. Straight and well developed slip lines were observed in almost all grains. An example is shown in fig. 13. In general all slip lines in one grain had the same orientation. In some grains of the specimens with the higher fatigue loads, slip on two different slip planes was observed.

The slip lines were supposed to be crack nuclei, which was supported by the following evidence. (1) Debris was extruded by several slip lines. (2) The cracks were indicated in cross sections of the specimens, see fig. 15. (3) Application of a deep etch made the slip lines broader and deeper as might be expected for micro-cracks. This is illustrated by fig. 14 which shows the same area as fig. 13. Slip lines caused by a static tensile loading

$\leftarrow\rightarrow$ direction of fatigue load

Magnification 410 ×, oblique illumination. Electropolished and etched before fatigue testing. Fatigue load 5000 cycles with $S_{max} = 20$ kg/mm² and $S_{min} = 1$ kg/mm² (nominal stress in specimen).

Fig. 13 Fatigue slip lines on the surface of the cladding of 2024-T3 Alclad sheet specimens, not etched after loading

The micrograph shows practically the same area as fig. 13, the surface now being etched for 8 minutes in Fuss etchant, which removed approximately 4μ of the material.

Fig. 14 Fatigue slip lines on the surface of the cladding of 2024-T3 Alclad sheet specimens, after deep etching

are shown in fig. 16. The oblique illumination reveals the static slip lines as (light or dark) surface steps. Such slip lines were almost fully eliminated by the same deep etching, which transformed the fatigue slip lines into grooves. (4) Application of a tensile load after the fatigue test, leading to plastic elongation of the core, opened many slip lines, see fig. 17. Most unopened slip lines in this figure originated from the static load.

The slip lines on the cladding (fig. 13) and the cracks shown in the cross section of the specimen (fig. 15) clearly indicate that the nucleation of the micro-cracks occurred along crystal planes. For a determination of the orientation of the planes the method used by Girard (ref. 9) was adopted. With a micro-hardness machine (Vickers) small impressions were made in several grains. The impressions yielded visible slip lines in three or four directions in each grain. One of the directions was the same as for the fatigue slip lines. Since static deformation in aluminium predominantly occurs on $\{111\}$ planes, this apparently applies to fatigue crack nucleation in the cladding as well.

For the longest cracks the rate of crack penetra-

$\leftarrow\rightarrow$ direction of fatigue load

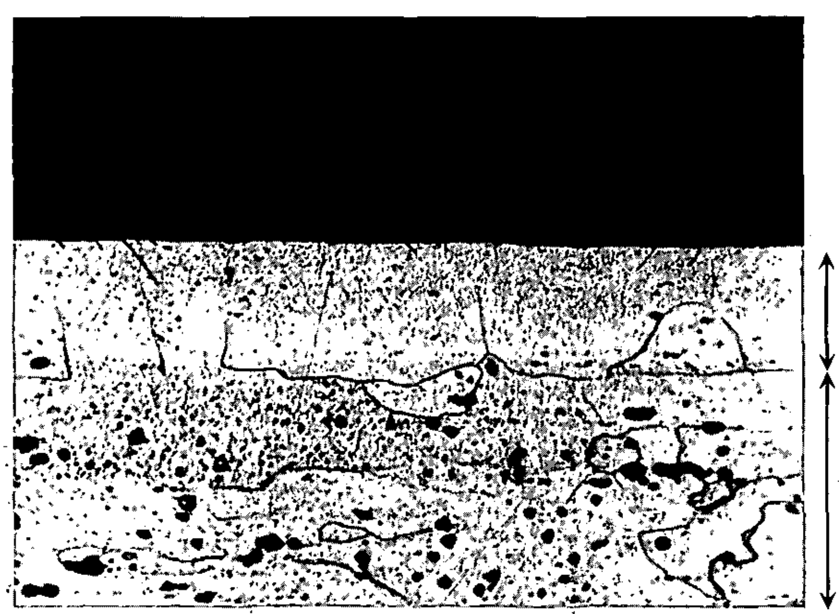

Magnification 250 ×. Fatigue load 20,000 cycles with $S_{max} = 20$ kg/mm^2 and $S_{min} = 1$ kg/mm^2 (nominal stresses in specimen)

Fig. 15 Micro-cracks in the cladding of 2024-T3 Alclad sheet material

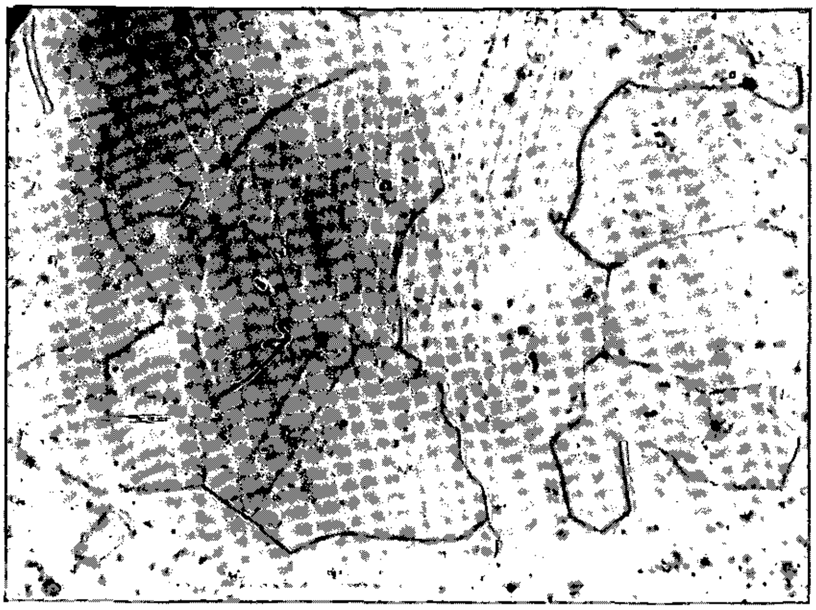

Magnification 410 ×, *oblique illumination*. Electropolished and etched before static loading until S = 38 kg/mm^2 (nominal stress in specimen) No fatigue loads applied.

←→ direction of static loading

Fig. 16 Slip lines on the surface of the cladding of 2024-T3 Alclad sheet specimen after a single tensile loading (not etched after loading)

←→ direction of fatigue load and subsequent static load

Magnification 440 ×. Fatigue load 5000 cycles with S_{max} = 35 kg/mm^2 and S_{min} = 1 kg/mm^2 (nominal stresses in specimen). A subsequent static loading induced a 7.6% plastic elongation. Note the static slip lines ending in the right-hand fatigue crack.

Fig. 17 Fatigue micro-cracks in the cladding of 2024-T3 Alclad sheet material, opened by a plastic elongation of the specimen.

tion into the cladding, as measured on micrographs such as shown in fig. 15, was in the order of 0.001 to 0.0025 μ/cycle or 10 to 25 Å/cycle.

4.5 *Crack propagation in aluminium alloy sheet specimens with a central slit*

The sheet material 2024-T3 Alclad used to study crack nucleation in the cladding (see previous section) was also used for studying crack propagation initiated by a small central slit.

The purpose of the tests was to study whether the cracks would show a tendency to grow along crystal planes. Microscopic observations were made at the surface of the specimen and on microsections, parallel to the surface. Tests were also carried out on specimens which had the cladding removed before fatigue testing, i.e. in the bare condition.

The dimensions of the specimen are shown in fig. 18. The central slits with the sharp saw cuts initiated cracks after a small number of cycles. The tests were performed in a vertical Schenck pulsator at a frequency of approximately 40 cycles per second. The crack length was recorded as a function of n, the number of cycles. When the longest crack had a length $l = 10$ mm the test was stopped. The crack length l is defined in fig. 18. From the results the crack rate dl/dn was calculated. Seven specimens were tested, four specimens with the cladding removed by emery-paper. The stresses applied are indicated in fig. 19, which also shows the crack rates obtained as a function of the crack length.

Cracks started at the central slit were growing through the full thickness of the sheet specimen, the crack front being virtually perpendicular to the sheet. If a cladding was present the cracks were simultaneously growing in the core and the cladding.

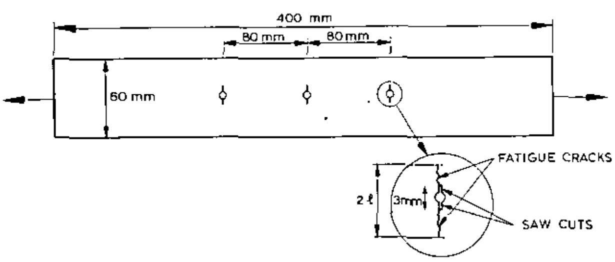

Sheet thickness 2 mm. The central slits consist of a hole (diameter 1 mm) and two saw cuts (depth 1 mm and width 0.25 mm).

Fig. 18 Sheet specimen of 2024-T3 Alclad with three central slits, used for crack propagation.

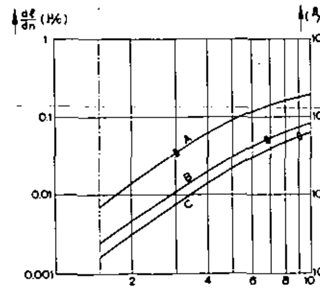

Fig. 19a

2024-T3 Alclad		
Spec.	S_{min}	S_{max}
A	1	9
B	1	7
C	1	6

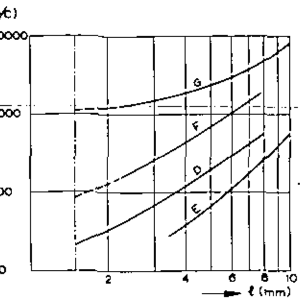

Fig. 19b

2024-T3 bare		
Spec.	S_{min}	S_{max}
G	2	15
F	1	9
D	1	6
E*)	1	5

Stresses in kg/mm² on gross area of specimen.

*) Specimen E was first tested at $S_{max} = 6$ kg/mm² until $l \approx 3.5$ mm.

□ indicates the crack length until which the crack in the cladding (specimens A, B and C) was clearly growing along crystal planes.

Fig. 19 The crack rates obtained in the 2024-T3 specimens shown in fig. 18.

The growth of the crack in the cladding predominantly occurred along slip planes if the crack rate was not too high. An example is shown in fig. 20. For higher crack rates the slip line density increased and the obvious correlation between the path of the crack and the orientation of the slip planes was gradually lost, i.e. beyond the possibilities of observations. In fig. 19 it has been indicated

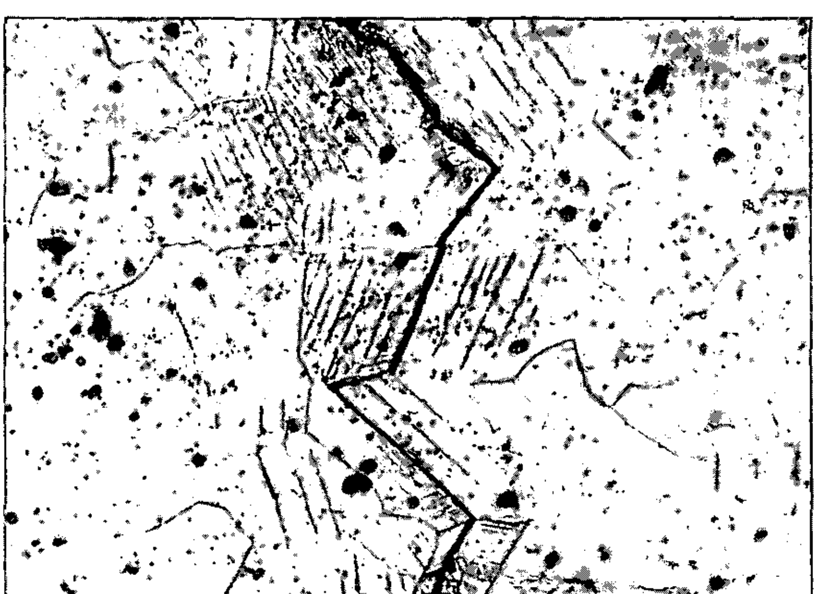

Micrograph of the surface (300 ×), electropolished and etched before fatigue test. Specimen shown in fig. 18. Load and crack rate data given in fig. 19. $l = 2.3$ mm, $dl/dn = 0.004\ \mu/c = 40$ Å/C.

growing direction

Fig. 20 Crack propagation along slip lines in the cladding of specimen C.

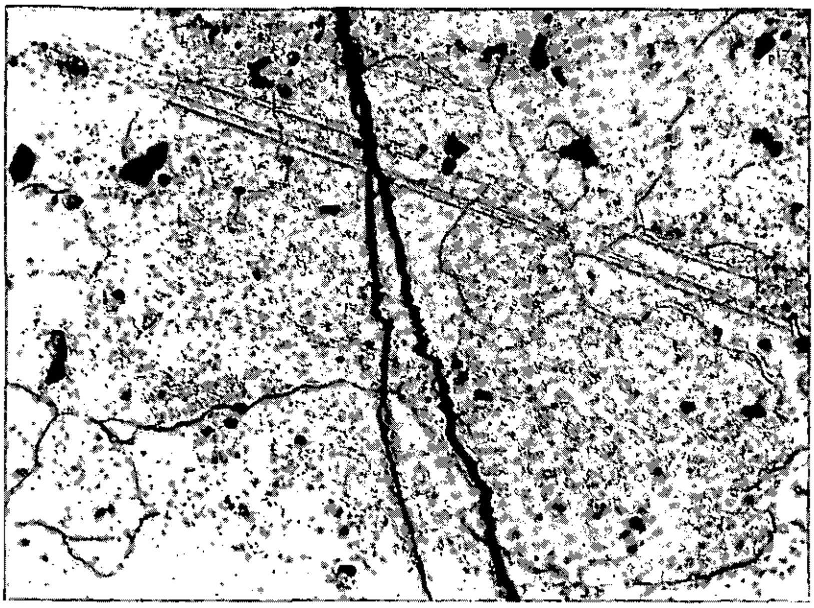

Micro-section (300 ×) just below cladding.

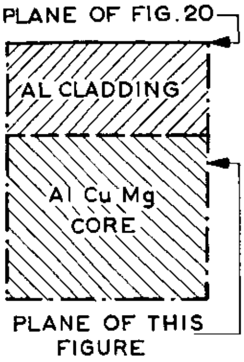

Fig. 21 The same area as shown in fig. 20 after removal of the cladding.

until which crack rate the crack was clearly growing along slip planes.

Fig. 21 shows the same area as fig. 20 after the cladding and a little bit of the core had been removed. The picture has changed drastically. A correlation with crystallographic planes cannot be observed.

The results of the bare (unclad) specimens were somewhat surprising. Micro-sections had always shown the path of a fatigue crack in the Al Cu Mg alloy to be fairly irregular and apparently uncorrelated to the crystal structure, apart from the very beginning of the crack growth when the crack rate was still very low. However, it was now observed that at the surface of the specimen there was a pronounced correlation with slip planes. Examples are shown in figs 22 and 23. In fig. 22, showing two large grains, the correlation with slip planes is clear in the left-hand grain, whereas in the right-hand grain the correlation is not evident. Fig. 23 shows a striking example of a crack alternately growing on two different slip planes. Although the correlation of crack growth with slip planes was not always as pronounced as shown in figs 22 and 23 it was observed in all specimens D, E, F and G. In fact the impression was obtained, that the correlation was about the same at all values of the crack length and the crack rate covered by fig. 19b.

← direction of growth

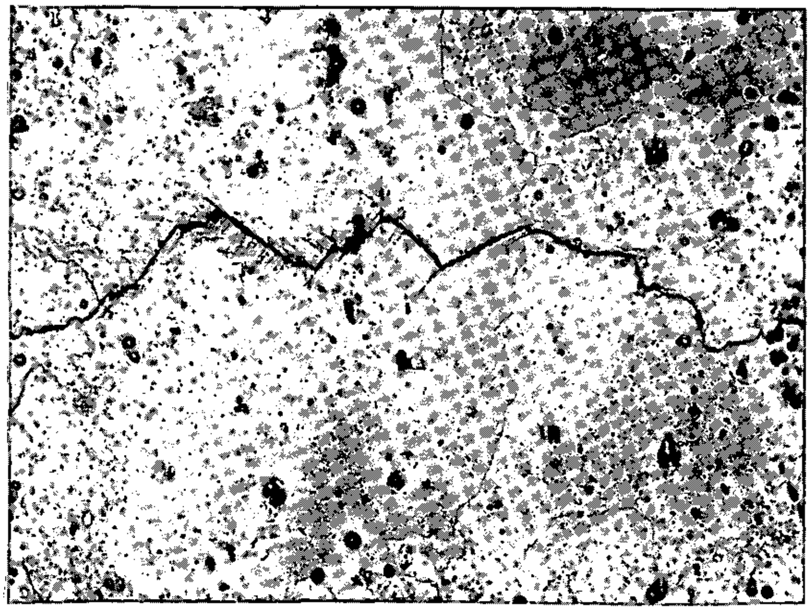

Micrograph of the surface (230 ×), electropolished and etched before fatigue test. Type of specimen shown in fig. 18. Load and crack rate data given in fig. 19 (F). l = 4.5 mm, dl/dn = 0.06 μ/c = 600 Å/C.

Fig. 22 Crack propagation along slip planes at the surface of specimen F (bare).

→ direction of growth

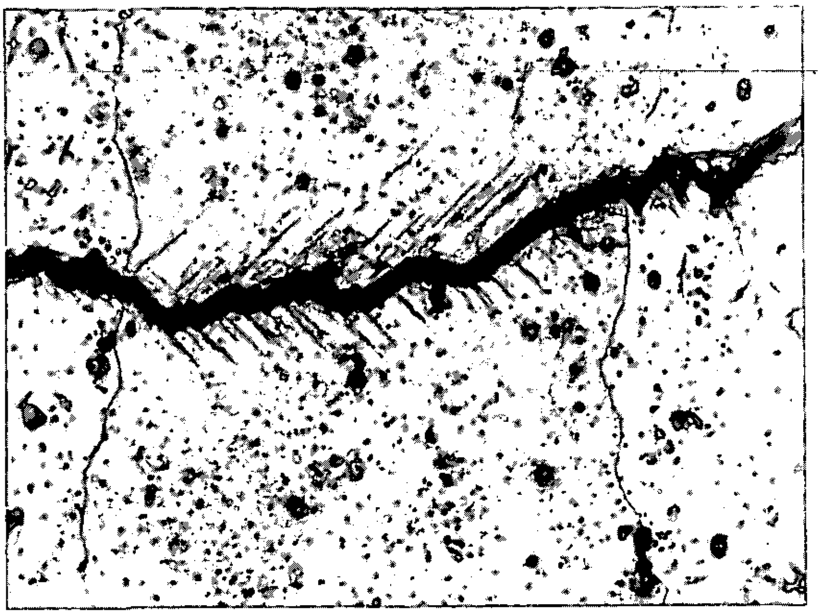

Micrograph of the surface (420 ×), electropolished and etched before fatigue test. Type of specimen shown in fig. 18. Load and crack rate data given in fig. 19 (G). l = 2.6 mm, dl/dn = 0.16 μ/c = 1600 Å/C.

Fig. 23 Crack propagation along slip planes at the surface of specimen G (bare).

At the higher crack rates slip lines were more frequently observed. At the highest crack rates, specimen G for $dl/dn = 0.6$ μ/c (= 6000 Å/C), the correlation was somewhat less clear, since the slip lines became more wavy.

The removal of 0.1 mm of the surface of the bare specimens again changed the pictures considerably; compare fig. 24 with fig. 22. Fig. 25 shows a detail of fig. 24. Micro-sections of the central plane of the sheet (i.e. after removing half the thickness) showed almost the same picture, see for example fig. 26. At a depth of 0.1 mm the crack path was perhaps somewhat more reminiscent of a correlation with crystal planes than at the central plane of the sheet. Further it could be thought that the same applied to low crack rates as compared with high crack rates.

However, again the impression was obtained that the microscopic picture did not depend to a great extent on the crack rate. One feature observed was that persistent branching occurred at low crack rates (see fig. 26), whereas the branches

← direction of growth

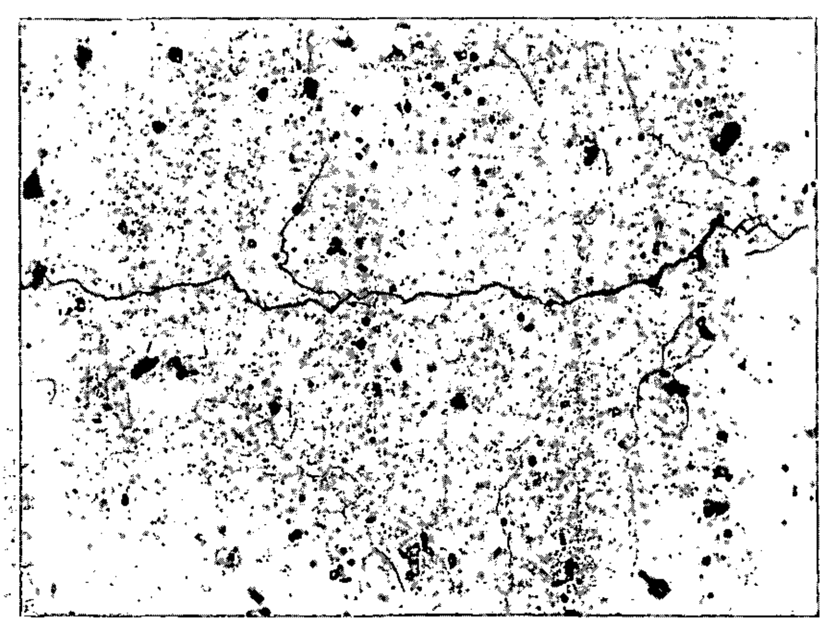

Micro-section (200 ×) parallel to and 0.1 mm below the surface of the bare specimen F. Type of specimen shown in fig. 18. Load and crack rate data given in fig. 19. l = 6.8 mm, dl/dn = 0.15 μ/c = 1500 Å/C.

Fig. 24 Micro-section of crack in specimen F (bare), 0.1 mm below the surface.

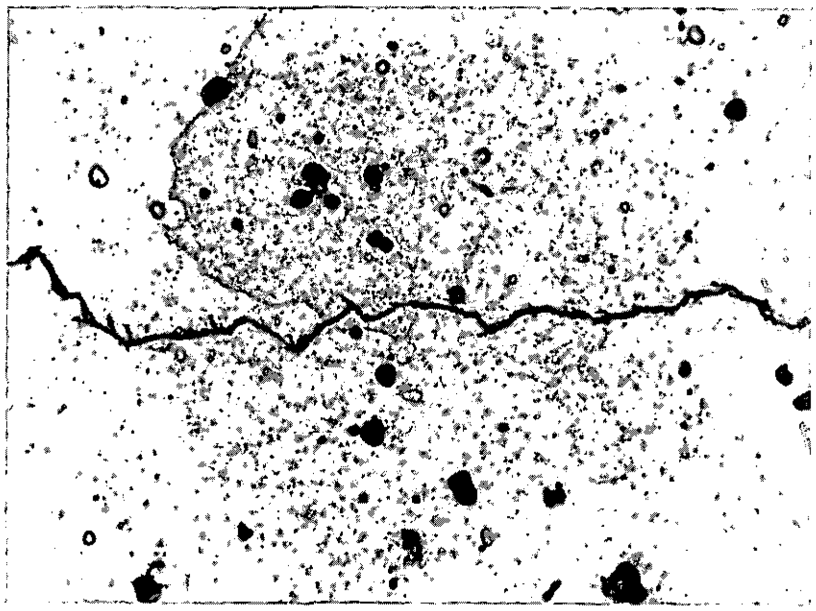

Fig. 25 Detail of fig. 24 (500 ×).

→ direction of growth

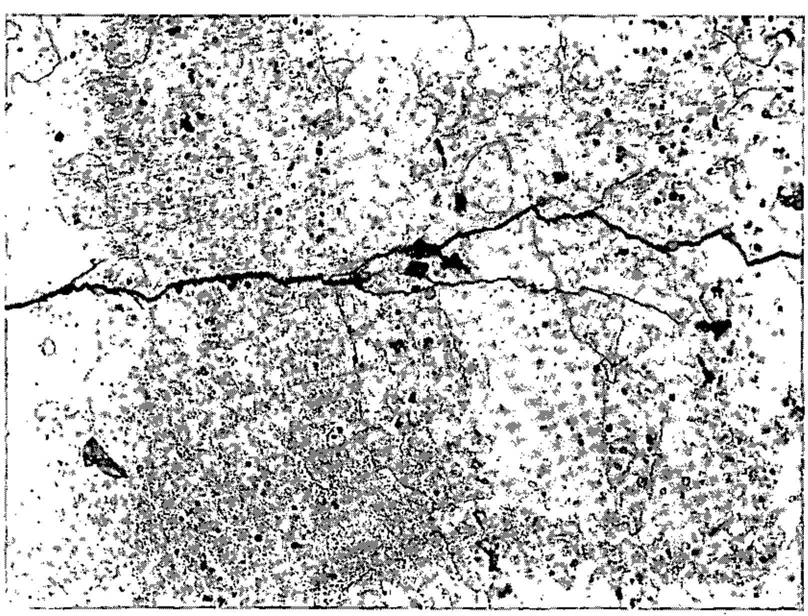

Micro-section (185 ×) parallel to the sheet surface and 1 mm below the surface (sheet thickness 2 mm). Type of specimen shown in fig. 18. Load and crack rate data given in fig. 19 (E). l = 4.4 mm, dl/dn = 0.005 μ/c = 50 Å/C.

Fig. 26 Micro-section at the central plane of the sheet of specimen E (bare).

were relatively short at a high crack rate (see fig. 25). No clear differences were noticed between cracking according to the 90°-mode and the 45°-mode, neither at the surface nor at the interior of the material. The two modes were discussed in section 4.2.

It certainly may be concluded that a pronounced correlation of the crack path with crystal planes was found at the surface and that the correlation at the interior of the material was much weaker or beyond the possibilities of observation. Secondly the microscopic observations do not suggest an essential difference between fatigue fractures of the 90° and the 45°-mode.

5 The nucleation of fatigue cracks

This chapter starts with a survey of information from microscopic studies and their interpretations. One interpretation outlines crack nucleation as a consequence of the escape of dislocations at the free surface. Evidence confirming this view is discussed. Alternative theories are briefly reviewed.

The majority of microscopic investigations on fatigue cracks has been concerned with the nucleation rather than the propagation. Classical studies were conducted by Gough et al. (refs 10 and 11). Their results will be summarized first.

For aluminium Gough and co-workers came to the following conclusions:

1. In a fatigue test slip occurs on the {111} planes in the ⟨110⟩ directions (12 slip systems). Slip occurs on that slip system for which the resolved shear stress on the slip plane in the slipping direction is a maximum ("maximum resolved shear stress" criterion, see also Appendix A).
2. The above conclusion applied to single crystals as well as polycrystalline specimens. This is in agreement with the elastic isotropy of aluminium.
3. Micro-cracks initially have a crystallographic orientation. The slip zones, however, have a fairly wavy character and this also applies to the microcracks. Probably the waviness will be related to the easy occurrence of cross slip in aluminium for circumventing obstacles.
4. When micro-cracks are growing the direction of the propagation can change over to another slip plane. Sometimes the crack follows a very irregular path, apparently in no relation to the crystal structure.

Observations as made by Gough have been confirmed by later investigations, partly on aluminium alloys, viz. by Forsyth (ref. 12), Weinberg and Bennett (ref. 13), Hempel and Schrader (ref. 14), Girard (ref. 9) and Alden and Backofen (ref. 15). The investigations of Forsyth with an electron microscope showed the slip zones to consist of a large number of short, sometimes wavy, slip lines. Between the slip zones fine slip was observed. Forsyth defines the slip zones as striations and slip in these zones is indicated as "coarse slip" involving large avalanches of dislocations. In the slip zone the surface is roughened and ridges* and valleys are formed.

Similar observations were made by Wood (ref. 16) on copper and brass. Wood has attributed this to slip on parallel planes. The possibility of forming a crack nucleus, according to Wood, is demonstrated in fig. 27. The dislocations involved have different signs in the tension part and the compression part of the load cycles. In a similar way a ridge may be built up. Dislocations of one sign have to escape at the free surface above the center line of the groove (or ridge) and dislocations of the opposite sign have to escape below that line. This systematic feature is a requirement of the mechanism. Consequently the mechanism cannot operate if dislocation movements are fully reversible, because surface steps formed during a positive stress increment would be eliminated by the subsequent negative stress increment. May (ref. 17) pointed out that a random selection of the slip planes for the to-and-fro slipping movements in a slip zone implies a certain probability of arriving at a groove. If a large number of dislocation sources is involved the statistical aspect as indicated by May cannot be ruled out. A very elegant model to explain the phenomenon of extrusions and intrusions as described by Forsyth (ref. 12) was published by Cottrell and Hull (ref. 18). The interaction of two dislocation sources active on different slip systems gives the required non-reversibility. The sequence of slip movements is shown in figure 28 and needs no further explanation. Objections against the model have been made by Backofen (ref. 19) based on the evidence that extrusions and intrusions do not occur on different slip systems as the model requires. Still it is felt that some interaction of different slip systems may indeed prevent the dislocation emission of one source from having a fully reversable effect on the geometry of the free surface. Mott (ref. 20) has suggested that a screw dislocation anchored at a cavity at one side and ending at the free surface at the other side will move along a closed circuit during cyclic loading and thus will extrude the material in the circuit. The crevice left behind the extrusion may become a crack nucleus. This model is considered to be somewhat more artificial. It is also difficult to see

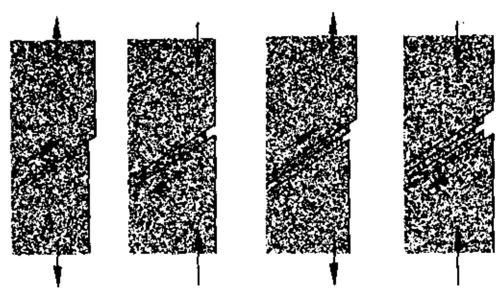

Fig. 27 Schematic view of the model of Wood for crack nucleation (ref. 16)

* Not to be confused with slip-band extrusions also described by Forsyth.

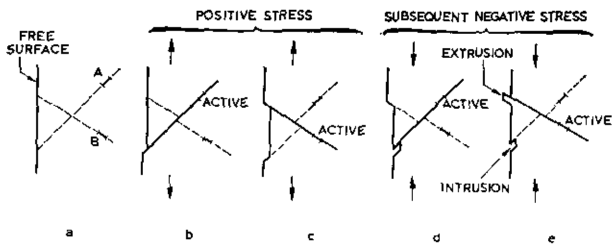

A and B are two dislocation sources. A being more easily activated than B. In fig. d and e one may also assume that the dislocation loops emitted in fig. b and c are returning to their sources in the same sequence, which will lead to the same surface topography.

Fig. 28 The formation of extrusions and intrusions by two dislocation sources on intersecting slip planes according to Cottrell and Hull (ref. 18)

how it could explain crack propagation. In another publication Mott (ref. 21) has suggested that a part of the sources will emit dislocations only during the positive stress increments, and another part will do so during the negative stress increments. Fleischer (ref. 22) has indicated that dislocation sources near the free surface will emit dislocations more easily in one direction than in the opposite direction due to the presence of the free surface. So sources will preferably operate "one way". This leads to the idea expressed by Mott. It can explain the occurrences of intrusions and extrusions, provided again that the dislocation loops do not return on reversal of the load and eliminate the surface steps. Fleischer suggests that a return need not occur if the loops are either trapped in some way or annihilated by dislocations of opposite sign.

Other geometrical reasons for the non-reversibility of the dislocation emission of one source may be added here. Fig. 29 shows a Frank-Read source emitting dislocation loops in the tension and in the compression part of the cycle. If the dislocations in fig. 29a meet the obstacle A it may be by-passed by cross-slip towards a higher or lower slip plane. After reversal of the stress the dislocations will meet again with the same obstacle. It is unlikely that cross-slip will occur now in exactly the same way, also because the dislocation does not approach the obstacle in the same direction if the latter is not too far removed from the source, see fig. 29b. Cross-slip as a requirement for fatigue has been emphasized by several authors, notably by Alden (ref. 23). Secondly if the dislocations have to cut through a screw dislocation at B in fig. 29a they will contain a jog. Let it be assumed that the jog on moving creates vacancies. The vacancies are mobile and will diffuse to other more favourable locations. In fig. 29b the dislocations should create interstitials. It is thought that this also will not lead to a reversible phenomenon. Both examples of fig. 29 are simplified. In view of the high dislocation density in the slip zones the actual process will be more complicated. But the complexity will rather promote the non-reversibility than allowing the emission to be reversible. Since the matrix of heat-treated aluminium alloys is dispersed with small coherent precipitates a reversibility of dislocation movements is considered to be still more unlikely than for pure metals. Finally it may be argued that a full reversal of all dislocation movements would not be compatible with a cyclic strain-hardening.

a Tension part of cycle b Compression part of cycle

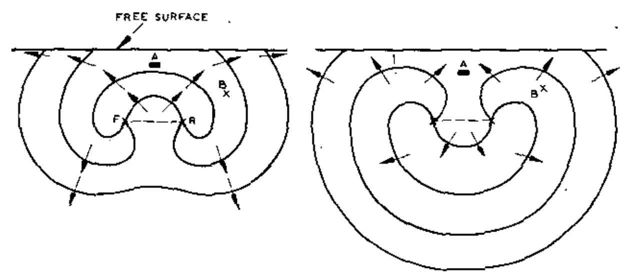

Slip plane = plane of figure
FR = Frank-Read source
A = obstacle.
B = screw dislocation cutting through the slip plane. Arrows indicate dislocation movement.

Fig. 29 Frank-Read source emitting dislocation loops under alternating stressing

A chemical reason for the non-reversibility was indicated by Thompson, Wadworth and Louat (ref. 24). Dislocations escaping from the material at the free surface are forming steps in the surface. This involves that small rims of material are freshly exposed to the environment. For aluminium there will be a very rapid oxidation and this may well prevent dislocations of opposite sign, emitted by the same sources during reversion of the load, from emerging at the surface on exactly the same planes.

From the foregoing it is concluded that the escape of dislocations at the free surface will not be a completely reversible phenomenon and the formation of ridges and valleys will occur as a geometrical consequence of dislocation movements. The deepest valleys are envisaged as fatigue crack nuclei.

An investigation performed by Alden and Backofen (ref. 15) has given conclusive evidence with respect to the role of the free surface. A thick anodic coating (1000 Å) on an annealed aluminium specimen prevented an escape of dislocations at the surface. Fatigue failures could not be obtained at a strain amplitude which would have given a fatigue life of about 10^5 cycles if an anodic coating had not been present. Still there was considerable cyclic plastic straining at the interior of the material. After removal of the coating and subsequent fatigue loading the normal fatigue life was again obtained. This investigation shows that the slip movements at the free surface are essential for the formation of the fatigue nucleus, and at the same time, that cyclic strain-hardening does not necessarily imply fatigue damage.

Additional evidence in favour of a nucleation model based on dislocation movements at the free surface as sketched in fig. 29 stems from investigations on copper. Both Thompson (ref. 25) and Backofen (ref. 19) found in fatigue studies that the slip movements should have a component perpendicular to the free surface in order to nucleate cracks. Other fatigue theories do not require such a slip component.

It is realized that the simple model for crack nucleation by the formation of surface grooves requires material transport. Vacancies and cross-slip could account for this, see also chapter 6.

Obviously it is difficult to define when crack nucleation has been completed and crack propagation is starting. It should be expected that both have several aspects in common which will be discussed in chapter 6.

Some alternative theories for the formation of fatigue nuclei are discussed in the literature and will be briefly reviewed. Gough (ref. 10) has postulated that the initiation of the fatigue crack is a consequence of the limit of local strain hardening being exceeded. This idea was picked up by Orowan (ref. 26) who argued that the local exhaustion of ductility will involve a local increase of stress which ultimately leads to cracking. Stroh (ref. 27) has analysed the stress field around a piled-up group of dislocations. The stress can become very high and high enough for local cleavage. It is thought that in aluminium near the free surface high stresses can not be set up. Relaxation of such stresses due to cross-slip or activation of other dislocation sources should occur with relative ease.

Another school of thought does not consider a local increase of stress but the deterioration of strength due to cyclic slip. Holden (ref. 28) performing an X-ray diffraction investigation concluded that subgrains are formed as a consequence of the cyclic plastic deformation. Boundary angles are fairly large and therefore micro-cracks are assumed to form in these subgrain boundaries. Cracking occurs through linking up these micro-cracks. The same idea was adopted by Valluri (ref. 29). Although no detailed mechanism is given of the linking-up procedure this is probably assumed to be related to static failure, in this case a localized static failure. There are two essential differences with the model of Wood. First, a free surface is not required for fatigue crack nucleation. Secondly the model implies that a certain amount of material (plastic enclave) has to be prepared by cyclic slip movements in order to become weakened and to allow crack nucleation (or extension). In other words the crack nucleation will have a discontinuous character rather than being more or less continuous as for the model of Wood. A somewhat related theory was proposed by Mott (ref. 30). He argued that cyclic strains will give such a disordered structure that local recrystallisation will occur. The accompanying volume contraction will induce tensile stresses sufficiently large to create cracks. Also for the model of Mott the free surface is not essential and it also involves a preparation of the material to become critical for fatigue crack nucleation.

The question whether the free surface is essential or not does not offer a strong argument in favour or against fatigue theories. All theories do involve cyclic slip, and since the restraint at the free surface is less than for the interior of the material, cyclic slip will always be concentrated at the free surface, also for a homogeneous stress distribution. So it has to be expected that cracks will anyhow originate at or rather near the free surface. Microscopic evidence in general points to a nucleation at the free surface apart from crack nucleation at inclusions.

Theories involving a local deterioration of strength are not considered to be realistic in view of the results of Alden and Backofen and Thompson as discussed before. The deterioration requires cyclic slip movements, but it is not required that dislocations escape at the free surface and that the Burgers vector of these dislocations has a component perpendicular to the free surface.

A model based on vacancy condensation is discussed by Oding (ref. 31). Obviously vacancies will be produced in regions with severe cyclic slip. However, many of them will be trapped by dislocations, grain boundaries, foreign atoms, precipitates and the surface of the material. It is difficult to specify their contribution to the fatigue process in any detail, especially in the presence of a high dislocation density and stress gradients. It is considered doubtful that coagulation of vacancies to a cavity or a microcrack near or at the surface will prevail over the geometric process mentioned before.

In summary it can be said that there are four types of theories on the nucleation of fatigue cracks.

1. Nucleation is a geometric consequence of dislocation movements at the free surface, involving the formation of intrusions, see fig. 27.
2. Nucleation occurs as a localized failure due to an increase of stress in a cyclically strain-hardened region.
3. Nucleation occurs as a localized failure due to a deterioration of strength as a consequence of cyclic plastic strain.
4. Nucleation is due to a coalescence of vacancies.

Cyclic slip is required for all theories and this makes a discrimination between the theories a delicate problem. The most conclusive evidence in favour of the first type of the theories was already mentioned: Alden and Backofen found that a thick anodic coating prevented crack nucleation in aluminium, although considerable cyclic slip did occur. Both Thompson and Backofen found for copper that crack nucleation is stimulated by a slip vector with a component perpendicular to the free surface. If these results have to be extrapolated to aluminium alloys it should be said that the evidence is not too abundant. On the other hand experimental evidence in favour of the other theories and in conflict with the first group of theories is also absent. One aspect not yet mentioned is the crack nucleation under cyclic loads for which both the maximum and the minimum load are compressive. Under such conditions cracks are nucleated also in the Al Cu Mg alloys (ref. 32). It is somewhat difficult to see that nucleation under compressive stress is a consequence of a localized static failure.

For the time being it is thought that the most logical explanation for the nucleation is that it occurs as a geometrical consequence of dislocation movements, although the process is likely to be more complex than indicated in fig. 27. An inherent feature of this fatigue model is that cyclic strain hardening per se cannot be regarded as fatigue damage. In the following chapter on crack growth several aspects are further analysed. The complications due to the presence of precipitates are discussed in chapter 10. It is thought that it need not essentially change the nucleation mechanism.

6 A dislocation model for crack growth

In the previous chapter the initiation of a crack nucleus was, according to Wood's model, visualized as a geometric consequence of dislocation movements at the free surface of a material. Dislocations of opposite sign, escaping from the material in the rising part and the falling part of a load cycle, may form intrusions and extrusions, an intrusion becoming a crack nucleus. It is now suggested that the contour of the tip of a crack may be regarded as a free surface capable of trapping dislocations. This could account for crack growth. Several aspects of the suggestion are considered in this chapter, while alternative mechanisms are discussed hereafter.

The probability of a dislocation running into a crack appears to be low in view of the "low thickness" of the crack. However, it is considerably increased by the stress concentration introduced by the crack. Fig. 30 shows in a rather schematic way how an intrusion is formed in the crack tip region during one load cycle. The intrusion implies a certain amount of crack growth. Some implications of fig. 30 will be further analysed.

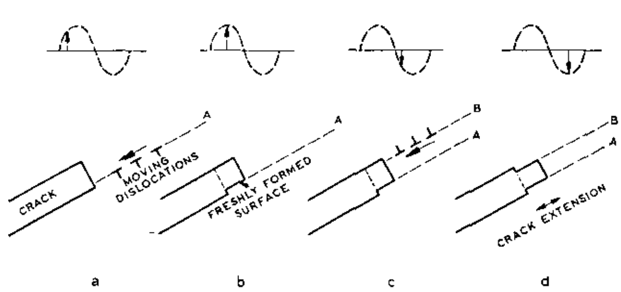

Fig. 30 Four subsequent stages of a simple mode of crack extension during one cycle.

In fig. 30 the slip planes A and B both cut through the tip of the crack. If either slip plane A had been below the crack or slip plane B above the crack the same amount of crack extension would occur, provided that the dislocations were in some way locked near the crack, preventing them from running backwards on reversal of the load. However, if the two slip planes A and B change places, an extrusion instead of an intrusion is formed and no crack extension occurs. So similar to crack nucleation, crack growth requires a systematic difference between the dislocation movements in the rising and the falling part of the load cycles.

In fig. 30 the contour of the crack tip is sketched as being rectangular. It is more likely that it will be rounded or tapered. Local plastic strains at the tip of the crack will blunt the crack when the loading increases and sharpen the crack when the stress decreases. For high stress amplitudes this was clearly shown for aluminium specimens by Laird and Smith (ref. 33). Another complication is the oxidation which on aluminium and its alloys occurs very rapidly. It may be expected that the edges of the crack will be covered by a thin oxide film. During an increase of the stress the crack will blunt and the brittle oxide film at the tip of the crack will be partly disrupted. An emerging of dislocations into the crack will then be relatively easy. During a decrease of the stress the situation is less favourable in view of the crack sharpening and the oxide layer being in a state of compression. One might think that the number of dislocations entering into the crack during the rising part of the cycle will be larger than during the falling part. Although this is likely to be true it must be said that the amount of slip in the crack tip region will be equal for both half cycles. If the latter were not true one should observe a shifting of one edge of the crack relative to the opposite edge. However, microscopic observations, for instance at grain boundaries, do not indicate such shifts.

Considering dislocations moving towards the crack tip it may be expected that some dislocation climb induced by vacancies and also some cross slip will occur. The cyclic slip in the crack tip region will produce vacancies and interstitials, but the number of vacancies will prevail since they are more easily generated (see ref. 34). Since in the rising and falling part of a load cycle dislocations of different signs will move towards the crack the vacancy induced dislocation climb in both half cycles will occur in opposite directions. This is schematically illustrated in fig. 31 which also shows the effect of crack blunting and sharpening of the oxide film. The dislocation climb provides the systematic deviation of reversible dislocation flow required for the mechanism shown in fig. 30. It would even be possible that the dislocations acting in both half cycles were emitted by the same source.

The above mechanism can also be described in other terms. Dislocation climb can be envisaged as a precipitation of vacancies on the dislocation. If the dislocations then enter the crack as indicated in fig. 30 the crack extension is in fact due to vacancies being transported to the crack by the dislocations.

Fig. 30 is based on the movement of edge dislocations. For screw dislocations cross slip in aluminium and its alloys easily occurs. If cross slip occurs in the two half cycles in different directions a similar picture as fig. 31 could be obtained for screw dislocations. Also in this case it might be associated with dislocations of the same source. From an energy point of view it is thought that the formation of intrusions (crack growth) will prevail since it involves a strain energy release whereas the formation of extrusions does not. Hence the strain energy release can provide the driving force for systematic cross slip required for crack growth. It should then be expected that the "tensile stress

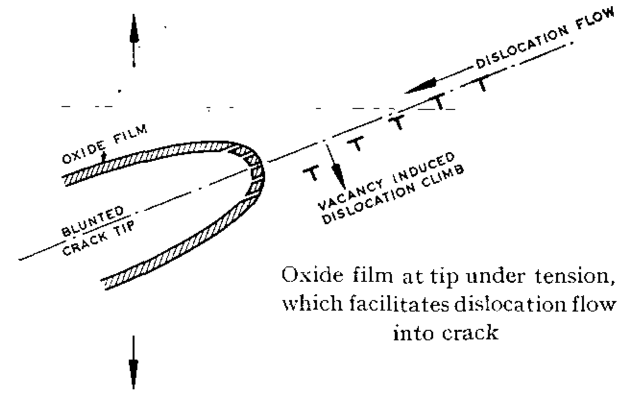

a. Rising part of the load cycle.

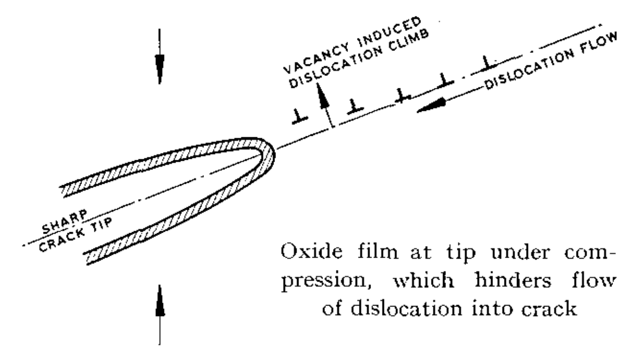

b. Falling part of the load cycle. Similar pictures apply to screw dislocations. Dislocation climb is then replaced by cross slip, promoted by strain energy release involved in crack extension.

Fig. 31 Further evaluation of the crack growth mechanism presented in fig. 30.

over the crack'' will be a controlling factor for the crack growth. This aspect is further discussed in chapter 11.

Until now dislocation flow into the tip of the crack was considered. One might wonder whether a crack tip can act as a dislocation source itself and what the consequences would be under a cyclic load.

If the crack front is wavy as indicated in fig. 32, the shear stress concentration at A will be significantly larger than the average concentration along the crack front. Since the augmentation of the stress at A is a very localized phenomenon, a leveling-off is not likely. It is now assumed that a dislocation will be generated at A which can start as a dislocation of a very short length. Its length will increase when the dislocation moves away from the crack. At the very beginning of the generation, only a small number of atomic bonds have to be disrupted. This will be facilitated by thermal vibrations of the atoms. The required shear stress will be much lower than the theoretical value for the perfect lattice. The emission of a dislocation at A will not affect the shape of the crack front at A and it then should be expected that an avalanche of dislocations will be generated.

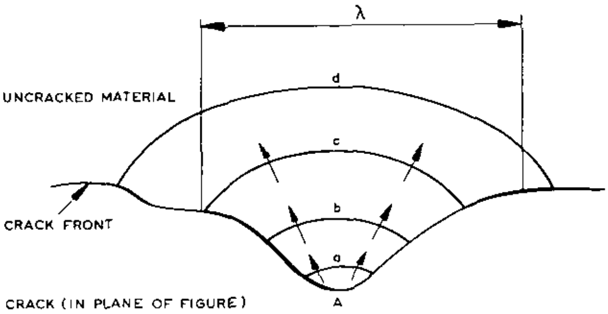

A dislocation generated in region A is shown in successive positions a, b, c and d. The generation leaves the shape of the crack front unaltered and avalanches of dislocations will be emitted.

Fig. 32 Crack extension by dislocation generation at a wavy crack front.

One might ask whether an irregularly shaped crack front, such as sketched in fig. 32 could occur. Mc Evily and Boettner (ref. 35) studying alloys with various stacking fault energies γ, found a straight crack front for a low and a curved crack front for a high value of γ. Also Crussard et al. (ref. 36) observed that the crack front is non-crystallographic. However, it may be asked whether fractographical studies give information on a relevant scale, i.e. whether the dimension λ in fig. 32 can be observed under the microscope. Since λ is a dimension of a hypothetical model this question remains unanswered here. Considering the multitude of slip systems and the many ways to affect dislocation movements it is intuitively stated that a wavy crack front will be the rule rather than an exception. At the same time it is realized that dislocation generation at the crack tip may be much more complicated than indicated in fig. 32.

Another aspect of the model in fig. 32 is the reversibility. Dislocations emitted by the crack front may return to the crack front on reversal of the load. However, if a part of them has been locked or annihilated, the mechanism is non-reversible. Moreover, those dislocations which do return will not enter the crack on exactly the same slip plane as explained before. So the returning of dislocations may still imply some crack extension. Secondly the irreversibility may be due to an emission of dislocations of the opposite sign at A on reversal of the load, which then could annihilate fully or partly the dislocations emitted in the first half cycle. This could still imply crack extension.

The emission requires a disruption of the oxide

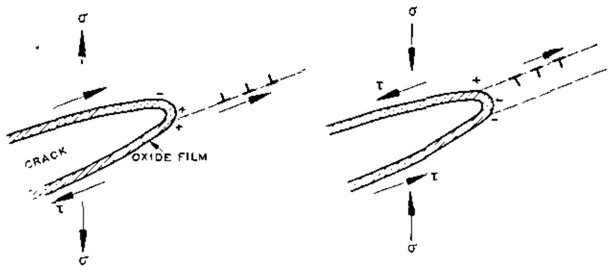

a Increase of stress b Decrease of stress.

+ oxide film under tension
— oxide film under compression.

Fig. 33 Dislocation emission by the tip of the crack on different slip planes during the rising and falling part of a load cycle.

film. This will occur at a location at which the film is under tension. A qualitative indication of the tension in the film is given in fig. 33*. Assuming that the dislocation emission occurs on the plane(s) associated with the disruption of the oxide film, the emission will occur on different slip planes in the two half cycles, see fig. 33. Consequently crack extension will occur in a way similar to that shown in fig. 30.

Dislocation emission by the crack has some resemblance to a static shear failure. This is further discussed in chapter 9.

The foregoing considerations were concerned with a single slip system being active. It will be pointed out in the following chapter that slip on two different families of crystal planes is likely to to occur. This still allows crack growth in a similar way as indicated in fig. 30, which is illustrated in fig. 34. The example in this figure implies the formation of two intrusions by two different slip systems. The sum of both intrusions is the crack extension. Here also there is a possibility of forming extrusions into the crack instead of intrusions into the material. For persistent crack growth it is again required that the occurrence of intrusions dominates the occurrence of extrusions.

There are some essential differences with crack extension by one slip system. An important feature of fig. 34 is, that it shows that crack extension by two different slip systems allows without any difficulty, crack growth in an arbitrary non-

* The indications of tension and compression in the oxide film in fig. 33 could be made intuitively. They find some substantiation in eqs (B33) and (B34) of Appendix B (σ_r for $\theta = \pm \pi$ and σ_θ for $\theta = 0$).

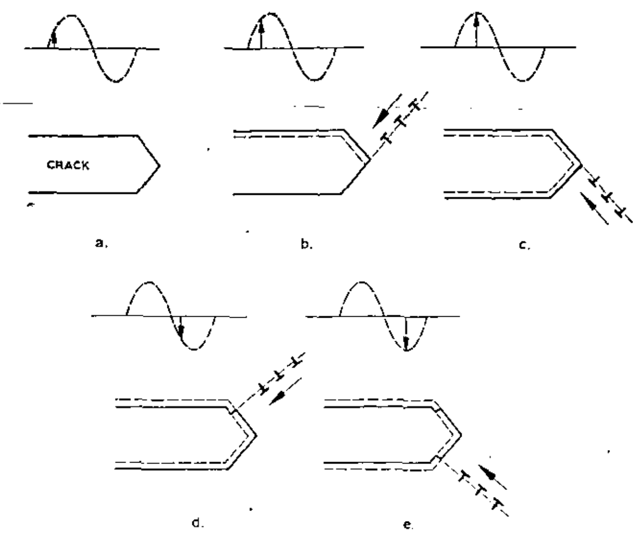

Fig. 34 Crack extension in one load cycle by dislocation movements on two different sets of crystallographic planes.

crystallographic direction*. Another phenomenon which can easily be explained is branching of fatigue cracks, such as shown in figs 25 and 26. The simultaneous occurrence of two differently orientated intrusions emanating from the tip region is possible due to the activity of two slip systems. If both intrusions grow separately by trapping dislocations, branching has occurred. If both cracks trap comparable numbers of dislocations they may be competing for some time before one of them becomes dominating.

The discussion in this chapter, although concerned with crack growth, is partly applicable to crack nucleation. Additional aspects were the dislocation generation by the crack front itself and the strain energy release, stimulating the formation of intrusions rather than extrusions. Accepting for the moment the concept that nucleation and growth are a geometric consequence of dislocation movements, it is clear that the discussion presented so far, which has yielded some more or less plausible mechanism, can neither give an accurate nor a complete picture. Other mechanisms based on the same concept are possible. In the following chapter the above model for crack growth will be compared with experimental evidence. Alternative theories for crack extension will be discussed in subsequent chapters.

* In ref. 35 (fig. 17a) a crack growth model was suggested requiring slip on different slip systems in the two half cycles. The mechanism involved a relative edge displacement in each cycle equal to the crack extension. This is not compatible with microscopic evidence, showing that no displacement occurs.

7 Crack nucleation and propagation along crystal planes

As a consequence of the model for the nucleation and the growth of fatigue cracks discussed in the two previous chapters, crack propagation will occur along a single crystal plane if dislocation movements are largely confined to that family of parallel planes. If slip occurs on two or more crystal planes the orientation of the crack does not necessarily have to be a crystallographic orientation. In this chapter microscopic evidence on this topic is analysed. For this purpose calculations were made on the ratio of resolved shear stresses on different slip planes and on the stress distribution around cracks. The calculations are described in Appendices A and B.

For the probability of slip on one, or more than one slip plane, the following aspects are important:
(1) The shear stress distribution.
(2) The resolved shear stress on the various slip systems.
(3) The restraint on slip for the various slip systems and the strain hardening.

In aluminium and aluminium alloy specimens without cracks, the shear stress distribution may be assumed to be homogeneous. Slip predominantly occurs on the $\{111\}$ planes in the $\langle 110\rangle$ directions. In each of the four slip planes there are three slip directions involving 12 slip systems. The problem to be considered is not whether slip occurs on one or more than one slip system, but whether slip occurs on one or more than one crystal plane. For a given orientation $[hkl]$ of a uni-axial load with respect to the crystal structure, the resolved shear stress for all slip systems can be calculated. If the highest resolved shear stress on one of the four slip planes is $\tau_{\max,1}$ and the highest resolved shear stress on one of the other slip planes is $\tau_{\max,2}$ the ratio

$$r = \frac{\tau_{\max,2}}{\tau_{\max,1}} \ (\leqslant 1) \qquad (7.1)$$

might give an indication of the probability of the occurrence of slip on more than one slip plane. The probability will be high if r differs little from unity and will be low if r is much smaller than unity. In Appendix A the calculation of r is explained. The results are presented in fig. A4 as curves of constant values of r in the standard triangle. The projection method of orientations is not the usual stereographic projection, but a more simple projection on the cube plane (100), see fig. A2. This method allows an easier calculation of fig. A4.

From fig. A4 it follows that the ratio of the maximum resolved shear stresses on two different slip planes varies from 0.5 to 1.0. High values will be encountered more frequently than low values. On the average the r-value will be 0.83 (space-angle average). In other words the occurrence of slip on more than one slip plane seems to be a very realistic possibility.

The third aspect listed above is a complicating factor. Crack nucleation occurs at the surface of the material. Slip in the direction of the surface will meet with less restraint and strain hardening than slip movements parallel to the surface. Although the ratio r may have some meaning for the initiation of slip, continued slip may be largely controlled by the restraint. In this respect it is noteworthy that the aluminium cladding of the unnotched specimens discussed in section 4.4, showing abundant crack nuclei, revealed slip mainly in a single direction in each grain, despite the relatively high strain amplitude and crack rate.

The difference of the restraint on slip at the surface and at the interior of the material can also account for the difference of the modes of crack propagation, as discussed in section 4.5. Whereas the difference between fig. 20 (crack propagation in the cladding at the surface) and fig. 21 (crackpropagation in the core just below the cladding) might still be attributed to the differences of the material (pure aluminium vs. the aluminium alloy) similar differences were also found for the bare material, compare figs 22 and 23 with figs 24, 25 and 26. Again it is confirmed, that the much lower restraint on slip at the free surface promotes crack propagation along crystal planes. That the propagation changes from one plane to another several times in the same grain will be discussed hereafter. First it may be observed that a propagation which is apparently uncorrelated to crystal planes, does not exclude that such a correlation is present on a much finer scale, beyond the resolving power of the microscope.

After a crack has been nucleated and has become larger than a single grain, the front of the crack is moving through a number of grains at the same time. If the propagation in each of these grains had to occur on a single slip plane, this would not be compatible with the coherence of the fracture surface at the grain boundaries. The crack growth occurring simultaneously in adjacent grains will therefore be subjected to a restraint on the path of the crack, mutually exerted by one grain on the other one. This mutual influence is obviously smaller at the surface of the specimen, but it is not absent. It is thought that it is responsible for the changes of orientation of the crack path at the surface such as shown in fig. 22. In other words the path of the crack at the surface is to some extent dictated by the path of the crack in the grains just below the surface.

The path of the crack could also be affected by inhomogeneities of the material such as inclusions, etc. They will promote an irregular course of the crack. Their influence is not further considered here.

As an explanation for the fairly irregular path of the crack at the interior of the material two arguments were already mentioned, viz. (1) the restraint on slip which might provoke slip on more than one crystal plane and (2) the coherence of the fracture surface from grain to grain, by which the crack is not free to follow a single crystal plane in each grain. In addition to these arguments attention will now be paid to the effect of the stress distribution.

For a crack in an infinite sheet, a solution for the stress distribution is available from the theory of elasticity. There are some restrictions on the validity of the solution. (1) At the tip of the crack, plastic deformation will occur (which removes the stress singularity). (2) The assumed elastic isotropy only applies approximately. (3) Cracks do not have a zero tip radius. (4) Specimens have a finite size, and notches are an additional geometric complication. In applying the results of the stress calculations one should keep the restrictions in mind. They need not be serious objections since qualitative information is looked for.

Dislocation movements are controlled by shear stress and therefore most calculations relate to this stress. A summary of the equations used, together with a brief discussion is presented in Appendix B. Calculations of the shear stresses τ_2, τ_3, τ'_2 and τ'_3, defined below, were made for the cases of plane stress and plane strain. The principal stresses in the plane of the sheet specimen are denoted by S_1 and S_2. The third principal stress S_3, being perpendicular to the sheet, is equal to zero for plane stress and equal to $\nu(S_1 + S_2)$ for plane strain, where ν is Poisson's ratio. The definitions of τ_2 and τ_3 are:

$$\tau_2 = \frac{|S_1 - S_2|}{2}$$

$$\tau_3 = \text{the larger value of } \frac{|S_1 - S_3|}{2} \text{ and } \frac{|S_2 - S_3|}{2}$$

If S_1 and S_2 have opposite signs the maximum shear stress is τ_2, which is acting on a plane perpendicular to the sheet. If S_1 and S_2 have the same sign τ_3 is the maximum shear stress and τ_3 is acting on a plane which makes an oblique angle with the sheet. In view of the model for crack extension discussed in the previous chapter, it was thought desirable to calculate shear stresses on planes which pass through the tip(s) of the crack. If such planes are perpendicular to the sheet, the shear stress is indicated by τ'_2. For planes passing through the tip of the crack and making an oblique angle α with the sheet, the shear stress is indicated by τ_α, and τ'_3 is the maximum value of τ_α if α varies from 0 to 90°.

Calculations were made for the stress in the tip region of the crack. Although they are valid for a crack in an infinite sheet they will qualitatively apply to cracks in specimens of finite dimensions, see Appendix B. The stress distributions are presented as curves along which the shear stresses, defined above, are constant. The curves are presented for a single value of the shear stress. Along radial lines emanating from the tip of the crack, the stress is inversely proportional to the square root of the distance to the tip.

The shear stress distribution around the tip of a crack perpendicular to the tensile loading, is shown in fig. B5. For plane stress, τ_3 is highly dominating τ_2, whereas for plane strain the reverse is true. As long as the size of the plastic zone is small as compared to the sheet thickness, the state of stress around the tip of the crack will rapidly change from plane stress at the surface to (approximately) plane strain at the interior of the sheet. According to a suggestion of Liu (ref. 37) plane stress will approximately apply to the full thickness of the sheet, if the size of the plastic zone, p, has increased to half the sheet thickness, t. Equations for the size of the plastic zone were derived in section B5 of Appendix B, see eqs (B31) and (B32). Substitution of $p = \frac{1}{2}t$ in eq. (B32) gives:

$$\frac{l}{t} = 1.7\left(\frac{S_0}{S}\right)^2$$

where l = crack length, S_0 = yield strength of the material and S should be interpreted as the nominal stress amplitude. Since S_0/S will be considerably larger than unity, l will be a multiple of t before plane stress applies through the full thickness of the specimen. For cracks of the order of the sheet thickness or smaller, the major part of the crack front will be in a state of approximately plane strain.

Fig. B8 shows the distribution of the shear stress on planes through the tip of the crack. A comparison with fig. B5 shows large differences. It is also found here that τ'_3 dominates τ'_2 for plane stress and the reverse is true for plane strain. In the latter case the maximum shear stress (τ'_2) is found on planes perpendicular to the sheet, which are not in line with the crack, but at an angle $\theta \approx$ ● 70° with the plane of the crack. This θ-value will probably be affected by plastic deformation, but it is not expected that it goes down to zero. Hence it may be assumed, that the τ'_2 distribution will promote dislocation flow to the tip of the crack from a positive and a negative θ-direction. As explained in chapter 6, this would imply a growth of the crack which under the microscope would seem to occur in no relation to the crystal planes. Whereas the four available slip planes will set certain limitations, it may be expected that on the average (i.e. on a macroscopic scale) a crack surface, perpendicular to the loading direction, will be the result. In other words the 90°-mode of fracture mentioned in section 4.2 is associated with a state of plane strain.

At the surface of the specimen (plane stress) τ'_3 (dominating τ'_2) shows a flat maximum around $\theta = 0°$ with α-values of 45° or slightly larger. Also in this case one should expect a propagation in the direction $\theta = 0°$ but now on a plane making an angle of approximately 45° with the loading direction. (Theoretically an alternation between $\alpha = +45°$ and $\alpha = -45°$ might still give a fracture surface macroscopically perpendicular to the loading direction. However, such an alternation is not likely to occur in view of the coherence of the fracture surface.) Consequently the 45°-mode of fracture should be associated with plane stress. The transition from the 90°-mode to the 45°-mode, illustrated in figs 5 and 6 and described in section 4.2, seems to confirm the above reasoning. Unpublished results on the influence of the sheet thickness on the crack propagation (ref. 38) show that the transition is completed at a larger value of the crack length in the thicker sheet material, thus confirming the above reasoning.

The above explanation for the transition from the 90°-mode to the 45°-mode emphasizes the importance of the shear stress on planes through the tip of the crack, which is an argument in favour of the model for crack extension, presented in the previous chapter. It should also be concluded, that the explanation of the transition from the 90°-mode to the 45°-mode on the basis of the difference between the states of stress, implies that the fracture mechanism is not necessarily different for the two modes of the fatigue fracture. This is further discussed in chapter 9.

Forsyth (ref. 39) has divided the fatigue process in a stage I and a stage II. In the former, cracks are produced along crystallographic planes which, according to Forsyth, are associated with single slip. Amongst other factors it should be promoted by low stress amplitudes. For the second stage he assumes, that crack extension occurs partly by cleavage and does not occur on the primary slip plane. In the second stage Forsyth observes a tendency for the crack to grow perpendicularly to the loading direction even on a microscale.

Girard (ref. 9) testing Al-4% Cu specimens ($S_m = 0$) at low stress amplitudes ($N \approx 10^6$ to 10^9 cycles) found clear evidence of cracking along {111} planes. Changes from one slip plane to another within the same grain frequently occurred. He reports values of the crack rate in the order of 1 to 3 Å cycle, which is low indeed and which seems to confirm Forsyth's stage I concept. It should be noted that Girard made his observations on the surface of the specimens without sectioning. His results are in good agreement with those reported in section 4.5, for much higher crack rates.

In a recent study on an aluminium alloy with 7.5% Zn and 2.5% Mg, Forsyth and Stubbington (refs 40 and 41) made observations similar to those found in the present study on the 2024-T3 alloy. Specimens loaded in reversed plane bending, showed crack growth along slip planes at the surface of the specimen and apparently non-crystallographic crack growth at the interior of the specimen, which is again referred to as stage I and stage II crack growth. The crack growth at the surface is assumed to occur in the same way as the crack nucleation. The two stages are not identical to the 45°- and the 90°-mode of fracturing defined in section 4.2, since these modes are concerned with macroscopic features of the fractures surface.

Similar observations were made by McEvily and Boettner (ref. 35), who tested pure aluminium monocrystal specimens. At the surface, crack growth occurred along {111} planes, but about 10μ below the surface the fracture surface became irregular and non-crystallographic. They concluded that stage I and stage II occurred simultaneously along the crack front, stage I occurring at the specimen's surface. This is in agreement with the observations of the present study on the 2024-T3 material (section 4.5).

An attempt will be made now to explain the results on the aluminium sheet specimens described in section 4.3. It was observed there, that in general the fracture surfaces did not coincide with a {111} plane. This observation, however, was concerned with the macroscopic fracture surface over the full thickness of the specimen. A correlation with slip planes at the surface was indicated in some cases, see for example figs 9 and 10. So far the results are in agreement with the evidence summarized above. It is remarkable, however, that the low stress amplitudes promoted macroscopically flat surface fractures in these aluminium specimens. This would require a reasonably constant balance between the slip activities on different slip systems. Another feature was the persistently oblique crack growth in the left hand grain of specimen B (fig. 7). A similar result was obtained by McEvily and Boettner (ref. 35) in several monocrystal specimens of pure aluminium, their conditions being somewhat different. In their test the mean stress was zero and they found the fracture surface to be a {111} plane. The crack rates were of the same order of magnitude as found for specimen B of the present study. However, in specimen B the fracture surface of the oblique crack was not flat and consequently could not be a crystal plane. McEvily and Boettner explained the oblique growth as a consequence of the resolved shear stress being a maximum on that {111} plane. It is thought that in addition to this, the effect of the oblique crack orientation on the stress distribution could play a part. As explained in section B6 of Appendix B the oblique orientation ($\beta \neq 90°$) hardly affects the distribution of τ_2, τ_3 and σ_θ (tensile stress perpendicular to radial lines emanating from the tip of the crack), see figs B1, B2 and B7, but a pronounced effect occurs on the distribution of τ'_2, see fig. B6. For the specimens of McEvily and Boettner it may be assumed that the major part of the crack front was in a state of plane strain and then τ'_2 is highly dominating τ'_3 (see Appendix B). Consequently the oblique crack gives a τ'_2 distribution, stimulating crack growth in that oblique direction. The results of McEvily and Boettner may then be seen as an additional indication of the importance of the shear stress on planes through the tip of the crack.

It is doubtful whether the oblique crack found in the present study (fig. 7), allows the same explanation, since in view of the low thickness of the specimen it is not sure whether plane strain still applied. Based on eq. (B32) the size of the plastic zone is estimated at 0.1 to 0.2 mm, the sheet thickness being 0.4 mm. If the state of plane stress was already present in the full thickness, τ'_3 was dominating τ'_2 and since τ'_3 has a maximum at a θ-value approximately perpendicular to the direction of loading, the persistently oblique crack orientation is difficult to explain, the more so since the plane of the fracture was not a crystal plane.

It has to be admitted that a fully satisfactory explanation of the present results of the aluminium specimens (section 4.3) has not been reached. The results of the aluminium cladding (sections 4.4 and 4.5) were much better in accordance with the ideas developed in chapters 5 and 6. The cladding is backed up by a low ductility aluminium alloy core which, when cracks in the cladding are present, largely prevents crack opening. In the pure aluminium specimens this restraining effect is absent, and it may be that creep in the annealed material occurred, thus complicating the phenomenon.

A clear example of crack growth along crystal planes was recently found under alternating compressive stresses in a specimen of the 7075-T6 alloy (ref. 42). In a comparative study on several types of lugs, one series of lugs were provided with an undersized hole. By drawing a tapered pin through the hole, its diameter was expanded 3% to obtain the correct diameter. This operation introduced extremely high residual stresses around the hole, which were compressive and which proved to have a highly favourable effect on the fatigue properties. The compressive residual stresses had a biaxial character to which the fatigue loading of the specimen added an alternating tension. A specimen which endured 20 million cycles showed considerable fretting corrosion in the hole. It was subsequently sectioned, which revealed that cracks had emanated from pits formed by the fretting action. Fig. 35 shows an example of these cracks. The correlation with crystallographic planes is obvious. The cracks were growing from grain to grain in a more or less random fashion. The crack rate is unknown but its magnitude can be estimated. If the crack propagation had covered 25% to 100% of the fatigue life the average crack rate was 4 to 1 Å/c, which is fairly low indeed. Probably the resulting alternating stress was largely in the compressive range. In Appendix B it was shown that the stress distribution for a crack loaded in compression was similar to that for a crack subjected to pure shear. For the latter case the distributions of τ_2 and τ_3 are given in fig. B9 and the distributions of τ'_2 and τ'_3 in fig. B10. The upper and lower parts of fig. B10 apply to plane stress and plane strain respectively, the distributions being symmetric with respect to the plane of the crack ($\theta = 0$). Again the restriction to planes through the tip of the crack considerably modifies the shear stress distribution. It may well be assumed that the cracks in fig. 35 were practically in a state of plane strain and then fig. B10 shows that τ'_2 is again highly dominating τ'_3. The distribution of τ'_2 shows a pronounced maximum in line with the crack as could be expected intuitively. Two secondary maxima occur at $\theta = \pm 125°$. One might be tempted to explain the growth along crystal planes by the former maximum, and the zig-zag character by the latter maxima. It is agreed that this involves some speculation. It is still interesting to see that extensive crack growth along crystal planes is possible at the interior of a specimen, whereas this did not occur in the sheet specimens loaded in tension, as described in section 4.5. In those specimens it did occur at the surface and was promoted by the lack of restraint. In the specimen of fig. 35 one might say that it occurred, since the biaxial compressive stresses prevented crack opening, and sliding along the crack is the only way to cause growth of the crack. The latter is conceivable if occurring on a slip plane. From this point of view the result of fig. 35 would afford some further substantiation to the crack growth conception proposed in chapter 6.

←→ direction of loading

Material: 7075-T6 Lug specimen with expanded hole (3%). $K_t = 3.5$, $S_m \pm S_a = 12.5 \pm 8$ kg/mm² (nominal stress). Specimen sectioned after 20 million cycles (168 ×).

Fig. 35 Fatigue cracks grown in an aluminium alloy lug specimen with high compressive residual stress (ref. 42).

The discussion in this chapter will now be summarized. Crack nucleation and propagation at the surface occurs predominantly along crystal planes, which is made possible by the lack of restraint on slip. At the interior of the material there is an increased restraint on slip and the coherence of the fracture surface implies another type of restraint. Moreover, at the interior there will approximately be a state of plane strain, provided that the stress amplitudes and the crack length are not too high and this will promote slip activities on more than one slip plane. As a consequence, the crack at the interior of the material follows an irregular path which may be apparently uncorrelated to the crystal planes. Under a compressive fatigue load, crack propagation along slip planes may be the only possible way of crack growth, also at the interior of the material.

The macroscopic fracture features defined as the 90°-mode and the 45°-mode are associated with a state of plane strain and a state of plane stress respectively, as indicated by the calculation of the distributions of the shear stress on slip planes through the tip of the crack. The two modes do not necessarily imply a different fracture mechanism.

8 The problem whether crack growth occurs in every cycle

In chapter 6 crack growth was suggested to be a geometrical consequence of dislocation movements at the tip of the crack. It is expected that the dislocation activity in the tip region is a fairly continuous process, i.e. such activity will occur in each cycle. It is not necessary that these dislocation movements will imply crack extension in each cycle, but on the basis of the model one should expect that crack extension is also a fairly continuous process occurring in the majority of cycles, if not in all. This problem is discussed in the present chapter. Fractographic studies give some information on this topic and will be reviewed first.

In the last ten years crack propagation in aluminium alloys received considerable interest in view of the problem of assessing the "fail-safe" characteristics of aircraft structures. In general such studies are concerned with large sheet specimens and cracks visible to the naked eye, rather than microcracks. Fig. 36 shows results of an NLR study (refs 7 and 8) on 2024 Alclad sheet specimens. The crack rate dl/dn was plotted as a function of the crack length for three values of the stress amplitude. Fractographic examination revealed growth lines, especially in the cladding, see fig. 37. Although there is some variation in the spacing, the pattern allows average spacings to be determined with the aid of the microscope. Results of such measurements were plotted in fig. 38. The correlation between the spacing and the crack extension per cycle is obvious. On the average the spacing is somewhat larger than the crack extension per cycle, but not yet twice as large. This suggests that the growth lines are successive positions of the crack front and that there was crack extension in more than 50% of the cycles. It should be pointed out that measurements of the spacings were made in those area's, where they could be observed most clearly. This might well have introduced a bias towards measuring somewhat larger spacings. The scatter in fig. 38 reflects the local variations in crack speed which probably will be due to local changes of the material properties. The conclusion drawn here is; that crack extension did occur in almost every cycle and probably in all cycles.

Growth lines in the core of the aluminium alloy sheet specimens were more difficult to observe than in the cladding. This experience was also reported by Forsyth, Ryder et. al. (ref. 43). It is thought that crack extension in almost every cycle as revealed by the cladding, will imply the same for the core, even if the growth lines cannot be observed there.

In the literature similar studies led to the same conclusion, i.e. the spacing between growth lines corresponds to the crack extension in one cycle (refs 44, 36 and 45). Strong evidence was offered by Ryder (ref. 46), by Laird and Smith (ref. 33) and

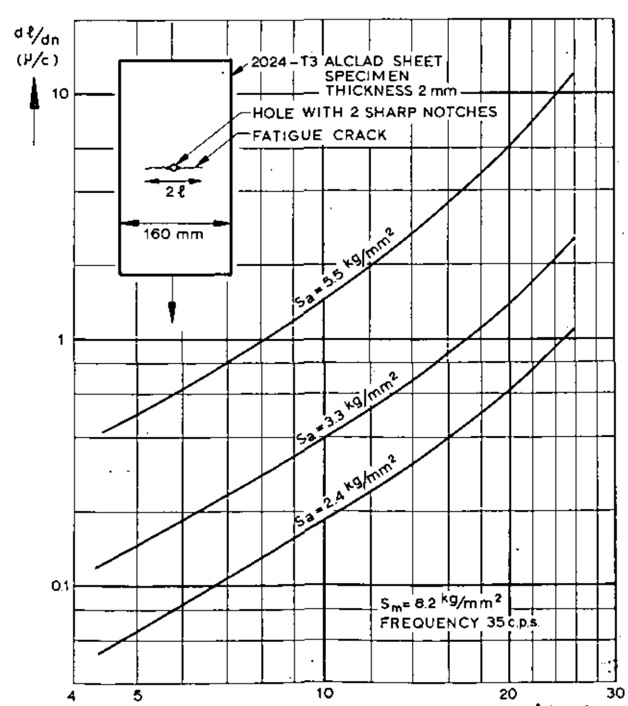

Fig. 36 Crack rate as a function of crack length in an Al-alloy sheet specimen. Results from (ref. 8).

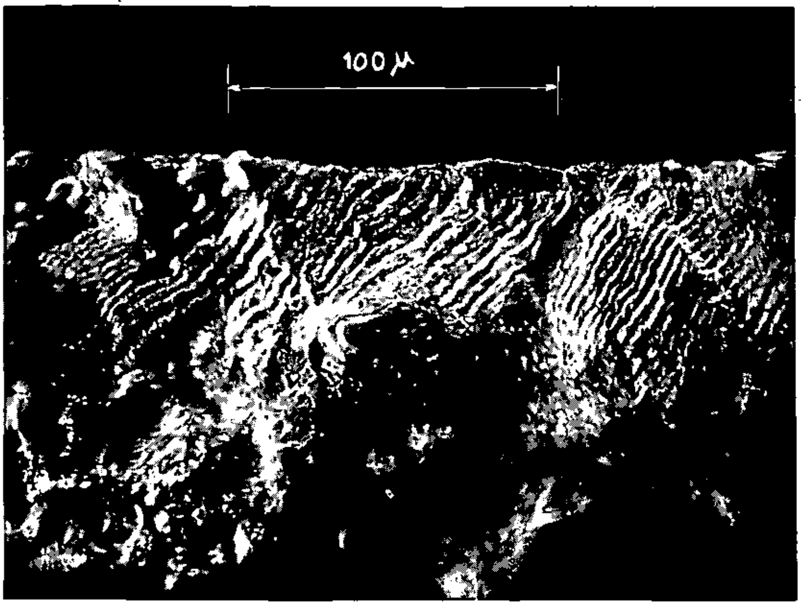

←

Direction of crack propagation. Nominal thickness of the cladding is 100 μ. Magnification (450 $\times$).

Fig. 37 Growth lines in the cladding layer of an 2024-Alclad sheet specimen (ref. 7).

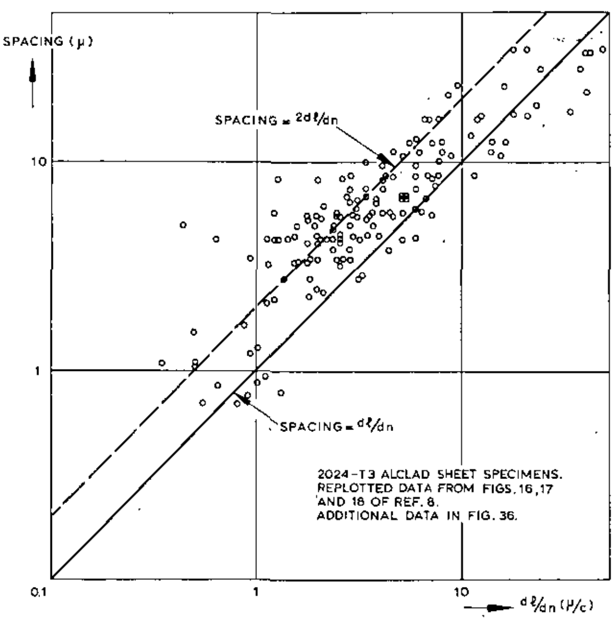

Fig. 38 The spacing between growthlines as a function of the crack rate. Test data from (ref. 8).

by Matting and Jacoby (ref. 47). They performed tests on aluminium and aluminium alloy specimens with a constant amplitude, inserting periodically a single more severe load cycle. On the fracture surface the growth lines of the high load cycles could be identified and the number of growth lines between them (18, 9 and 10 respectively) did correspond exactly to the number of low load cycles applied between two high load cycles. This proved *the 1 : 1 correspondence between the number of* growth lines and the number of load cycles.

A summary of the width of spacings as found in several publications, including the results of some other materials, is given in table 4. Several investigations were made with the optical microscope. The smallest spacing to be observed in this way, will be in the order of 0.5 μ. In other investigations an electron microscope was employed. The smallest spacing was reported by Christensen (ref. 48), viz. 0.02 μ = 200 Å.

Before discussing the meaning of the measurements of the spacings of growth lines to some further extent, it is useful to consider the following question: What are the orders of magnitude of the crack rate which are of interest for the present study? Micro-cracks start early in the fatigue life, but it takes a considerable number of cycles before they become visible by the naked eye. For a simple specimen or a small component the major part of the fatigue life is covered by this invisible cracking. Once the crack obtains a technically visible size, the crack rate is so high that only a small portion of the fatigue life remains until final rupture occurs. This means that the crack growth study on the 2024-T3 sheet specimens, unnotched and notched by a central hole (K_t = 2.66), as reported in section 4.1 is relevant to the above question. The orders of magnitude of the crack rate obtained there were collected in table 1.

From a comparison of the results of table 4 for growth-line spacings and table 1 for crack magnitudes, the following conclusions can be drawn. In the first part of a fatigue test on an unnotched or a notched specimen the crack rate has a value much lower than the smallest spacings observed. Still in this part of the fatigue life the most characteristic beginning of the fatigue fracture is formed. Towards the end of a fatigue test the crack rate at-

TABLE 4

Survey of spacings between growth lines reported in the literature as results of fractographical studies.

Investigator (Reference)	Material[1])	Spacing, order of magnitude	
		(μ)[2])	Burgers vectors[3])
Zappfe and Worden (49)	Al-alloy	0.5	2000
	Mild steel	0.6	2500
Forsyth (44)	Al-alloy	0.3–3	1000–10000
Ryder (46)	Al-alloy	0.5	1750
Forsyth, Ryder, Smale and Wilson (43, 50)	Al-alloy and Al-cladding	0.2–40	700–140000
Crussard, Plateau et al. (36, 51)	Al-alloy	0.2	700
	Mild steel	0.2	800
	18–8 stainless steel	0.2	800
	Steel	0.05	200
Schijve and Jacobs (52)	Ni-alloy	1–2[4])	4000–8000
Schijve, Broek and De Rijk (8)	Al-alloy	0.7–1.2	2500–4000
	Al-cladding	1.2–40	4000–140000
Tokuda (53)	Steel	0.02–0.16	80–600
Christensen (45, 48)	Al-alloy	0.4–2.5	1400–9000
	Al-alloy	0.02–1.2[5])	70–4000
Bockrath and Christensen (54)	Ni-alloy	0.2	800
Laird and Smith (33)	Al	10–100	35000–350000
	Ni	1	4000
Matting and Jacoby (47, 55)	Al-alloy	0.4–4	1400–14000
	Mild steel	0.5	2000
McGrath, Buchanan and Thurston (56)	Al-alloy	5	20000
	Cu	2–5	8000–20000

[1]) Al-alloys in this column were high strength precipitation hardened Al-alloys of the Al Cu Mg type of the Al Zn Mg type, except for Jacoby and Matting, which studied a medium strength Al Mg alloy.

[2]) Values in this column are measured from micrographs in the referenced publications. If only one value is indicated, this is a minimum value.

[3]) The Burgers vector was assumed to be equal to the closest interatomic distance. This is not correct for all materials but a better procedure would not affect the order of magnitude of the spacings. Values are derived from those in the previous column and are rounded.

[4]) Measured on fracture surface of a turbine blade failed in service.

[5]) Values from the graph in figure 26 of Christensen (ref. 48).

tains values corresponding to the order of magnitude of the spacings given in table 4. So the available evidence on growth lines gives no direct answer to the question, whether there is crack extension in the majority of cycles of a normal fatigue test.

An appreciable part of the data compiled in table 4 was obtained with large sheet specimens and propagation of cracks with a length which cannot be considered as small. Some of the studies, however, were made on small specimens without mentioning the crack size for the micrographs and one may expect from the magnitude of the spacings, that the values of the crack length probably were relatively large, i.e. the major part of the fatigue life had elapsed at the values concerned. The lack of data on fractographical studies with large magnifications for small crack sizes may have several reasons, viz. (1) There will be experimental difficulties in locating the crack nucleus in an electron-microscope replica. (2) Magnifications may be too small to show growth lines with a small spacing. (3) Crack extension may occur in each cycle without forming a growth line. (4) Finally crack extension may be a discontinuous process in the micro-stage with large number of cycles without crack extension. Some thought will now be given to these arguments except for the first argument which has no physical relevance to the problem considered.

The smallest spacings mentioned in table 4 are in the order of 0.02 μ to 0.2 μ or 200 Å to 2000 Å.

Although details smaller than 200 Å may be observed under the electron-microscope, one should not overlook that not the spacings have to be observed, but the growth lines with a width smaller than the spacings and probably considerably smaller, depending on the material. No limit for the possibility of observation will be estimated here, but is may be said that a crack, propagating at a speed lower than 10 Å/c, will not allow a detection of growth lines, supposing that they are formed at all. Values below 10 Å/c apply to a fatigue test at low stress amplitudes (see table 1).

The electron microscope will only allow the detection of growth lines if they are a physical reality, i.e. if they are ridges or grooves. This raises the question how the growth lines are formed. According to Forsyth et al. (ref. 43) the lines are ridges, formed by plastic deformations and the zone between two spacings should have been a brittle crack extension. The width of the lines is supposed to be larger for a more ductile material and at the same time the brittle zone should be smaller. The plastic deformation implies blunting of the crack which stops the growth. Laird and Smith (ref. 33), testing aluminium and nickel, consider the lines to be grooves instead of ridges. They agree with Forsyth et al. on the blunting of the crack and they show convincing evidence of this by sectioning cracked specimens. On reversal of the load the crack is closed, also by plastic deformation, but at the crack tip this does not completely occur, leaving there a pipe-line hole. In the next cycle crack growth starts from this hole which then leaves a groove on one or on both surfaces of the crack as revealed by microscopic evidence. Laird and Smith noticed that the difference with Forsyth's observations may be due to the type of material and moreover to the high stress amplitudes used. Investigations of Forsyth et al. were made on aluminium alloys. McGrath et al. (ref. 56) found both grooves and ridges on pure copper and suggest that they might form interlocking fracture surfaces. Matting and Jacoby (ref. 55) studying an Al Mg alloy suggest that crack extension starts on one slip plane and is completed on another slip plane, thus forming growth markings. So microscopic studies give a variety of answers. Further microscopic studies on this topic are certainly worthwhile. It is expected that the topography of the growth line will depend on the type of material, especially on the ductility of the material, and probably also on the type of stressing, i.e. on the magnitude of the stress amplitude as well as the mean stress.

In fig. 37 the cladding shows visible growth lines for which it was established that the spacing did correspond to the crack growth per cycle. Although most times growth lines could not be detected in the aluminium alloy core adjacent to the aluminium cladding, it still has to be presumed that crack growth in each cycle also occurred there. Apparently crack extension in each cycle in this aluminium alloy does not necessarily involve visible growth lines. The fracture surfaces of the 2024-T3 alloy shown by McGrath et al. (ref. 56) reveal an irregular pattern of lines which they consider to be growth lines. Forsyth et al. (ref. 43) noted that growth lines are better visible in the more ductile materials.

Along intuitive lines one may argue that some blunting of the crack at the maximum tensile load will occur if the crack extension per cycle is as large as the values indicated in table 4. A difficult question is how this blunting will be reduced during the reversal of the load. If cracks are closed during the minima of the stress this might affect the shape of the growth lines. So S_{min} could have an important influence. The blunting (and the sharpening) will be more pronounced at higher amounts of plastic strain around the tip of the crack and one should expect an increased visibility for larger crack rates and for more ductile materials. Similarly one should expect a decreased visibility for smaller crack rates and less ductile materials. One might question, whether a crack rate of 100 Å/c or 35 b/c in an alloyed material with a limited amount of ductility could produce growth lines visible by the electron microscope. It is likely that this will not be the case. So it seems that fractographical studies will be unable to provide a satisfactory answer to the question whether crack propagation in the micro-stage does occur in each cycle or not.

In table 1, summarizing the orders of magnitude of crack rates in unnotched and notched specimens, values for $dl/dn < 1$ b/c are mentioned, the lowest value being 0.1 b/c. For such values of the crack rate a number of cycles is required to propagate the crack one atomic distance, which is the smallest value for crack extension. One might think that this will give the crack extension a probabilistic character, i.e. it might become a matter of chance whether there will be crack extension in a certain cycle or not. Although the probability aspect in crack propagation cannot be denied, it should be realized that $dl/dn < 1$ b/c may imply that crack extension will not occur over the complete length of the crack front, but only over a part of the front, with an average over the complete front smaller than one atomic distance per cycle.

Fractographical studies of growth lines (refs 44, 51 and 47) show that these lines are continuous over the grain boundaries, suggesting crack propagation along the entire crack front. However, this need no longer apply if the crack rate is of the order of magnitude of 1 b/c. On the contrary, if the crack extension is so small, the amount of slip occurring in the tip region will also be small. Local slip is obviously very sensitive to local conditions, i.e. the dislocation arrangements, precipitates, etc. They may easily affect the crack rate, especially when the latter is very small.

The recent NLR study (section 4.1), from which figs 1 to 4 were drawn, confirmed that there was a good deal of variability in the propagation of micro-cracks. The scatter was larger than for the propagation of macro-cracks, which in aluminium alloys is usually very low (ref. 7).

Girard (ref. 9) studied crack propagation in small notched Al-4% Cu specimens by filming through a microscope. The endurances ranged from 10^6 to 10^9 cycles. Girard mentioned a value for the average crack rate corresponding to 1 b/c. If crack propagation occurred along one slip plane he observed that the crack rate was substantially constant. This did not apply if the crack followed a more complex path. Recently the NLR has built a small fatigue machine in combination with a microscope. The crack growth was followed at a magnification of 500 times. Stroboscopic light was employed. Limited results available now on 2024-T3 specimens indicate the same trend. As long as the crack followed a straight path its growth made the impression of being a continuous process. The frequency of testing was 50 cycles/second whereas Girard employed the ultrasonic frequency of 90,000 cycles/second. When a change of orientation of the crack occurred it was preceded by a slowing down of the growth (at the surface). Then no crack growth was observed for some time after which growing continued in another direction. The first part of this new crack extension sometimes occurred quite rapidly. It is thought that the direction of growth before the change of orientation could not be maintained, because it was not compatible with the path of the crack below the surface. This restraint released the shear stress on the slip system being active at the surface, and the crack growth slowed down. Crack growth along another slip plane required an increase of shear stress on that plane, which was effectuated after the crack below the surface had gone through some further growth. Such a process leads to unbalanced crack extension at the surface and probably it will occur at the interior of the material as well. Crack growth in certain grains with at the same time no or less crack growth in other grains, implies a locally discontinuous crack growth, which in the extreme case can account for crack rates lower than one atomic distance per cycle. Locally discontinuous crack growth will further be stimulated by inhomogeneities of the material.

Another consequence of locally discontinuous crack growth may be branching of the crack. If crack growth is locally slowed down for some reason, it may be continued along another path thus forming a branch. Further complications may come from inclusions which, when they are approached by a growing crack, may initiate secondary cracks.

Although the above complications will certainly occur, the locally discontinuous character of the growth of the crack need not essentially affect the model for crack growth explained in chapter 6. Such discontinuities are essentially different from the discontinuous propagation proposed in certain fatigue theories, which is in fact an inherent feature of the theories. They were briefly referred to in chapter 5 and will be given further attention in chapter 9. It is thought that the evidence discussed in this chapter is not in favour of discontinuous crack growth as an essential feature of the fatigue phenomenon.

The discussion in this chapter will now be summarized. Fractographical studies of growth lines have shown for macro-cracks that crack extension occurs in every cycle. For micro-cracks such evidence is missing. For unnotched and notched aluminium alloy specimens the orders of magnitude of the crack rate vary from 0.1 to 10,000 atomic distances per cycle. An important part and most times the major part of the fatigue life is expiring at crack rates, for which the fracture surface offers no proof of crack extension in each cycle. Several reasons were discussed explaining why crack extension occurring in each cycle need not be revealed by growth lines on the fracture surface. From the crack propagation model, discussed in previous chapters, it was concluded that continuous crack propagation is a consequence of the continuity of cyclic slip. The continuity of cyclic slip may be affected by locally varying stress conditions along the crack front and by local structural inhomogeneities. This will apply especially at low crack rates, but it will not upset the crack propagation model, even for crack rates lower than one atomic distance per cycle. The latter implies that crack extension does not simultaneously occur along the entire crack front.

9 The difference between low-level and high-level fatigue

In this chapter differences between low-level and high-level fatigue are considered. In the literature it is frequently suggested that there are such differences and that a high-level fatigue failure shows some similarity with a static failure. Aspects discussed here are the transition from fatigue failures to a static failure and fatigue crack propagation at low and high speeds.

It is usual to extend S–N curves into the low fatigue life range by drawing a curve to the vertical stress axis with a horizontal tangent at the ultimate stress S_u, see for instance fig. 39. This procedure is based on the experience that a specimen in a constant-load-amplitude test with S_{max} slightly lower than S_u, if it does not fail in the first cycle, can endure a considerable number of cycles, say in the order of 1000, before complete fracture occurs. One might be led to believe that there is no smooth transition from a fatigue fracture to a static fracture. In a test with S_{max} beyond the yield limit, considerable plastic straining occurs in the first cycles, but due to strain-hardening the strain amplitude and the hysteresis decrease rapidly. However, if the strain amplitude in a test is kept constant instead of the load amplitude, the latter may increase and a fracture in a low number of cycles can be obtained. Such tests were performed notably by Coffin and Tavernelli (ref. 58) and Smith, Hirschberg and Manson (ref. 59). Data for 2024-T3 of the former group of investigators have been reproduced in fig. 40. Contrary to fig. 39 this figure suggests a gradual transition from fatigue failures to the static failure.

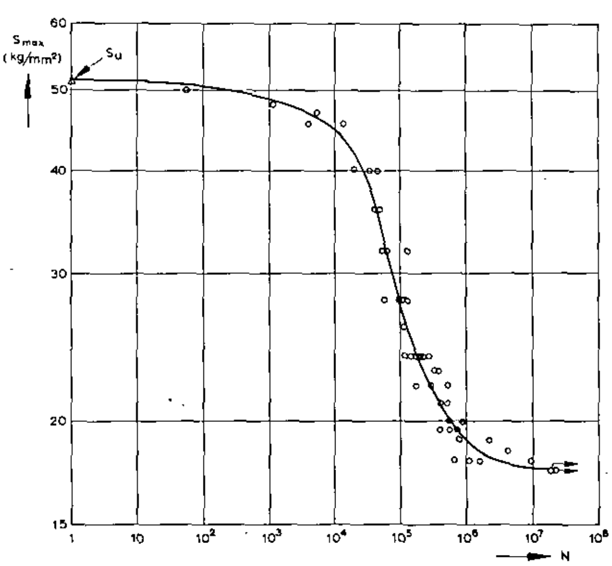

Fig. 39 S–N-curve ($R = 0$) for unnotched specimens of 2024-T3 material (ref. 4).

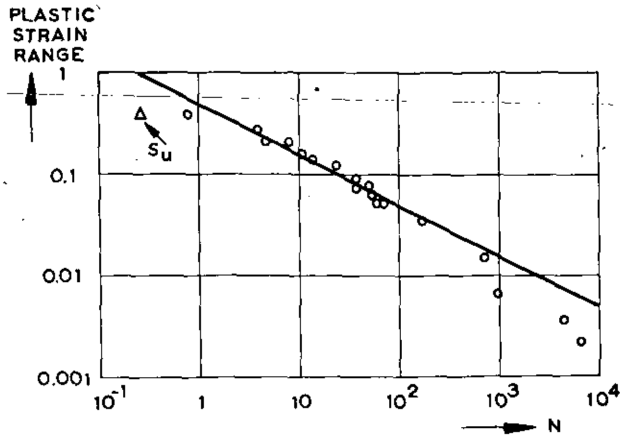

Fig. 40 ε-N-curve for unnotched specimens of 2024-T4 material (ref. 58).

The linear relationship shown by fig. 40 is analytically represented by

$$N^{\alpha}\varepsilon = C \tag{9.1}$$

This relation, first proposed by Manson (ref. 60), was shown to be valid for a variety of materials, a usual value for α being 0.5. Its validity, however, was restricted to low endurances, say $N < 10^4$. Fatigue tests with such low endurances have been labelled in the literature as high-level fatigue tests, especially in those publications which wanted to emphasize that the mechanism of fracture in these tests should be different from that occurring in tests giving high endurances, i.e. low-level fatigue tests. According to Coffin and Tavernelli (ref. 58) the plastic strain (true strain) in a static tensile test fits well into the above relation, if it is assigned an endurance $N = \frac{1}{4}$ cycle. This might suggest that high-level fatigue and a static failure imply the same fracture mechanism. The idea was further stimulated by publications of Wood (ref. 61), who introduced the term "delayed static fracture" to describe a high-level fatigue failure. The idea was picked up by Valluri (ref. 29) to develop a cumulative damage theory.

From a phenomenological point of view there is a large difference between a static failure and high-level fatigue failures in aluminium alloys. The static failure is preceded by necking down and generally starts at the interior of the specimen, spreading outwards. In fatigue, even in high-level fatigue, necking is not observed (ref. 62) and the crack starts from the outside growing inwards. The result that the elongation in a static test satisfies eq. (9.1) for $N = \frac{1}{4}$ cycle then seems to be somewhat fortuitous.

The NLR study (ref. 4), partly described in section 4.1, showed that crack propagation also occurred in tests giving low endurances. Fig. 6 illustrates that on the fracture surface of specimen 1A12 (endurance 5500 cycles) the characteristic 90°-mode, starting from an edge of the cross section, is present. The extent of the crack at the moment of final fracture was larger than the 90°-mode area, although probably not very much larger. A fatigue load with a high maximum stress will produce a final fracture after a small amount of fatigue cracking. The higher S_{max} is, the smaller is the fatigue nucleus required for the final fracture, the latter being considered as a static fracture since it involves relatively much plastic deformation. Nevertheless as long as some crack propagation has preceded the final fracture, the specimen has essentially failed because of fatigue.

Laird and Smith (ref. 33), testing aluminium specimens could show crack growth occurring in each cycle for an endurance somewhat below 1000 cycles. There is no reason to see why this should not apply to aluminium alloys as well. Table 4 shows indeed maximum crack rates for these alloys of the same order of magnitude as Laird and Smith found for aluminium. Consequently the term "delayed static fracture" seems to be inappropriate for high-level fatigue of these materials.

Instead of following the phenomenological approach one could also wonder whether there is a certain similarity in the atomic fracture mechanisms for static and high-level fatigue failures. Obviously this is an ambituous question, since it may be argued that these mechanisms are not yet understood. The cup and cone failure in a tensile test has been discussed by Cottrell (ref. 63). He adheres to the idea that such a fracture starts from inclusions by internal neckings, which view is based on work of Tipper and Puttick. Internal necking is considered as a consequence of slip and should not require fracture by cleavage in the material itself or by micro-cracks nucleated by coalescence of dislocations. If this view is correct, some similarity with fatigue seems to be possible, since both could be considered as the geometrical consequence of slip movements. In high-level fatigue, crack propagation rates will be in the order of 10^3 to 10^5 b/c. For such magnitudes of the crack rate some terms used in the literature seem to be very appropriate. Crussard et al. (ref. 36) are speaking about "glide decohesion" or "decohesion along glide planes". Cottrell (ref. 64) in a discussion on crack propagation in Al-alloy sheet material, described a shear failure as "catastrophic ductile fracture by the propagation of a group of dislocations which causes complete sliding off. It is essentially failure by plastic instability, rather than by fracture in the strict sense".

The alternative fracture mechanism is, using Cottrell's terminology, "fracture in the strict sense". Fracture anyhow implies a disruption of atomic bonds. This also applies to sliding off. For fracture in the strict sense, for instance for cleavage, it is thought that a high tensile stress is required for the disruption of the bonds, rather than a high shear stress. A high tensile stress can be set up with the aid of internal stresses, but as explained in chapter 5, it is difficult to see how this should occur at the surface of a material. It might occur slightly below the surface (or ahead of a crack) and then form internal micro-cracks, presumably of a submicroscopic nature. Studies on static fracture of Al-5% Cu by Beevers and Honeycombe (refs 65 and 66) have shown that static fracture occurs in coarse slip bands formed just prior to failure and that the resolved shear stress on the slip planes (mostly {111} planes, sometimes {100} planes) is still a suitable criterion for the onset of ductile fractures. One might feel that this confirms the sliding-off mechanism, but the conclusion drawn by Beevers and Honeycombe was that ductile fracture is a shear failure from a macroscopic point of view only. On an atomic level they think that static fracture is still due to local stresses built up around pile-ups causing small micro-cracks rather than further glide. They also point out that inclusions are not so important for a static failure in this alloys as they may be for other metals. Probably it will remain difficult to prove or disprove such a mechanism on the basis of microscopic studies since what would be needed is microscopic evidence of such micro-cracks. Even then the micro-cracks do not yet give the complete story. The cracks have to be linked up. In Holden's fatigue theory (ref. 28) such micro-cracks are supposed to be formed by an intensive sub-structure formation with an increasing misorientation. Also he assumed that these micro-cracks are linked up. Although it is an essential part of the crack growth it is not specified whether this linking up should be considered as cleavage or sliding off.

Micro-cracks caused by local high stresses around dislocations should be preceded by considerable strain hardening. In a static test the hardening is clearly observed from the stress-strain curve. However, in high-level fatigue an increasing hardening in aluminium-copper alloys is not observed, at least not as a bulk phenomenon, see chapter 10. It is argued there that more reasons exist to believe that cyclic strain-hardening is not the same as strain-hardening in a static test. In fact the former appeared to be absent in the 2024-T3 alloy, apart from some hardening in the very first cycle. For the time being the question, whether cracking "in the strict sense" occurs below the surface or ahead of a crack and thus could contribute to high-level fatigue, has to remain unanswered.

The preceding discussion was mainly concerned with high-level fatigue and its differences or similarities with a static fracture. Coming now to the differences between low-level fatigue and high-level fatigue, the crack propagation results of section 4.1 imply that it should be a matter of differences in crack propagation. Microscopic studies, discussed in chapter 7, do not indicate such a difference. However, table 1 shows orders of magnitude of the crack rate varying from 0.1 to 10,000 atomic distances per cycle and it is certainly not self-evident that this complete range could be covered by the same fracture mechanism.

In the fatigue model explained in chapter 6, crack extension has been described as a geometric consequence of dislocation movements. Two different mechanisms were mentioned. (1) Dislocations moving towards the crack and flowing into the crack at the tip region. If this happens in a systematic way, crack extension will occur (dislocation-absorption mechanism). (2) Instead of an absorption of dislocations, a generation of dislocations at the tip of the crack can also involve crack extension (dislocation-generation mechanism), which requires high shear stresses.

The first mechanism was considered to be responsible for crack nucleation, while it also can easily account for crack growth at a low rate. The second mechanism requires high shear stresses and should therefore be associated with high crack rates. Although the absorption and the generation mechanisms appear to be different, this can be looked upon as a question of definition. Both are essentially "sliding off" mechanisms. In the absorption model, sliding-off starts at the interior and moves towards the tip of the crack. In the generation model, sliding-off starts at the tip of the crack and moves towards the interior of the material. Both mechanisms may be active at the same time, although it is thought that the former one will prevail at low crack rates and the latter one at high crack rates. It is practically impossible to make quantitative statements about the individual contributions of both mechanisms to crack extension.

The crack propagation at the surface in the 2024-T3 alloy (section 4.5) was clearly associated with crystal planes. Fig. 23 shows that the crack had alternately been growing along two different slip planes. The slip lines of one orientation are almost exclusively found at one side of the crack, while the slip lines of the second orientation mainly occur at the opposite side of the crack. This strongly suggests that sliding off was initiated by the crack, i.e. the generation mechanism was predominantly active, as could be expected at that high crack rate.

As pointed out in chapter 7, the crack propagation at the interior of the material was apparently less associated with crystal planes, which was explained by arguments based on restraining effects on slip and crack growth and the type of shear stress distribution. Under such conditions one might more easily imagine that the dislocation absorption mechanism is active. It should be admitted, however, that at high rates, say in the order of 10,000 b/c, a detailed picture is somewhat beyond imagination. The absorption as well as the generation mechanisms are both simplified concepts and may be considered as representing two classes of possible mechanisms.

In chapter 7, the difference between the 90°-mode and the 45°-mode of fatigue crack propagation was explained on the basis of the state of stress, the former being associated with plane strain and the latter with plane stress. One might think that the absorption mechanism will prevail in the 90°-mode and the generation mechanism in the 45°-mode. Although a weak correlation might be present, it is thought that the correlation is not a plausible one at all crack rates.

This chapter can be summarized as follows. A difference between a static tensile fracture and a high level fatigue fracture is that the former starts at the interior of the material, whereas the latter starts at the surface and essentially involves fatigue crack propagation. Both might occur as a consequence of "sliding off" and it is expected that a high-level fatigue crack is formed that way.

A difference between high-level and low-level fatigue should essentially be a difference of crack growth. For crack growth a dislocation absorption and a dislocation generation model were proposed. It is thought that the former prevails at low-crack rates and the latter at high-crack rates.

10 Cyclic strain-hardening and the Bauschinger effect

The model for the growth of a crack, proposed in chapter 6, is further developed in chapter 11 in order to explore the problems of a quantitative treatment. The amount of slip in each cycle will obviously play an important part and therefore it is necessary to know the cyclic strain-hardening properties of the aluminium alloy concerned. These properties, including the Bauschinger effect are discussed in this chapter. Since they are only known as bulk properties, attention is also paid to the aspect of the local phenomena in the crack tip region.

Hardening implies an increased resistance against deformation. Frequently the yield stress is measured to indicate that hardening has occurred. More information is provided by determining a complete stress-strain curve. Under cyclic loading with a constant stress amplitude the width of the stress-strain hysteresis loop may decrease as a function of the number of cycles. In other words, the induced strain amplitude becomes smaller. Similarly in a test with a constant strain amplitude a narrowing of the hysteresis loop implies an increasing of the required stress amplitude. In the literature both phenomena are referred to as cyclic strain-hardening. The opposite effect is called cyclic strain-softening.

The yield stress gives a useful indication of the precipitation hardening. However, for strain-hardening this indication is not unambiguous in view of the Bauschinger effect. For a cylindrical specimen, pulled in tension to a certain amount of plastic strain, the yield stress in tension has been raised, whereas the yield stress in compression has not been raised to the same amount and may even have decreased.

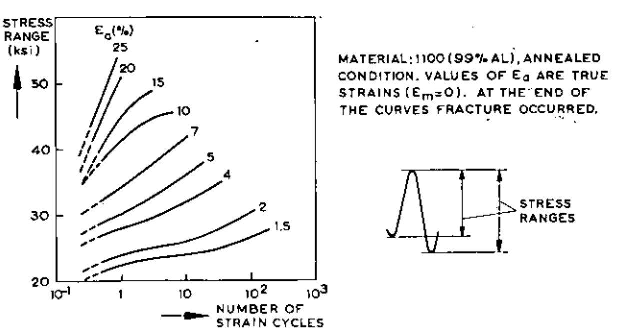

Fig. 41 Stress range required for cyclic straining of aluminium specimens in the annealed condition. (Results of ref. 58.)

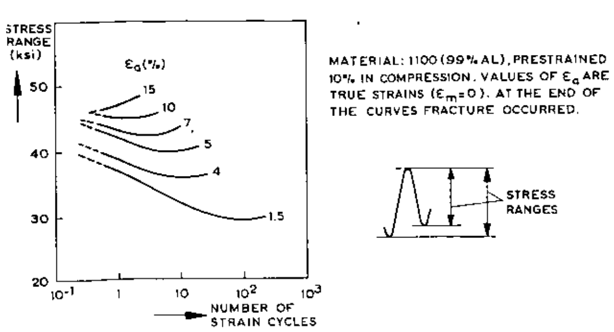

Fig. 42 Stress range required for cyclic straining of prestrained aluminium specimens. (Results of ref. 58.)

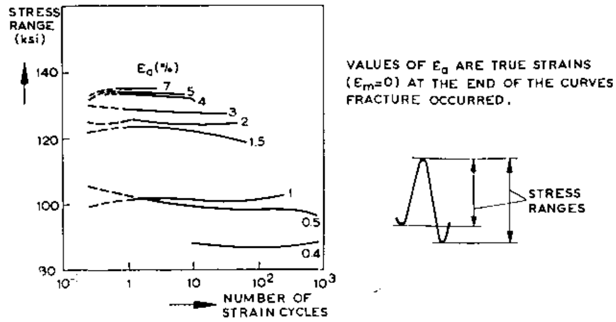

Fig. 43 Stress range required for cyclic straining of 2024-T3 aluminium alloy specimens. (Results of ref. 58.)

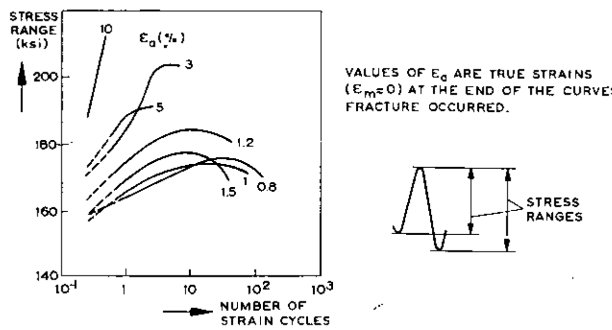

Fig. 44 Stress range required for cyclic straining of 7075-T6 aluminium alloy specimens. (Results of ref. 58.)

A large number of tests to study cyclic strain-hardening of a variety of materials were carried out by Coffin and Tavernelli (ref. 58). Specimens were axially loaded with a constant strain amplitude. A record was made of the stress amplitude required for maintaining a constant strain amplitude. Results for annealed aluminium, prestrained aluminium and two aluminium alloys are reproduced in figures 41 to 44. The annealed aluminium shows cyclic strain-hardening. The prestrained aluminium (10% prestrain in compression) shows cyclic strain-softening at the lower values of the strain amplitude. For the aluminium alloys the 2024-T3 alloy, which is of most interest for the present study, shows a very peculiar behaviour, i.e. it exhibits neither cyclic strain-hardening nor cyclic strain-softening, contrary to all other materials tested by Coffin and Tavernelli. The 7075-T6 alloy shows cyclic strain-hardening. The typical behaviour of the 2024-T3 alloy was confirmed by measurements of Dugdale (ref. 67) on the alloy L65 and by measurements of Smith, Hirschberg and Manson (ref. 59) on the alloy 2014-T4. These alloys are largely the same as 2024-T3. The results Dugdale obtained during tests with a varying strain amplitude are still more important for the present study. He first performed tests with a constant strain amplitude as a basis for comparison with a test in which the strain amplitude was changed a few times. The stress amplitudes required in the latter test are indicated in fig. 45 as a function of the sum of the absolute values of the applied strain increments (cumulative plastic strain). Fig. 45 shows that after a change of the strain amplitude, the stress amplitude became immediately constant again and approximately equal to the stress amplitude required at that strain amplitude in a constant-strain-amplitude test.

Material L65 (Al Cu Mg), specimens are axially loaded

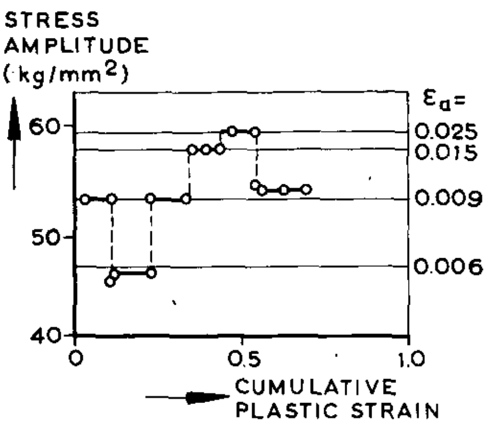

The thin horizontal lines apply to constant strain-amplitude tests. The thick horizontal line segments apply to a test with the strain amplitude varying between the indicated values.

Fig. 45 The stress amplitudes required during a test with a varying strain amplitude. Results of ref. 67.

Systematic measurements on the Bauschinger effect in aluminium alloys are scarce. Kuntze and Sachs (ref. 68) presented results, reproduced here in fig. 46, showing the yield stress as a function of the amount of prestrain. For $S_{0.03}$ (yield stress for 0.03% permanent elongation) a Bauschinger effect was obviously found. On the other hand, the prestrain had only a small effect on the yield

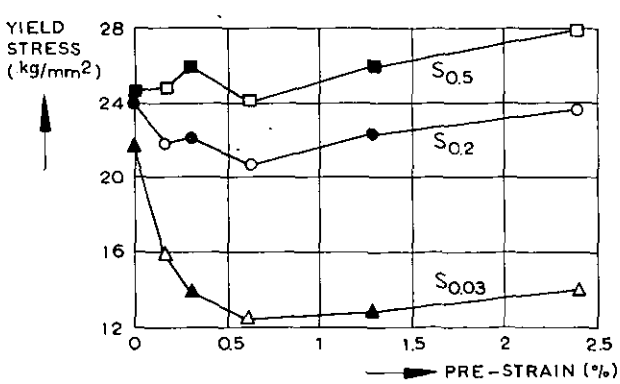

Open data points refer to yield stress in tension after pre-compression. Black data points refer to yield stress in compression after pre-tension. Material is duralumin ("geglüht" = annealed?, composition and heat treatment not specified).

Fig. 46 The Bauschinger effect in an Al-Cu alloy. Results of ref. 68.

stress for 0.2% and 0.5% permanent elongation. Results of a later date were published by Sachs and co-workers (refs. 69, 70 and 71). They performed tests on specimens of the 2024-T3 alloy and employed larger prestrains. They found that the yield stress in tension (compression) was raised by a preloading in compression (tension). Results of greater interest for the present study were obtained by measuring the stress-strain behaviour after a few preload cycles. Fig. 47 shows the stress-strain curve in tension after 2 to 7 prestrain cycles. Apart from the difference in elongation at fracture, there are only small differences between the curves. They are all clearly different from the stress-strain curve of the virgin material. This is further illustrated in fig. 48 showing the yield stress during the successive applications of positive and negative strains. After two cycles the yield stress has stabilized at a constant value. The major part of the increase of the yield stress is already obtained after the first cycle.* Fig. 49 shows the stresses required to induce

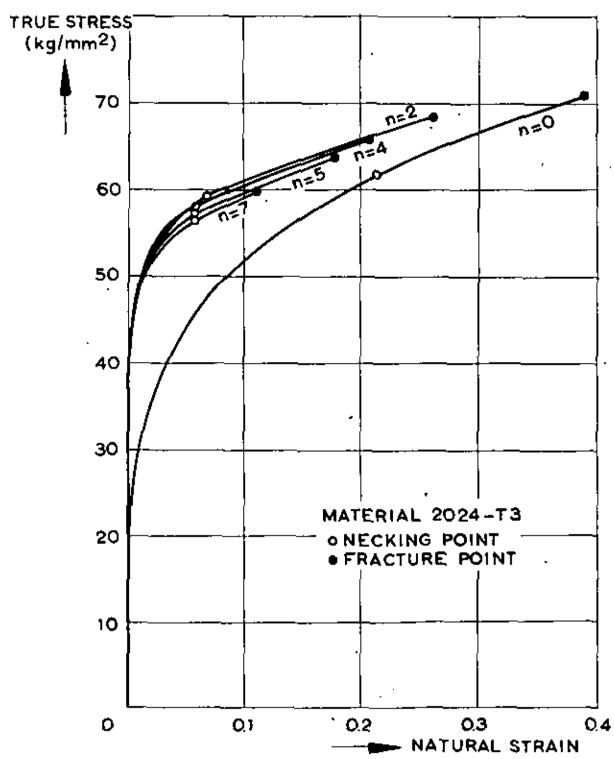

n = number of strain cycles consisting of a positive and a negative strain increment $\varepsilon = 0.12$. Specimens were axially loaded.

Fig. 47 The effect of cyclic prestraining on the stress-strain curve in tension. Results of ref. 70.

* It is somewhat unsatisfactory to see that the yield stresses in tension and compression remain persistently different. The specimens were probably made of extruded bar. The material was heattreated before manufacturing the specimens. The anomalous behaviour remains unexplained, but it is thought that it will not invalidate the trends observed from the results.

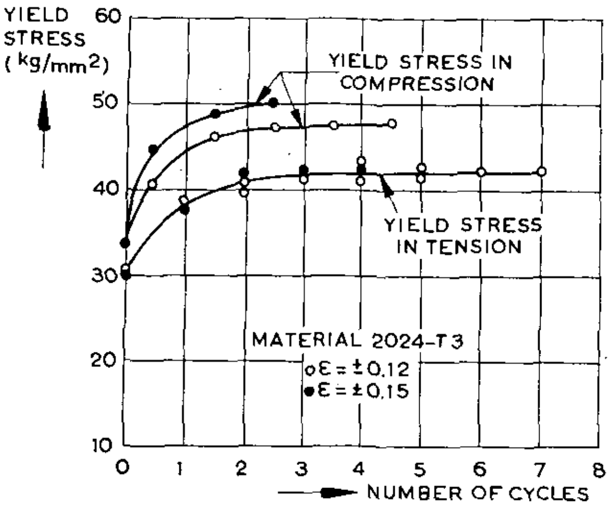

Specimens were axially loaded. Strain cycles consisted of a positive and a negative strain increment ε.

Fig. 48 The yield stress in tension and compression during a small number of plastic strain cycles. Results of ref. 70.

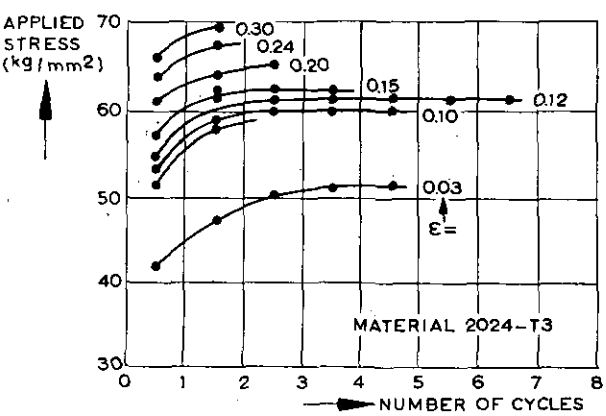

Specimens were axially loaded. Strain cycles consisted of a positive and a negative strain increment ε.

Fig. 49 The stress required to induce plastic strain cycles. Results of ref. 70.

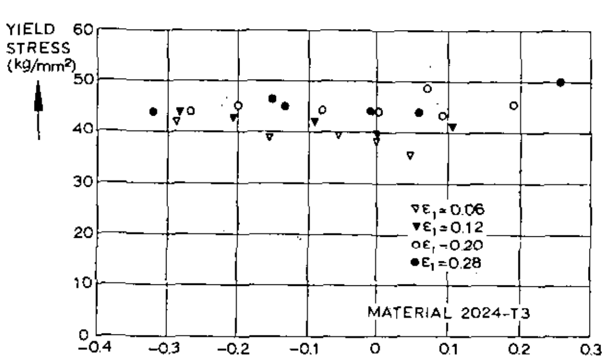

Specimens were axially loaded
ε_1 = positive prestrain
ε_2 = subsequent negative prestrain

Fig. 50 The effect of a positive and negative prestrain increment of unequal absolute magnitude on the yield stress. Results of ref. 71.

plastic strain cycles of constant strain amplitude. They confirm again that the effect of plastic strain cycles on the stress-strain behaviour is stabilizing in one or two cycles. Fig. 49 also confirms the results of Coffin et al., Smith et al. and Dugdale on cyclic strain-hardening, discussed before. Finally fig. 50 shows results of Liu and Sachs (ref. 71) of a study on the effect of one positive prestrain ε_1 and a subsequent negative prestrain ε_2 on the yield stress in tension. In these tests ε_1 and ε_2 usually were of unequal absolute magnitude. Although there is a fair amount of scatter, a tendency towards a constant yield stress is observed.

It is concluded from the above experimental evidence that the plastic behaviour of the 2024-T3 alloy under cyclic loading is surprisingly simple. The stress-strain behaviour is noticeably affected by the first load cycle, but after that first cycle it is not further affected to a great extent.

The dislocation concepts referred to in the literature for explaining the Bauschinger effect and cyclic strain-hardening and softening in pure metals, are concerned with dislocation pile-ups and the formation or destruction of a sub-structure. It is also supposed that the dislocation arrangements for cyclic and uni-directional plastic strains are different. Although these aspects may have some importance for aluminium alloys, it is believed that they will be overshadowed by the presence of the precipitates and their interactions with dislocations. This is a most complex problem. Some information from the literature will be summarized below.

In aluminium alloys the precipitation takes place in the following steps: (1) Supersaturated matrix, (2) Guinier-Preston (GP) zones, (3) coherent precipitates, (4) non-coherent precipitates. An extensive description was given by Hardy and Heal (ref. 72) (see also ref 34). In the Al Cu system there are two types of Guinier-Preston zones, indicated by GP1 and GP2. The coherent precipitates are indicated by θ' and the final precipitate by θ (Cu Al_2). GP zones give the maximum hardness. Formation of the final precipitate implies overageing. In the Al Cu and the Al Cu Mg system, the zones are in the form of platelets with an orientation parallel to the cube planes. In the Al Zn system on the other hand, the zones are spherical. In the Al Cu and Al Cu Mg system the coherency strains around the GP2 zones are supposed to be the major factor in the hardening mechanism. In the Al Zn system, however, the coherency strains are small and the hardening is largely due to the precipitates being obstacles for dislocation movements (dispersion hardening). So a generalization between Al Cu and Al Cu Mg alloys on one hand, and Al Zn Mg alloys on the other hand, does not seem reasonable from the physical point of view. It might well be that the differences in the precipitation hardening mechanisms are responsible for the difference in ductility of the 2024-T3 and the 7075-T6 alloy, the latter one being less ductile, and the difference in cyclic strain-hardening of both alloys, as shown in figs 43 and 44.

Microscopic studies on the interaction between dislocations and precipitated zones were mainly made on the Al-4% Cu alloy. Some relevant results of static tests, based on studies of Thomas et al. (refs 73, 74 and 75), Dew-Hughes and Robertson (ref. 76), Greetham and Honeycombe (ref. 77), Beevers and Honeycombe (refs 78, 65 and 66) and Rakin and Buinov (ref. 79) will be summarized.

In the supersaturated matrix (as—quenched condition) or a lightly aged material (GP1 zones) slip lines can be observed and are relatively straight. Dislocations pass through the GP1 zones. For bowing between the zones the distances between the zones are too small. Avoiding the zones by cross slip might be possible, but apparently passing through the zones does not offer too many difficulties. The thickness of the zones (located on the cube planes) is a few atomic distances. In the overaged condition slip lines are also easily visible. Dislocations do not pass through the incoherent precipitate θ ($CuAl_2$), but the distances between the particles are large enough to allow a bowing between the precipitates, which leaves dislocation loops around them. Also in this condition the hardness is relatively low. The most interesting case is the condition: aged to maximum hardness with predominantly GP2-zones and some θ' (coherent precipitate). In this condition slip lines are very difficult to observe. They are more wavy. Dislocations seem to be able to pass through GP_2 zones and θ' particles, but probably a part of the dislocations are either bowing around the precipitates or circumventing them by cross slip. Once dislocations have passed through a zone or a θ'-particle, subsequent dislocations on the same slip plane will find less difficulty in doing the same. This could imply an absence of strain-hardening. At the same time dislocation movements will produce vacancies which will enhance diffusion. Indications of strainageing during plastic deformation were obtained by Greetham and Honeycombe (ref. 77). Rakin and Buinov (ref. 79) have stated that plastic deformation on the one hand will cause a partial resolution of GP zones and on the other hand will cause stabilization of a certain proportion of the zones and θ'-particles, their transformation into θ' and θ-particles respectively, and the appearance of new GP-zones. If resolution and precipitation proceed both at the same time one might think that the average state of precipitation need not be affected very much. Obviously the phenomenon of the interaction between dislocation movements and the precipitation is a rather complex one.

Passing on to cyclic plastic deformation it is still more difficult to outline qualitatively the process going on in the structure of the material. Microscopic investigations meet with the same difficulty as for undirectional plastic straining, viz. slip lines are very difficult to detect in the fully age-hardened material. Hunter and Fricke (ref. 80) could easily observe slip in pure aluminium, almost directly after the beginning of a fatigue test. However, for the bare 2024-T3 and 7075-T6 material they rarely noticed any slip before cracking was observed. Extensive studies were made by Forsyth and Stubbington (refs 12, 81, 82 and 83), which showed that unambiguous information is not easily obtained for aluminium alloys. They conclude from their findings that fatigue in these alloys is a rather local phenomenon. In slip zones softening occurs, which consequently leads to a further localization of subsequent slip movements. The major problem was to explain the softening. Both overageing and resolution of the precipitates involve softening. For the Al-Cu system Forsyth (ref. 81) has advanced the idea, that Cu-atoms in the slip zones are migrating away to the edges of the zones and, after precipitating there, leave a soft depleted zone. For the Al Zn Mg alloy, fatigue tested at room temperature, he suggests that the precipitates have dissolved under the action of cyclic stress, leaving a more random distribution of the solute atoms, therefore causing the zones to be softer. In a recent study Forsyth (ref. 84) reports results of an Al-7.5% Zn-2.5% Mg alloy tested in torsion. Under the electron microscope bands were observed, which were apparently free from precipitates. He remarks that "such bands only clearly developed under torsional fatigue stress where the conditions prevail for active slip and inactive crack growth. When a tensile stress is present as in direct stressing fatigue, the slip bands develop into cracks with virtually no observable advanced slip band deterioration". The type of loading (tension or torsion) may indeed have some effect on the phenomena (see also chapter 11). Forsyth (ref. 57) also considers the possibility of dislocations passing through the precipitates, which would increase the free slip length of dislocations. This might have an autocatalytic character and as a result the zones and the coherent precipitates would become smaller. The process could then be conceived as resolution, the more so since zones becoming smaller may become too small for being stable (ref. 72).

In conclusion it should be said that the author finds it difficult to accept the idea that localized cyclic slip, involving high dislocation densities and a high production of vacancies, is compatible with a resolution of the precipitates only, since the conditions are an optimum for enhanced precipitation. It is believed that the opinion expressed by Rakin and Buinov (ref. 79), based on a study of Al-4% Cu under uni-directional deformation (see preceding discussion), might apply to cyclic slip as well, i.e. there will be a partial resolution of the smaller GP zones and a stabilization and formation of other zones at the same time.

If softening in the slip zones occurred, it would obviously concentrate cyclic slip. At first sight it may seem plausible that the local character of fatigue cracks is related to the local softening. This aspect needs some careful reconsideration, since several arguments against it can be raised. (1) In fully hardened aluminium alloys the yield strength is relatively high and under low-level fatigue loads a limited number of slip zones should be expected anyhow. (2) Under high-level fatigue, slip is a widely spread phenomenon. So if softening occurs by cyclic slip it should be measurable in specimens loaded at high load levels. However, hardness measurements on 2024-T3 specimens, having fatigue lives in the order of 10^4 cycles ($S_{min} = 0$; S_{max} between the yield stress and the ultimate stress) did not reveal any noticeable change of hardness (unpublished NLR results). Hardness measurements around a tip of a crack also failed to show a drop of the hardness. The latter observation was also made by Frost, Holden and Phillips (ref. 85). The cyclic strain-hardening properties of 2024-T3, discussed in this chapter are another aspect which is not easily reconciled with the softening conception. (3) If the fatigue slip zones would harden rather than soften, cyclic slip movements would stop in the zones. Instead of being transferred to other slip zones it is likely that slip movements then will occur at the edges of hardened zones, because the zones were initiated there due to a locally higher stress (inhomogeneous stress distribution on a micro scale). This stress concentration is not eliminated by the hardening, on the contrary, it will be aggravated, since the possibilities of leveling-off the local shear stress decrease by the hardening. That would involve that the fatigue slip zones should become wider. These arguments support the view that the local character of fatigue in aluminium alloys at low load amplitudes need not a priori be a consequence of local softening. In fact the macro-behaviour is suggesting that the softening does not occur.

Figs 47 to 50 show that the stress-strain behaviour is largely affected in the first load cycles, but not afterwards. After the first cycle yielding apparently requires a higher stress. The following reasons are now suggested as a qualitative explanation. A certain number of free or loosely bonded dislocations are present in the material. These dislocations are forced into more stably tangled positions in the first strain increments. After exhaustion of these dislocations in one or a few cycles the yield strength has increased. A second reason might be related to the state of precipitation. Dislocations may be assumed to cut through GP1 zones. One might expect that a part of the GP1 zones will be destroyed or resolved and that another part will grow towards GP2 zones, implying higher coherency strains. Even without dislocations cutting through GP1 zones one could assume that an increased diffusion activity will favour the growth of GP1 zones to GP2 zones at the cost of smaller GP1 zones. If the transition GP1 → GP2 occurs it is somewhat surprising to see that only a few strain cycles are required to reach a constant cyclic hardening. Of course the material condition is not necessarily stable since breakdown and building-up of zones may both proceed and balance each other.

From the two arguments explaining the behaviour in the first cycles the second one should have some bearing on the absence of cyclic strain-hardening and cyclic strain-softening. One might indeed speculate that resolution and increased precipitation are in perfect balance. There is another less speculative argument which originates from the typical result that, after the first cycles, reversal of plastic strain always gives the same yield stress (see fig. 50). This behaviour is schematically illustrated in fig. 51a and will now be discussed. In aluminium-copper alloys in the aged

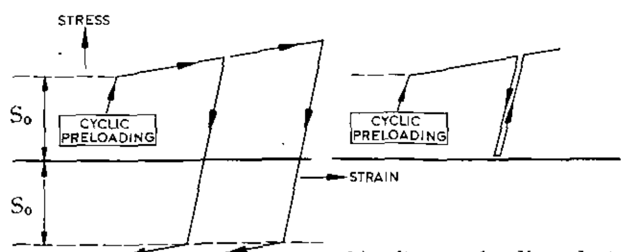

Fig. 51 Schematic illustration of the yield stress behaviour of Al Cu alloys after cyclic preloading.

condition, the dislocations are not straight but curling between the GP zones, following as much as possible the potential valleys. Slip implies dislocation movements over potential hills to other potential valleys (ref. 34). If the potential hills all had the same intensity one would not expect any strain-hardening (ideal plastic body). The precipitated zones would exert a frictional force on the dislocations. However, the topography of the potential hills and valleys will show some statistical variability. It is expected that a dislocation, after having overcome a number of potential hills, will meet a potential hill (or rather a series of hills) which is high enough to stop its movement under the applied stress*. This implies strain-hardening and an increasing stress is required for more plastic strain, even after an intermittent elastic unloading during which the dislocations stay in potential valleys. What occurs when the plastic strain is reversed (fig. 51a)? The dislocations have to move in the opposite direction and meet with potential hills which they had overcome in the preceding plastic strain. Since it may well be assumed that the statistical distribution of the intensities of these hills will be independent of the preceding plastic strain, the reversal of plastic strain will require an approximately constant yield stress as schematically indicated in fig. 51a. The explanation is also compatible with the result that the 7075-T6 alloys (Al Zn Mg) do show cyclic strain-hardening contrary to the Al Cu alloys, since for the Al Zn alloys the hardening is largely a dispersion hardening rather than an internal strain-hardening. If the dislocation movements in the 2024-T3 alloy were reversible the dislocations would always meet the same obstacles. However, it is thought that dislocation movements, passing so many potential hills and valleys, are not likely to be reversible. Moreover, growth of some GP zones and resolution of others are another factor in promoting the irreversibility, which will blur out any strain-history effect.

In addition to the interaction of dislocations and precipitates, other dislocation mechanisms might contribute to the remarkable behaviour of the aluminium-copper alloys. Frictional forces on dislocations, having a constant character, could indeed contribute to the observed behaviour. However, mechanisms which imply a permanent locking of dislocations or a formation of a sub-structure, are thought to be incompatible with the experimental data discussed before.

It will now be considered whether the strain-hardening behaviour, observed as a bulk phenomenon in unnotched specimens under high alternating strains, can be representative for the occurrences in the local region around the tip of a crack. In fact this was assumed by Valluri (ref. 29) in suggesting that fatigue is a high-level fatigue phenomenon up to endurances in the order of one million cycles. To analyse this point an estimate of the size of the plastic zone will be made.

For a micro-crack a state of plane strain will predominantly exist along the crack front. The size of the plastic zone is then calculated from eq. (B32) of appendix B. If a low and a high fatigue load are characterized by $S_a = \frac{1}{4}S_{0.2}$ and $S_a = \frac{1}{2}S_{0.2}$ respectively, a substitution of these values for S in eq. (B32) gives sizes of the plastic zone of 2% and 8% of the crack length. If $l = 0.02$ mm is taken as a characteristic small value for the crack length (see l_t in figs 1 and 2) the size of the plastic zone is ranging from 4000 to 16000 Å. For a dislocation density of 10^{10} per cm^2 the number of dislocations in the plastic zone then ranges from 50 to 750. The density of the GP2 zones will probably be somewhat larger (ref. 34).

If the numbers of dislocations and precipitates in the plastic zone are in the order of 1000 or higher one might think that the phenomena going on, could be much the same as bulk phenomena, i.e. a continuum approach could be acceptable. However, for a low stress amplitude lower numbers are expected and the local slip activity around the tip of the crack might have an inhomogeneous character as a function of the number of cycles. The same will apply to the nucleation period. In this period the crack rate will be of about the same magnitude as for a crack length of 0.02 mm (see section 4.1) and it may then be assumed, that the amount of slip will also be of the same order. The initial crack rates are varying from 0.1 to 10 b/c (see table 1). Reference was previously made to the work of Girard (ref. 9), who observed that crack growth at a rate as low as 1 b/c could be a continuous process. This observation was made with the optical microscope in tests with an extremely high frequency (90,000 cycles/sec.). A discontinuous effect of the precipitates on the crack growth was clearly beyond the possibilities of observation. At the same time Girard's results indicate that crack growth at such

* Consider dislocations overcoming on the average 20 potential hills during a plastic strain increment. With an average spacing of 250 Å for the GP zones (ref. 34) the average movement $d = 5000$ Å. The plastic shear strain $\gamma_p = \varrho db$, ϱ being the density of moving dislocations and b the Burgers vector. For $\varrho = 10^{10}$ dislocations per cm^2 and $b = 3$ Å one finds $\gamma_p = 1.5 \times 10^{-2}$. This is a reasonable order of magnitude as compared with the elastic shear strain γ_e which, for $\Delta\tau = 20$ kg/mm^2, is equal to 0.8×10^{-2}.

a low rate could be considered as a continuous process, if looked at on a somewhat larger scale. For the time being, it is tentatively assumed that the local character of cyclic slip in the first phase of a fatigue test at a low amplitude, has no other implication than a discontinuous proceeding of the crack nucleation and initial growth, without an essential modification of the fatigue mechanism.

The major points of the present chapter will now be summarized. Under cyclic plastic strain the aluminium-copper alloys show a very remarkable behaviour. Only in the first few cycles the stress-strain behaviour is noticeably affected, but afterwards the alloys show neither cyclic strain hardening nor cyclic strain softening. Moreover, after reversal of the plastic strain, there is a tendency towards a constant yield stress, irrespective of the strain history. A tentative explanation for the behaviour has been given.

The microscopic observations on the interaction between dislocations and precipitates were reviewed. A consistent picture of all processes in the material was not yet obtained. Probably resolution of some Guinier-Preston zones and nucleation and growth of other ones are occurring simultaneously and may balance each other. To explain the local nature of slip in low-level fatigue a local softening is not required.

Estimates were made of the size of the plastic zone around the tip of micro-cracks. They showed that the number of dislocations and precipitates in the plastic zone were large, except with small cracks at low stress amplitudes. In the latter case crack growth will probably not be fully continuous, although it is thought that it will not be essentially different.

11 Further evaluation of the fatigue model

In chapters 5 and 6 the nucleation and the growth of a fatigue crack were described as being geometrical consequences of dislocation movements at the surface and in the crack tip region respectively. Various aspects of this fatigue model were further studied in chapters 7 to 10 by analysing relevant experimental evidence. The picture obtained was still qualitative. In this chapter the essential elements of the previous chapter are recapitulated first. Secondly, the variables governing the crack extension are indicated. Finally, the first steps of the quantitative evaluation are considered.

The analysis in the previous chapter has led to the following ideas on fatigue in aluminium-copper alloys. Cracks are nucleated right at the beginning of a fatigue test. This nucleation is a geometrical consequence of dislocations emerging at the surface and forming surface steps. If this happens in a systematic way grooves (intrusions) are formed from which the crack growth starts. The growth process is essentially the same, dislocations now flowing into the crack or, at higher growing rates, being generated by the crack. If all dislocation movements were fully reversible nucleation and growth would not occur. However, it was indicated that for several reasons the reversibility, especially near the surface or the tip of the crack, was not a likely process. Although irreversibility per se need not imply crack nucleation or growth, a few mechanisms were mentioned, which could explain that dislocation movements in the rising and the falling part of a load cycle will cause nucleation and growth. This will receive a further stimulus from the strain energy release involved in crack extension. A tensile stress normal to the crack is important for the efficiency of the conversion of slip into crack growth.

When slip is restricted to a single slip plane crack growth will have a crystallographic orientation. This occurs at the surface at both high and low crack rates. It apparently does not occur at the interior of the material. An explanation was given on the basis of restraint on slip, the coherency of the fracture surface and the shear stress distribution. In principle, crack extension will occur in each load cycle, except when the crack rate is still very low, i.e. lower than one atomic distance per cycle. Crack extension may still occur in each cycle then, but not everywhere along the crack front. The idea that a certain number of strain cycles is required to prepare the plastic zone around the tip of the crack for further crack extension was not accepted, although it may apply to other materials.

If there is a difference between low-level and high-level fatigue, this must be a difference in the crack growth mechanism. It was indicated that there may be two classes of crack growth mechanisms, characterized by dislocations flowing into the crack and dislocations being generated by the crack. The former will predominate at low crack rates and the latter at high crack rates. Both are essentially sliding-off mechanisms. A study on the microcrack propagation in notched and unnotched specimens of 2024-T3 sheet material indicated crack rate values varying as widely as from 0.1 b/c to 10,000 b/c.

The difference between the 90°-mode and the 45°-mode of the fatigue fracture was correlated with the state of stress, being plane strain for the former and plane stress for the latter. It was pointed out that these macroscopic fracture features would not necessarily have to be associated with different growing mechanisms.

Since crack extension is a consequence of cyclic slip, cyclic strain-hardening is an important aspect of the problem. One should except this to be a very complex process in a precipitation hardened aluminium alloy. Surprisingly enough, the cyclic strain-hardening behaviour of aluminium-copper alloys was fairly simple from a descriptive point of view. It was attempted to explain this behaviour by considering the interactions of dislocations and precipitated zones. It was further concluded that the observations on bulk hardening could apply to the plastic zone around the tip of micro-cracks.

Several explanations given for the fatigue mechanism as summarized above are far from rigorous. Assumptions, having a certain degree of plausibility, had to be made. At the present time this is obviously unavoidable for a fatigue theory. Some remarks on limitations involved and aspects which need further investigation, are given in the following chapter.

For a quantitative formulation of the fatigue model two questions have to be answered:

(1) How much slip occurs in the crack tip region and which are the variables governing this amount of slip?
(2) How effective is the slip in the crack tip region in causing crack extension, i.e. which fraction of the moving dislocations effectively contributes to the crack extension, and which are the variables determining the efficiency of the conversion of cyclic slip into crack extension?

The amount of slip will depend on the applied stress, the geometry of the specimen, the size of the crack and the strain-hardening of the material. A quantitative analysis will be far from simple since both the stress distribution and the strain-hardening are not homogeneous throughout the specimen. Moreover, the strain-hardening will depend on the load history (and crack length) in the preceding load cycles. Simplifying assumptions therefore are not to be avoided.

With respect to the second question it cannot be assumed a priori that the same amount of cyclic slip will always involve the same amount of crack extension. From the discussion in chapter 6 it follows that for an axially loaded specimen, the tensile stress at the tip of the crack, i.e. the stress that will open the crack, will have an important effect on the efficiency of cyclic slip in producing crack growth. Obviously this tensile stress should include any residual stress being present. In addition the "crack tip radius" (the amount of crack blunting) could have some effect. It is thought, however, that the former effect will prevail, and for the time being the influence of the latter will be ignored.

It is more or less usual to define a cyclic stress by its mean value and its amplitude. However, for the material the mean stress is just one stress level to be passed in going from a minimum to a maximum or the reverse. Also the time spent in going from a minimum to a maximum (frequency, loading rate) has, within certain limits, a negligible effect, on the fatigue life. The landmarks are the maxima and the minima of the load-time history.

Constant-amplitude tests are considered only, i.e. S_{max} and S_{min} are constant.

The basic equation is:

$$\frac{\Delta l}{\Delta n} = \varphi m b \qquad (11.1)$$

$\Delta l/\Delta n$ is the crack rate, Δl being the crack extension in one cycle; m is the number of moving dislocations which possibly could, depending on circumstances, contribute to crack extension. This number cannot be equal to the number of all moving dislocations in the plastic zone, since many of the latter will never move far enough for having a possibility of flowing into the crack, or they may be moving in the wrong direction. It should be expected that m is correlated to the instantaneous size of the plastic zone. The symbol φ represents the fraction of the number of the m dislocations contributing effectively to the crack extension ($\varphi < 1$) and b is the magnitude of the Burgers vector. The two questions raised above are apparently concerned with m and φ repectively.

The shape of the plastic zone will not be accurately known, but its size can be estimated from the theory of elasticity (see Appendix B). Taking p as a characteristic dimension for the size of the plastic zone it was suggested above that m should be correlated with p, or:

$$m = f_1(p) \qquad (11.2)$$

It was pointed out before that the efficiency of the cyclic slip in producing crack extension depended mainly on the tension stress at the tip of the crack. The fraction φ will depend on this stress, called S_{tip}, the value of which will be characteristic for the distribution of tension stresses around the tip of the crack. S_{tip} will not be defined any further here; it will include the residual stress remaining from the previous load-time history. Analytically the assumption is represented by:

$$\varphi = f_2(S_{tip}) \qquad (11.3)$$

Substitution of eqs. (11.2) and (11.3) in eq. (11.1) gives:

$$\frac{\Delta l}{\Delta n} = b \cdot f_1(p) \cdot f_2(S_{tip}) \qquad (11.4)$$

In this form the essential elements of the model are still present in a way which can easily be understood. The complications are due to the problem of arriving at the functions f_1 and f_2 and finding suitable expressions for p and S_{tip}. Eqs. (11.1) and (11.4) apply to the n^{th} load cycle. Both p and S_{tip} in the n^{th} load cycle will depend on the distribution of stress and strain hardening at the end of the $(n-1)^{th}$ cycle, and on the cyclic change of the stress distribution in the n^{th} cycle itself. It is thought that solving this problem for each load cycle as a two-dimensional continuum problem is fully impracticable and simplified concepts will be necessary. This does not have to be an objection if the main features of the fatigue model, as outlined before, can be included in a reasonable way. Until now such an approach was only attempted by Head (ref. 86). It is thought, however, that his model does not satisfy the main elements of fatigue (ref. 87).

The functions f_1 and f_2, eqs. (11.2) and (11.3) require physical assumptions to be made. Instead of employing speculative arguments a first approach could be made by assuming them to be simple power functions.

The preceding illustrates the enormous difficulties involved in arriving at a quantitative model which gives full credit to the essential features of the fatigue phenomenon. The significance of qualitative models, such as developed in this thesis, is that they help to understand the influence of various factors on fatigue, that they give guidance in correlating observations and that they are required for planning meaningful research on the fatigue phenomenon.

12 Future prospects

In the present thesis the empirical evidence contained in the literature was analysed and new evidence from recent NLR-studies was added. Secondly, it was tried by employing simple dislocation concepts to present a fatigue model which could account for the empirical evidence. The analysis of available evidence and the formulation of a dislocation mechanism form the main part of the present study.

The analysis in this report might suggest that qualitatively the fatigue phenomenon in aluminium-copper alloys is more or less understood. However, various assumptions have been made indicating that several aspects require further investigation. It is thought that a study of the following topics could provide useful information.

(1) It was suggested that the crack rate was approximately constant during the first period of a fatigue test. The evidence for this was not too abundant and it would be useful to study this aspect in greater detail. Quantitative records of the development of micro-cracks should be made right from the beginning of a test. In such tests the stress amplitude and the mean stress should be varied within wide limits.

(2) A systematic study of the effect of a tensile stress, normal to the crack, on the crack growth behaviour on a microscopic scale is certainly worthwhile. It was pointed out that this stress was important for the conversion of cyclic clip into crack growth. More evidence is certainly desirable.

(3) Systematic fractographical studies to explore the presence of growth lines at low crack rates should be extended in view of the limited available evidence.

(4) Studies on the topography of growth lines and the shape of the tip of the crack may give useful information for specifying dislocation mechanisms in more detail.

(5) In view of the restraint on the crack path in polycrystals, mutually exerted by neighbouring grains, a study of the crack growth in specimens with a thickness much lower than the grain size may be elucidating.

(6) Crack growth studies at very low endurances, say N smaller than 500 cycles, are worthwhile. Such tests should be carried out with a constant strain amplitude.

The above proposals are all concerned with microscopic studies. It is thought indeed, that there is still ample room for microscopic studies, for both the optical and the electron microscope.

With respect to the dislocation concepts employed it may be said that there will be no certainty about a dislocation mechanism for fatigue, unless its occurrence can be proved by electron microscopy. With respect to such a proof there are probably no reasons to be optimistic. Still it is thought that studies on dislocation mechanisms are not at all futile since they can hardly be missed as guidelines for planning microscopic and other studies on the fatigue phenomenon.

It is obvious that for aluminium-alloys the problem of the interaction of dislocations and precipitates under cyclic loading might benefit from further study.

The above proposals aim at an improvement of the qualitative understanding of the fatigue phenomenon as it occurs in the metal. As said in the preceding chapter a qualitative knowledge is important, also from an engineering point of view, since it allows a better understanding of various factors affecting the fatigue behaviour. Moreover a qualitative model is a prerequisite for planning fatigue research.

For a quantitative treatment the continuum approach is unavoidable. The present study has shown that an elastic stress analysis may give useful indications for certain aspects of the fatigue problem. However, chapter 11 has illustrated that the information required for the quantitative development of the proposed fatigue model presents tremendously complex problems. Starting from simplifying assumptions studies of this nature could still be useful for such problems as "cumulative fatigue damage", the notch effect and the size effect. The cumulative fatigue damage problem can be defined as the problem of correlating the fatigue life under a load with a varying amplitude, with the fatigue lives under constant-amplitude loading. This problem, having importance in aircraft design, might turn out to be the least difficult one, since the material, the surface condition and the dimensions of the specimen do no enter the problem as variables.

13 Conclusions

The conclusions refer to aluminium alloys and more in particular to aluminium-copper alloys.

1. Fatigue cracks are nucleated at the free surface (if nucleation at inclusions is disregarded) since dislocation movements near the free surface are more easily initiated and since there is less restraint on plastic flow. The nucleation is a geometrical consequence of dislocations emerging at the surface, and the process of crack growth is essentially the same, dislocation movements then being concentrated at the tip of the crack. The dislocation movements in the rising and the falling part of a load cycle are partly irreversible, for which several reasons are given. A few mechanisms were indicated causing nucleation and growth. The growth receives a stimulus from the strain energy release involved in crack extension.
2. In addition to crack growth occurring as a consequence of dislocations flowing into the tip of the crack, cracks may also grow by dislocations generated by the tip of the crack. The former occurs at low crack rates and, since it requires high shear stresses, the latter predominantly occurs at high crack rates. Both are essentially "sliding off" mechanisms.
3. A tensile stress normal to the crack promotes the conversion of cyclic slip into crack growth.
4. Crack nucleation occurs right from the beginning of a fatigue test. For some time after the initiation the rate of growth will be approximately constant, after which it increases. Tests on notched and unnotched specimens of 2024-T3 material indicated orders of magnitude for the growth rate of micro-cracks ranging from 0.1 to 10,000 atomic distances per cycle.
5. Crack growth occurs along a crystal plane if slip is restricted to a single slip plane. This occurs at the surface for both low and high crack rates and is a consequence of the weak restraint on slip there. Crack growth along crystal planes apparently does not occur at the interior of the material since slip there occurs on more than one slip plane, as caused by the higher restraint on slip, the coherency of the fracture surface and the type of shear stress distribution.
6. New evidence for the previous conclusion was obtained in microscopic studies on the crack nucleation in the aluminium cladding of an aluminium alloy sheet material and the crack propagation in unclad aluminium sheet specimens (2024-T3 material).
7. For macro-cracks growth lines observed in fractographical studies show that there is crack extension in each load cycle. For micro-cracks such evidence is largely missing. A few reasons have been indicated which explain why growth lines are not observed in the latter case. Continuous crack propagation, also in the micro-stage, occurs as a consequence of the continuity of cyclic slip. A growth rate, lower than one atomic distance per cycle implies that crack extension does not simultaneously occur along the entire crack front. Inhomogeneities of the metal structure may locally upset the continuity of the crack growth, especially at low crack rates, without essentially modifying the crack growth mechanism.
8. Crack propagation was observed at high fatigue loads involving low endurances. A difference between low-level and high-level fatigue must be due to different crack growth mechanisms. Reference to such differences was already made in the second conclusion.
9. The difference between the 90°-mode and the

45°-mode of the fatigue fracture is associated with the state of stress, being plane strain for the former and plane stress for the latter. These macroscopic fracture features are not necessarily correlated with different growing mechanisms.

10. The aluminium copper alloys show a remarkable behaviour under cyclic plastic strain. Cyclic strain-hardening occurs in the first cycle, but subsequently neither cyclic strain-hardening nor softening is found. Secondly, on reversal of plastic strain there is a tendency towards a constant yield stress irrespective of the previous strain history. A tentative explanation for this behaviour was given based on the interaction of dislocations and precipitated zones.
11. For explaining the local nature of slip in fatigue at low amplitudes a local softening is not required.
12. Estimates of the size of the plastic zone around the tip of a micro-crack show that the numbers of dislocations and precipitates in this zone are large, except for the initial period in tests with a low stress amplitude. For a quantitative development of the suggested fatigue mechanism a continuum approach seems to be allowed.
13. The crack growth in a cycle depends on the amount of cyclic slip and the efficiency of the conversion of this cyclic slip into crack extension. The former is associated with the size of the plastic zone, p, and the latter with the stress at the tip of the crack, S_{tip}. The analytic function for the crack rate is proposed to be of the type $\Delta l/\Delta n = b \cdot f_1(p) \cdot f_2(S_{tip})$, b being the size of the Burgers vector. Both p and S_{tip} depend on the previous load-time history, S_{tip} includes residual stresses.

14 List of symbols, units and nomenclature

Symbols used in Appendices A and B are explained there.

b —Burgers vector, or size of Burgers vector ($b = 2.86$ Å for slip system {111} <110> in aluminium)
c —cycle
C —constant
GP1, GP2 —phases of precipitation (see chapter 10)
K_t —theoretical stress concentration factor
l —crack length for an edge crack and semi-crack length for a central crack
l_t —length of crack until which the crack rate is approximately constant and after which the crack growth starts accelerating (see section 4.1)
m —number of dislocations
n —number of load cycles, or rank number of load cycle
N —fatigue life until failure
N_l —fatigue life until a crack of length l
NLR —Nationaal Lucht- en Ruimtevaartlaboratorium (National Aero- and Astronautical Research Institute, Amsterdam)
p —size of plastic zone
r —polar co-ordinate from tip of crack, or shear stress ratio (see chapter 7)
R —stress ratio $= S_{min}/S_{max}$
S —stress on specimen
S_1, S_2, S_3 —principal stresses, S_1 and S_2 in plane of sheet, S_3 perpendicular to sheet
S_a —stress amplitude
S_m —mean stress
S_{max} —maximum stress
S_{min} —minimum stress
nominal stress on initial uncracked cross section
S_o —yield stress
$S_{0.2}$ —yield stress for 0.2% permanent set
S_u —ultimate tensile strength
t —sheet thickness
α —angle between slip plane through the tip of the crack and plane of sheet, or exponent in eq. (9.1)
β —angle between direction of loading and crack
γ —shear strain
δ —elongation after fracture in a tensile test
ε —strain
ε_a —strain amplitude
ε_m —mean strain
θ —polar coordinate from tip of crack, or phase of precipitation (see chapter 10)
λ —wave length (see fig. 32)
ν —Poisson's ratio ($\nu = 0.33$ for aluminium alloys)
ϱ —dislocation density
τ —shear stress
τ_2 —maximum value of shear stress on planes perpendicular to the sheet
τ_3 —maximum value of shear stress on planes at an oblique angle to the sheet
τ'_2 —shear stress on planes perpendicular to the sheet and passing through the tip of the crack
τ'_3 —maximum value of the shear stress on planes at an oblique angle to the

sheet and passing through the tip of the crack

—φ— —coefficient indicating the efficiency to convert cyclic slip into crack extension

Units

Å	=Ångström = 10^{-7} mm = 10^{4} μ
μ	= 10^{-3} mm
mm	=millimeter = 0.04 inch (1 inch = 25.4 mm)
b	=size of Burgers vector = 2.86 Å for slip system {111} ⟨110⟩ in aluminium
kc	=kilocycle = 1000 cycles
c.p.s.	=cycle/second
b/c	=crack rate of 1 atomic distance per cycle
Å/c	=crack rate of 1 A per cycle
1 kg/mm^2	=1422 psi

Nomenclature

90°-mode of fatigue fracture	—crack with a macroscopic fracture surface perpendicular to the direction of loading
45°-mode of fatigue fracture	—crack with a macroscopic fracture surface at an angle of 45° to the direction of loading and to the plane of the sheet.

Material designations of precipitation-hardened aluminium alloys (nominal compositions)

2024	Al—4.5% Cu—1.5% Mg, T3: naturally aged
2014	Al—4.4% Cu—0.4% Mg
L65	Al—4.3% Cu—0.7% Mg
7075	Al—5% Zn—2.5% Mg—1.5% Cu, T6: artificially aged.

15 List of references

1 SCHMID, E. UND BOAS, W., Kristallplastizität. Springer, Berlin (1935).

2 GILMAN, J. J., Cleavage, ductility and tenacity in crystals. Fracture, p. 193. John Wiley (1959).

3 SEEMANN, H. J. AND STAVENOW, F., Röntgenographische Untersuchungen über das Auftreten von Stapelfehlern in verschiedenen Al-legierungen. Z. Metallk. vol. 52, p. 667 (1961).

4 SCHIJVE, J. AND JACOBS, F. A., Fatigue crack propagation in unnotched and notched aluminium alloy specimens. N.L.R. Report (to be published shortly).

5 DE LANGE, R. G., Plastic replica methods applied to a study of fatigue phenomena. (Private communication, to be published in Trans. Am. Inst. Mech. Engrs.).

6 BROEK, D. AND SCHIJVE, J., The influence of the mean stress on the propagation of fatigue crack in aluminium alloy sheet. N.L.R. Report M. 2111 (1963).

7 SCHIJVE, J., Fatigue-crack propagation in light alloy sheet material. Advances in Aero. Sciences, vol. 3, p. 387, Pergamon Press (1960).

8 SCHIJVE, J., BROEK, D. AND DE RIJK, P., The effect of the frequency of an alternating load on the crack rate in a light alloy sheet. N.L.R. Report M. 2092 (1961).

9 GIRARD, F., Etude microscopique de la fissuration par fatigue à haute fréquence. Advances in Aero. Sciences, vol. 3, p. 357, Pergamon Press (1960).

10 GOUGH, H. J., Crystalline structure in relation to failure of metals, especially by fatigue. Proc. Am. Soc. Testing Mats., vol. 33, p. 3 (1933).

11 GOUGH, H. J. AND FORREST, G., A study of the fatigue characteristics of three aluminium specimens each containing from 4 to 6 large crystals. J. Inst. Metals, vol. 58, p. 97 (1936).

12 FORSYTH, P. J. E., The mechanism of fatigue in aluminium and aluminium alloys. Fatigue in Aircraft Structures, p. 20, Academic Press Inc., New York, (1956).

13 WEINBERG, J. G. AND BENNETT, J. A., Effect of crystal orientation on fatigue-crack initiation in polycrystalline aluminium alloys. NACA Tech. Note 3990, (1957).

14 HEMPEL, M. AND SCHRADER, A., Gleitspuren an der Oberfläche von biegewechselbeanspruchtem Reinaluminium. Archiv. Eisenh. w., vol. 28, p. 547 (1957).

15 ALDEN, T. H. AND BACKOFEN, W. A., The formation of fatigue cracks in aluminium single crystals. Acta Metallurgica, vol. 9, p. 352 (1961).

16 WOOD, W. A., Recent observations on fatigue failure in metals. Am. Soc. Testing Mats, Spec. Techn. Publ. No. 237, p. 110 (1958).

17 MAY, A. N., A model of metal fatigue. Nature, vol. 185, p. 303 (1960).

18 COTTRELL, A. H. AND HULL, D., Extrusion and intrusion by cyclic slip in copper. Proc. Roy. Soc. (A), Vol. 242, p. 211 (1957).

19 BACKOFEN, W. A., Formation of slip-band cracks in fatigue. Fracture, p. 435. John Wiley (1959).

20 MOTT, N. F., A theory of the origin of fatigue cracks. Acta Metallurgica, vol. 6, p. 195 (1958).

21 MOTT, N. F., The behavior of metals under reversed stresses. Dislocations and Mechanical Properties of Crystals, p. 458. John Wiley (1956).

22 FLEISCHER, R. L., Discussion. Fracture, p. 447. John Wiley, (1959).

23 ALDEN, T. H., Fatigue fracture in pure metals. J. of Metals, vol. 14, p. 828 (1962).

24 THOMPSON, N., WADSWORTH, N. AND LOUAT, N., The origin of fatigue in copper. Phil. Mag. (8), vol. 1, p. 113 (1956).

25 THOMPSON, N., Some observations on the early stages of fatigue fracture. Fracture, p. 354. John Wiley (1959).

26 OROWAN, E., Theory of the fatigue of metals. Proc. Roy. Soc. (A), vol. 171, p. 79 (1939).

27 STROH, A. N., The formation of cracks as a result of plastic flow. Proc. Roy. Soc. (A), vol. 223, p. 404 (1954) and vol. 232, p. 548 (1955).

[28] HOLDEN, J., The formation of sub-grain structure by alternating plastic strain. NEL Report PM 298, East Kilbride (1960).

[29] VALLURI, S. R., A unified engineering theory of high stress level fatigue. Aerospace Eng., vol. 20, p. 18 (1961).

[30] MOTT, N. F., Theories of fracture in metals. IUTAM Colloquium on Deformation and Flow of Solids, Madrid, p. 53, Springer Verlag (1955).

[31] ODING, I. A., Ueber den Mechanismus der Zerstörung bei der zyklischen Belastung von Metallen. IUTAM Colloquium on Fatigue, Stockholm, p. 178, Springer Verlag (1955).

[32] WOODWARD, R. A., GUNN, K. W. AND FORREST, G., The effect of mean stress on the fatigue of aluminium alloys. Proc. International Conf. on Fatigue of Metals, London 1956. The Inst. of Mech. Engrs., p. 158 (1956).

[33] LAIRD, C. AND SMITH, G. C., Crack propagation in high stress fatigue. Phil. Mag. (8), vol. 7, p. 847 (1962).

[34] SMALLMAN, R. E., Modern physical metallurgy. Butterworths Scientific Publications, London (1962).

[35] MCEVILY, A. J., BOETTNER, R. C., On fatigue crack propagation in f.c.c. metals. Acta Metallurgica, vol. 11, p. 725 (1963).

[36] CRUSSARD, C., PLATEAU, J., TAMHANKAR, R., HENRY, G. AND LAJEUNESSE, D., A comparison of ductile and fatigue fracture. Fracture, p. 524, John Wiley (1959).

[37] LIU, H. W., Discussion in Proc. Crack Propagation Symposium, Cranfield, vol. 2, p. 514. The College of Aeronautics (1961).

[38] BROEK, D. AND SCHIJVE, J., The effect of sheet thickness on the fatigue crack propagation in a light alloy sheet. N.L.R. Report (to be published shortly).

[39] FORSYTH, P. J. E., A two stage process of fatigue crack growth. Proc. Crack Propagation Symposium, Cranfield, vol. 1, p. 77. The College of Aeronautics (1961).

[40] FORSYTH, P. J. E., STUBBINGTON, C. A., Some observations on the initiation and growth of fatigue cracks in an aluminium 7.5% zinc 2.5% magnesium alloy. Royal Aircraft Est., Techn. Note Met. Phys. 334 (1962).

[41] STUBBINGTON, C. A., Some observations on air and corrosion fatigue of an aluminium—7.5% zinc—2.5% magnesium alloy. Metallurgia, vol. 68, p. 109 (1963).

[42] SCHIJVE, J., BROEK, D. AND JACOBS, F. A., Fatigue tests on aluminium alloy lugs with special reference to fretting. N.L.R. Report M. 2103 (1962).

[43] FORSYTH, P. J. E., RYDER, D. A., SMALE, A. C. AND WILSON, R. N., Some further results obtained from the microscopic examination of fatigue, tensile and stress corrosion fracture surfaces. Roy. Aircraft Est., Tech. Note Met. 312 (1959).

[44] FORSYTH, P. J. E., The application of fractography to fatigue failure investigations. Roy. Aircraft Est., Techn. Note Met. 257 (1957).

[45] CHRISTENSEN, R. H., Fatigue crack growth in metals. Douglas Engineering Paper No. 985 (1960).

[46] RYDER, D. A., Some quantitative information obtained from the examination of fatigue fracture surfaces. Roy. Aircraft Est., Techn. Note Met. 288 (1958).

[47] MATTING, A. AND JACOBY, G., Ueber das Verhalten von Schweissverbindungen aus Aluminiumlegierungen bei Schwingbeanspruchung. Teil II: Beitrag zum Mechanismus des Schwingungsbruches. Aluminium, vol. 38, p. 309 (1962).

[48] CHRISTENSEN, R. H., Cracking and fracture in metals and structures. Proc. Crack Propagation Symposium, Cranfield, vol. 2, p. 326, The College of Aeronautics (1961).

[49] ZAPPFE, C. A. AND WORDEN, C. O., Fractographic registrations of fatigue. Trans. Am. Soc. for Metals, vol. 43, p. 958 (1951).

[50] FORSYTH, P. J. E. AND RYDER, D. A., Fatigue fracture. Some results derived from the microscopic examination of crack surfaces. Aircraft Engineering, vol. 32, p. 96 (1960).

[51] PLATEAU, J., CRUSSARD, C., FAGUET, J., HENRY, G., WEISZ, M., SERTOUR, G. AND ESQUERRÉ, R., Etude microfractographique des surfaces de rupture par fatigue. Example d'application. Revue de Métallurgie, vol. 55, p. 679 (1958).

[52] SCHIJVE, J. AND JACOBS, F. A., Fractographical investigation and hardness measurements on a number of failed turbine blades of the J 65. N.L.R. Report M. 2079 (restricted) (1960).

[53] TOKUDA, A., Observation of the fatigue fracture surface of some carbon steels by electron microscope. Trans. Japan Inst. of Metals, vol. 1, p. 108 (1960).

[54] BOCKRATH, G. E. AND CHRISTENSEN, R. H., Master fatigue curves. Douglas Engineering Paper No. 999 (1961).

[55] MATTING, A. AND JACOBY, G., Die Zerrüttung metallischer Werkstoffe bei Schwingbeanspruchung in der Fraktographie. Aluminium, vol. 38, p. 654 (1962).

[56] MCGRATH, J. T., BUCHANAN, J. G. AND THURSTON, R. C. A., A study of fatigue and impact fractures with the scanning electron microscope. J. Inst. of Metals, vol. 91, p. 34 (1962).

[57] FORSYTH, P. J. E., A study of the damage caused by torsional fatigue in an aluminium alloy. Roy. Aircraft Est., Tech. Note Met. 310 (1959).

[58] COFFIN, L. F. AND TAVERNELLI, J. F., The cyclic straining and fatigue of metals. Trans. Am. Inst. Met. Engrs., vol. 215, p. 794 (1959).

[59] SMITH, R. W., HIRSCHBERG, M. H. AND MANSON, S. S., Fatigue behavior of materials under strain cycling in low and intermediate life range. NASA Tech. Note D-1574 (1963).

[60] MANSON, S. S., Behavior of materials under conditions of thermal stress. NACA Tech. Note 2933 (1953).

[61] WOOD, W. A., Some basic studies of fatigue in metals. Fracture, p. 412. John Wiley (1959).

[62] BENHAM, P. P. AND FORD, H., Low endurance fatigue of a mild steel and an aluminium alloy. J. Mech. Eng. Science, vol. 3, p. 119 (1961).

[63] COTTRELL, A. H., Theoretical aspects of fracture. Fracture, p. 20, John Wiley (1959).

[64] COTTRELL, A. H., Discussion in Proc. Crack Propagation Symposium Cranfield, vol. 2, p. 495. The College of Aeronautics (1961).

[65] BEEVERS, C. J. AND HONEYCOMBE, R. W. K., The deformation and fracture of Al—5% Cu crystals. Acta Met., vol. 10, p. 17 (1962).

[66] BEEVERS, C. J. AND HONEYCOMBE, R. W. K., The initiation of ductile fracture in pure metals. Phil. Mag. (8), Vol. 7, p. 763 (1962).

[67] DUGDALE, D. S., Stress-strain cycles of large amplitude. J. Mech. Phys. Solids, vol. 7, p. 135, (1959).

[68] KUNTZE, W. AND SACHS, G., Der Fliessbegin bei wechselnder Zug-Druckbeanspruchung. Mitt. der Materialprüfungsanstalten, Sonderheft 14, p. 77 (1930).

[69] LYNCH, J. J. RIPLING, E. J. AND SACHS, G., Effect of various stress histories on the flow and fracture characteristics of the aluminium alloy 24ST. Trans. Am. Inst. Mining Met. Engrs., vol. 175, p. 435 (1948).

[70] LIU, S. I., LYNCH, J. J., RIPLING, E. J. AND SACHS, G., Low cycle fatigue of the aluminium alloy 24ST in direct stress. Trans. Am. Inst. Mining Met. Engrs., vol. 175, p. 469 (1948).

[71] LIU, S. I. AND SACHS, G., *The flow and fracture* characteristics of the aluminium alloy 24ST after alternating tension and compression. Transm. Am. Inst. Mining Met. Engrs., vol. 180, p. 193 (1949).

[72] HARDY, H. K. AND HEAL, T. J., *Report on precipitation.* Progress in Metal Physics, vol. 5, p. 143, Pergamon Press (1954).

[73] THOMAS, G. AND NUTTING, J., The plastic deformation *of aged aluminium alloys.* J. Inst. Metals, vol. 86, p. 7 (1957).

[74] NICHOLSON, R. B., THOMAS, G. AND NUTTING, J., Electron-microscope studies of precipitation in aluminium alloys. J. Inst. Metals, vol. 87, p. 429 (1959).

[75] NICHOLSON, R. B., THOMAS, G. AND NUTTING, J., The interaction of dislocations and precipitates. Acta Met., vol. 8, p. 172 (1960).

[76] DEW-HUGHES, D. AND ROBERTSON, W. D., The mechanism of hardening in aged aluminium-copper alloys. Acta Met., vol. 8, p. 156 (1960).

[77] GREETHAM, G. AND HONEYCOMBE, R. W. K., The deformation of single crystals of aluminium—4.5% copper alloy. J. Inst. Metals, vol. 89, p. 13 (1960).

[78] BEEVERS, C. J. AND HONEYCOMBE, R. W. K., Ductile fracture of single crystals. Fracture, p. 474, John Wiley (1959).

[79] RAKIN, V. G. AND BUINOV, N. N., The influence of plastic deformation on the stability of precipitation particles in an Al—Cu alloy. *Translated from Fiz.* metal. metalloved, vol. 11, p. 61 (1961).

[80] HUNTER, M. S. AND FRICKE, W. G., Metallographic aspects of fatigue behavior of aluminium. Proc. Am. *Soc. Testing Mats. vol.* 54, p. 717 (1954).

[81] FORSYTH, P. J. E., Slip-band damage and extrusion. Proc. Roy. Soc. (A), vol. 242, p. 198 (1957).

[82] FORSYTH, P. J. E. AND STUBBINGTON, C. A., The *mechanism of fatigue failure in some binary and* ternary aluminium alloys. J. Inst. Metals, vol. 85, p. 339, (1957).

[83] STUBBINGTON, C. A. AND FORSYTH, P. J. E., Some *observations on the air and corrosion fatigue behaviour* of a ternary aluminium-zinc-magnesium alloy. Roy. Aircraft Est. Techn. Note Met. 258 (1957).

[84] FORSYTH, P. J. E., Fatigue damage and crack growth *in aluminium alloys.* Acta Met., vol. 11, p. 703 (1963).

[85] FROST, N. E., HOLDEN, J. AND PHILLIPS, C. E., Experimental studies into the behaviour of fatigue cracks. Proc. Crack Propagation Symposium, Cranfield, vol. 1, p. 167. The College of Aeronautics (1961).

[86] HEAD, A. K., The growth of fatigue cracks. Phil. Mag., vol. 44, p. 925 (1953).

[87] SCHIJVE, J., The relation between the endurances under variable-amplitude and constant-amplitude fatigue loading (in Dutch). N.L.R. Report M. 2050 (1958).

16 Summary in Dutch

In dit proefschrift wordt het vermoeiingsverschijnsel in aluminiumlegeringen aan een analyse onderworpen. Een dergelijke studie kan van betekenis zijn voor de techniek, ook indien alleen kwalitatieve kennis wordt verkregen over het nog steeds tamelijk mystieke begrip „vermoeiingsschade". De probleemstelling wordt gedefinieerd door de volgende vragen:

1 Hoe vindt het ontstaan van de eerste microscheur plaats?
2 Is er een essentieel verschil tussen het ontstaan en de groei van vermoeiingsscheuren?
3 Vindt scheurgroei plaats langs kristallografische vlakken?
4 Is er scheurgroei in iedere belastingswisseling en welke orden van grootte van de scheurlengte en de groeisnelheid moeten in aanmerking worden genomen?
5 Wat is de invloed van de spanningsamplitude op het scheurgroeimechanisme? Is er een essentieel verschil tussen de mechanismen voor hoge en lage spanningsamplituden?
6 Hoe is bij een wisselende belasting de spanning-rek-relatie van aluminiumlegeringen met een precipitatieharding?

In het proefschrift worden, voorafgaand aan de behandeling van deze vragen, de resultaten vermeld van proevenseries, die in verband staan met enige der bovengenoemde problemen. De resultaten zijn hoofdzakelijk afkomstig van microscopisch onderzoek. Voor ongekerfde en gekerfde proefstukken van een Al—Cu—Mg—legering werd de groeisnelheid van microscheuren bepaald. Het kristallografisch karakter van de vermoeiingsscheuren werd bestudeerd in aluminium proefstukken, in de aluminium plateerlaag van plaatmateriaal van een Al—Cu—Mg—legering en in ongeplateerd materiaal van dezelfde legering.

Vermoeiingsscheuren ontstaan in het algemeen aan het oppervlak van het materiaal, omdat glijden daar gemakkelijker plaats vindt. In overeenstemming met een mechanisme voorgesteld door Wood, wordt het ontstaan van een vermoeiingsscheur gezien als het gevolg van trede-vorming aan het oppervlak. Hiervoor is vereist, dat de dislocatiebewegingen niet volledig omkeerbaar zijn. Verschillende mogelijke oorzaken hiervan worden in het proefschrift besproken. Aangegeven wordt dat scheurgroei op dezelfde manier kan plaats vinden. Scheurgroei kan behalve als gevolg van dislocatiebewegingen, die in de tip van de scheur uitmonden, ook plaatsvinden door dislocatie-emissie uit de tip van de scheur. Beide mechanismen zijn in wezen afglijmechanismen. Het eerste mechanisme is van toepassing bij een kleine scheurgroeisnelheid en het tweede mechanisme zal overheersen bij hoge groeisnelheden. Zowel bij lage als bij hoge spanningsamplituden wordt scheurgroei waargenomen. Een normaalspanning loodrecht op de scheur zal de omzetting van dislocatiebewegingen in scheuruitbreiding bevorderen.

Scheurgroei langs en kristallografisch vlak vereist glijden op een enkel glijvlak. Dit vindt plaats aan het oppervlak van het materiaal bij lage en hoge groeisnelheden en hangt samen met de geringe beperkingen op het glijden naar het oppervlak toe. In het inwendige van het materiaal vindt in het algemeen glijden op meer dan één glijvlak plaats, als gevolg van de grotere beperkingen op glijbewegingen, de vereiste samenhang van het breukoppervlak en het karakter van de schuifspanningsverdeling (plane strain).

Het ontstaan van een microscheur begint direct bij het begin van een vermoeiingsproef. Nadat de scheur aanvankelijk een zekere periode met een ongeveer constante snelheid groeit, vindt een versnelling van de groei plaats. De orden van grootte der groeisnelheid volgend uit de proeven varieerden van 0,1 tot 10.000 burgersvectoren per wisseling. Dat scheurgroei in iedere wisseling plaats vindt kan met behulp van breukvlakstudies alleen voor tamelijk hoge groeisnelheden worden aangetoond. Voor kleine groeisnelheden wordt groei in iedere wisseling beschouwd als een natuurlijk gevolg van wisselend glijden in iedere wisseling. Bij zeer kleine groeisnelheden zullen locale materiaalstructuuromstandigheden de groei gemakkelijker beïnvloeden dan bij hoge groeisnelheden en een zekere discontinuïteit in de scheurgroei zal het gevolg zijn. Dit kan leiden tot scheurgroei, die niet overal langs het scheurfront plaats vindt en tot scheurgroeisnelheden, die gemiddeld kleiner zijn dan 1 burgersvector per wisseling.

Bij aluminiumlegeringen met een precipitatieharding moet worden verwacht, dat de interactie van dislocaties en geprecipiteerde zones een aanzienlijke complicatie vormt. Merkwaardigerwijs laat het plastisch gedrag van Al-Cu-Mg-legeringen onder een wisselende belasting zich eenvoudig beschrijven. Getracht is hiervoor een verklaring te geven.

Schattingen van de grootte van de plastische zone bij de tip van een scheur geven aan, dat de aantallen dislocaties en precipitaten in deze zone in het algemeen groot zullen zijn, uitgezonderd bij het begin van een proef met een lage spanningsamplitude. Een kwalitatieve uitwerking van het gegeven vermoeiingsmechanisme als een continuumprobleem wordt aanvaardbaar geacht. De eerste stappen hiertoe zijn aangegeven.

Berekeningen van de schuifspanningsverdeling bij scheuren zijn samengevat in een appendix. Uit deze berekeningen blijkt onder andere, dat de overgang van een vermoeiingsbreuk in een vlak, loodrecht op de grootste hoofdspanning, naar een vlak onder 45° met deze spanning verklaard kan worden uit de overgang van een twee-dimensionale rektoestand (plane strain) naar een twee-dimensionale spanningstoestand (plane stress).

Verschillende aspecten van de gegeven analyse zijn niet vrij van speculatie. In verband hiermee worden een aantal voorstellen voor voortgezet onderzoek gedaan.

APPENDIX A

The calculation of the maximum resolved shear stress ratio for two different slip planes of the slip system {111}<110>

A slip system is defined by a slip plane and a direction of slip in that plane. Fig. A1 shows a monocrystal specimen, subjected to a uni-axial load. The angle between the loading direction of the load and the slip plane is denoted by α and the angle between the direction of the load and the slip direction by β. The resolved shear stress τ for slip is defined as the shear stress on the slip plane in the slipping direction. From fig. A1 the following relation can be easily obtained:

$$\tau = \frac{P \cos \beta}{A_0/\sin \alpha} = \sigma_0 \sin \alpha \cos \beta \qquad \text{(A1)}$$

σ_0 is the nominal tensile stress in the specimen.

It was shown several decades ago that the resolved shear stress is an important parameter governing the initiation of first slip (maximum resolved shear stress criterion, Schmid's critical shear stress law); see for instance the text-book by Schmid and Boas (ref. 1).

In each of the four octahedral slip planes {111} there are three slip directions <110>. For an arbitrary orientation [hkl] of the load the resolved shear stress τ can be calculated for all 12 slip systems from eq. (A1). The maximum of the 12 τ-values is designated as $\tau_{max,1}$. This value is associated with one of the four slip planes. The maximum τ-value for the three other slip planes (9 remaining slip systems) is denoted by $\tau_{max,2}$. In chapter 7 it is assumed that the ratio

$$r = \frac{\tau_{max,2}}{\tau_{max,1}} \ (\leq 1) \qquad \text{(A2)}$$

is a parameter which could give an indication of the probability of slip occurring on one or more than one slip plane. The ratio r can be calculated if the slip system, associated with $\tau_{max,1}$ and $\tau_{max,2}$,

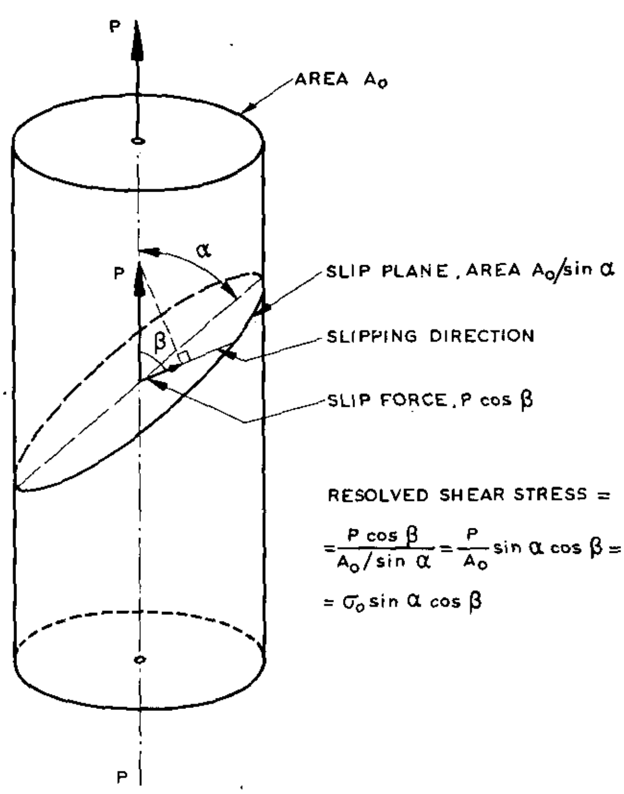

Fig. A1 Definition and formula for the resolved shear stress.

are known. To this end the resolved shear stresses for all slip systems were calculated for a variety of orientations in the stereographic triangle between [100], [110] and [111]. Within this triangle the maximum resolved shear stress, $\tau_{max,1}$, occurs on the slip system $(11\bar{1})$ [101]. The maximum resolved shear stress on one of the other slip planes occurs on either the slip system (111) $[10\bar{1}]$ or the slip system (111) [110].

Calculation of τ for an arbitrary orientation [*hkl*] of the loading is a simple mathematical procedure. As an example the relation for $\tau_{max,1}$ is given.

$$\frac{\tau_{max,1}}{\sigma_0} = \frac{(h+k+l)(h-l)}{(h^2+k^2+l^2)\sqrt{6}} \qquad \text{(A3)}$$

With two similar equations for $\tau_{max,2}$ the ratio r can be calculated. As an example the relation for the two slip systems (111) $[10\bar{1}]$ and $(11\bar{1})$ [101] is given.

$$r = \frac{(h+k+l)(h-l)}{(h+k-l)(h+l)} \qquad \text{(A4)}$$

Fig. A3, showing the maximum resolved shear stress ($\tau_{max,1}$) was constructed from eq. (A3) and for fig. A4, giving results for the maximum resolved shear stress ratio, eq. (A4) and another similar equation were used.

The method of projecting crystallographic orientations as used in figs A3 and A4 needs some explanation, since it is not a usual method. All orientations have been projected on the cube plane (100). This makes calculation of the plotting position of the direction [*hkl*] a very simple procedure since the ordinates are now k/h and l/h see fig. A2.

Fig. A3 was previously published by Von Göler and Sachs (ref. 2) in the conventional projection. Fig. A4 could have been constructed by combining some of the figures published by Diehl et al. (ref. 3) also in the conventional projection.

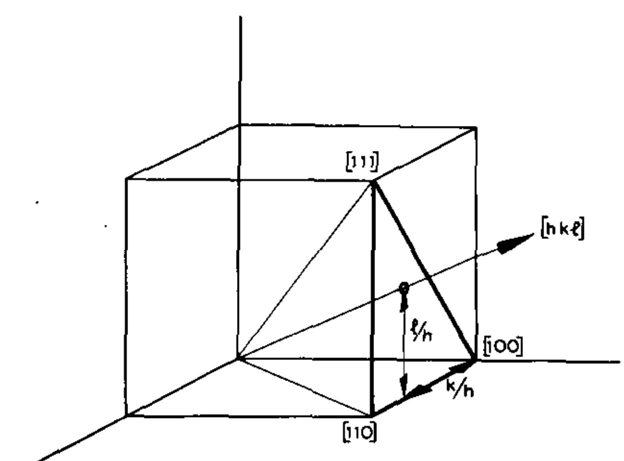

Fig. A2 Projection of the direction [*hkl*] on the cube plane (100).

Fig. A4 shows that the value of r can never be smaller than 0.5 and is per definition not greater than unity. The probability of an r-value to occur near unity is obviously much larger than the probability of an r-value near 0.5. The average value of r (space-angle average) is 0.83. Hence there is a slip plane on which the maximum resolved shear stress on the average is only 17% lower than on the slip plane carrying the stress $\tau_{max,1}$. It should be remembered than this conclusion is valid for face-centered cubic material for which slip occurs on the slip systems {111} <110>. It therefore applies to aluminium. Another restriction is that the equations apply to a monocrystal under uni-axial load.

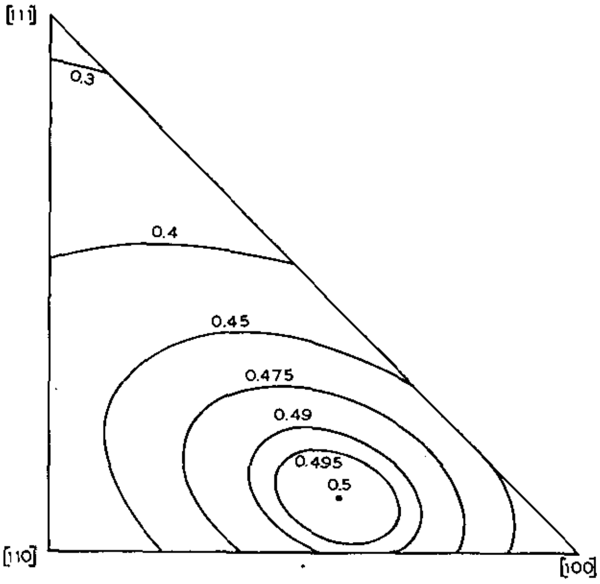

Fig. A3 Lines of constant maximum resolved shear stress in the stereographic triangle, slip system $(11\bar{1})$ [101] (projection on the cube plane (100) see fig. A2).

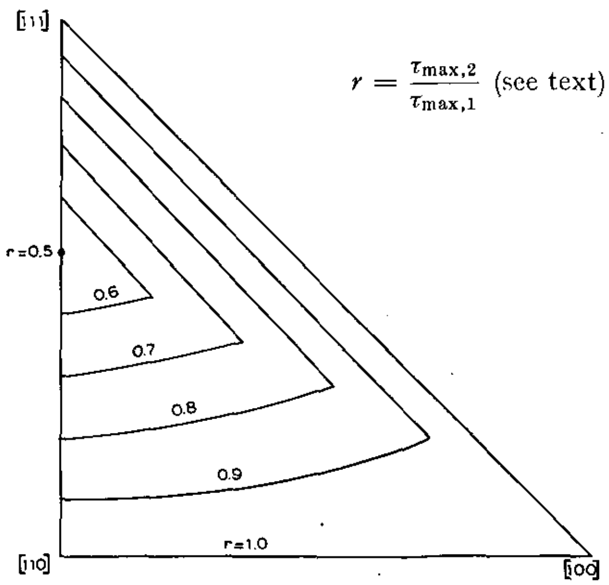

Fig. A4 Lines of constant r-values in the stereographic triangle (projection on the cube plane (100), see fig. A2).

List of references for Appendix A.

[1] SCHMID, E. AND BOAS, W., Kristallplastizität. Springer, Berlin. (1935).

[2] GÖLER, F. VON, AND SACHS, G., Das Verhalten von Aluminiumkristallen bei Zugversuchen. Geometrische Grundlagen. Z. für Physik, Vol. 41, p. 103 (1927).

[3] DIEHL, J., KRAUSE, M., OFFENHÄUSER, W. AND STAUBWASSER, W., Graphische Darstellung der Schubspannungsverhältnisse in Kubisch flächenzentrierten Kristallen. Z. für Metallk., Vol. 45, p. 489 (1954).

APPENDIX B

The shear stress distribution around the tips of a crack in an infinite elastic sheet.

Contents

Symbols and nomenclature

x, y —Cartesian coordinates
ξ, η —elliptic coordinates
r, θ —polar coordinates
$z = x + iy$ —complex variable
$\zeta = \xi + i\eta$ —complex variable
$\sigma_x, \sigma_y, \tau_{xy}$ —stress components, Cartesian coordinates
$\sigma_\xi, \sigma_\eta, \tau_{\xi\eta}$ —stress components, elliptic coordinates
$\sigma_r, \sigma_\theta, \tau_{r\theta}$ —stress components, polar coordinates
S_1, S_2, S_3 —principal stresses (S_3 perpendicular to the plane of the sheet = xy plane)
S —normal stress loading the sheet
τ_2 —maximum value of the shear stress on planes perpendicular to the sheet
τ_3 —maximum value of the shear stress on planes at an oblique angle to the sheet
τ —= (1/2)S
τ'_2 —shear stress on planes perpendicular to the sheet and passing through the tip of the crack
τ_α —shear stress on planes at an oblique angle α to the sheet and passing through the tip of the crack
τ'_3 —maximum value of τ_α if α varies from 0 to 90°
α —angle between a plane passing through the tip of the crack and the plane of the sheet
β —angle between S and the crack
ψ, χ —potential functions
ξ_0 —ξ-values for the boundary of an elliptic hole
ϱ —tip radius of the ellipse
a, b —semi major and minor axis of the ellipse
c —semi crack length (note: in the thesis the symbol l is used)
ν —ratio of Poisson (ν = 0.33 for aluminium alloys)
μ —coefficient of friction

B1: *Introduction*

In the present study of a fatigue model information was required on the shear stress distribution around the tips of a crack. More specifically the following problems were met:

(1) How is the shear stress distribution in a sheet loaded in tension affected by changing the angle between the crack and the loading direction from 90° to lower values?
(2) Are there any significant differences between the shear stress distributions for plane stress and for plane strain?
(3) What is the size of the plastic zone?
(4) What is the shear stress distribution for a sheet loaded in compression?

In the literature the analysis of the stress distribution in an infinite sheet with a crack has attracted much attention. For the questions raised above, however, additional computations were necessary, which are presented in this appendix. They are essentially based on the linear theory of elasticity.

The solutions offered by this theory are subject to several limitations associated with (1) the stress singularity at the tip of the crack, the strains being no longer very small, (2) the plasticity of the material, (3) the finite width of the specimen or an even more complicated geometry and (4) the assumed elastic-isotropic behaviour. Nevertheless it was thought that helpful indications could be obtained.

All calculations made in this Appendix pertain to an infinite sheet of an isotropic linearly elastic material with a Poisson ratio $\nu = 0.33$. The calculations partly have an asymptotic character, i.e. they are valid for the proximity of the tips of the crack. In view of the fatigue model calculations are also made for the shear stress on planes passing through the tip of the crack.

Some brief comments on the results are given in the last section. However, the implications for the present study are discussed in various chapters of the thesis.

B2: *The influence of the loading direction on the shear stress distribution around a crack in a sheet loaded in tension*

The problem of the stress distribution around a crack in an infinite sheet was analytically solved some fifty years ago by Inglis (ref. 1). Other solutions were published since then (ref. 2 and 3). Since the calculations of the stress distribution are

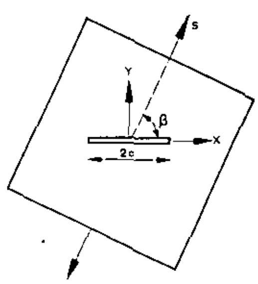

virtually impossible without a computer, calculated distributions were not published before 1955. Rothman and Ross (ref. 4), Cox (ref. 5), and Dixon (ref. 6), made calculations which were all limited to $\beta = 90°$, β being the angle between the loading direction and the crack (see the sketch). Since it was desirable for the interpretation of fatigue tests to know the effect of β on the shear stress distribution calculations were made for $\beta = 90°$, $75°$, $60°$ and $45°$ respectively. The analytic relations used for the calculations were taken from a textbook by Timoshenko and Goodier (ref. 7). The relations were based on the work of Stevenson. For an elliptic hole the solution is summarized below. The solution for a crack is then obtained if the minor axis of the elliptic hole tends to zero.

The elliptic coordinates ξ and η employed are related to the Cartesian coordinates, x and y, by:

$$x = c \cosh \xi \cos \eta,\ y = c \sinh \xi \sin \eta \quad \text{(B1)}$$

where c is half the crack length. The elliptic hole is represented by $\xi = \xi_0$.

With the definitions

$$z = x + iy\ (= c \cosh \zeta) \quad \text{(B2)}$$

and

$$\zeta = \xi + i\eta \quad \text{(B3)}$$

the relations between the stresses and the two complex potential functions, ψ and χ are:

$$\sigma_\eta + \sigma_\xi = 4\mathrm{Re}[\psi'(z)] \quad \text{(B4)}$$

$$\sigma_\eta - \sigma_\xi + 2i\tau_{\xi\eta} = 2\,\frac{\sinh \zeta}{\sinh \bar{\zeta}}[\bar{z}\psi''(z) + \chi''(z)] \quad \text{(B5)}$$

The number of primes indicates the order of differentiation while $\bar{z}$ and $\bar{\zeta}$ are the complex conjugates of z and ζ respectively. The stress notation is indicated in the figure below.

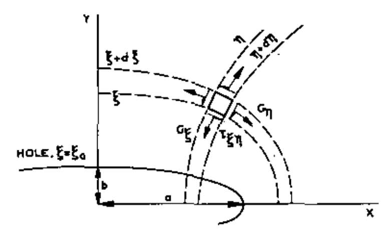

Boundary conditions to be satisfied are:
At the hole ($\xi = \xi_0$): $\sigma_{\xi_0} = 0$ and $\tau_{\xi_0\eta} = 0$
At infinity ($z \to \infty$): $\sigma_x + \sigma_y = S$ and $\tau_{xy} = \frac{1}{2}S \sin 2\beta$
The solutions for ψ and χ are:

$$4\psi(z) = Sc[e^{2\xi_0} \cos 2\beta \cosh \zeta + (1 - e^{2\xi_0 + 2i\beta}) \sinh \zeta] \quad \text{(B6)}$$

$$4\chi(z) = -Sc^2[(\cosh 2\xi_0 - \cos 2\beta)\zeta + \tfrac{1}{2}e^{2\xi_0} \cosh 2(\zeta - \xi_0 - i\beta)] \quad \text{(B7)}$$

For a crack the two equations are somewhat simplified by substituting $\xi_0 = 0$. The conversion relations for σ_x, σ_y and τ_{xy} are:

$$\sigma_x - \sigma_y = \sigma_\xi + \sigma_\eta \quad \text{(B8)}$$

$$\sigma_y - \sigma_x + 2i\tau_{xy} = \frac{\sinh \bar{\zeta}}{\sinh \zeta}(\sigma_\eta - \sigma_\xi + 2i\tau_{\xi\eta}) \quad \text{(B9)}$$

Since the shear stress is of major importance for fatigue the shear stress distribution was analysed for the tip region of the crack. Two shear stresses, indicated by τ_2 and τ_3 were calculated. Two of the principal stresses, S_1 and S_2 ($|S_1| > |S_2|$), are orientated in the plane of the sheet. The third principal stress, S_3, is perpendicular to the sheet and is equal to zero (plane stress).

$$\tau_2 = \frac{|S_1 - S_2|}{2} \quad \text{(B10)}$$

$$\tau_3 = \frac{|S_1|}{2} \quad \text{(B11)}$$

If S_1 and S_2 have opposite signs it follows that $\tau_2 > \tau_3$ and τ_2 is the maximum shear stress in the sheet. If S_1 and S_2 have the same sign, then $\tau_3 > \tau_2$ and τ_3 is the maximum shear stress in the sheet.

An electronic digital computer (Electrologica X—1) was programmed for calculating directly the x and y coordinates of a large number of points of the curves along which either τ_2 or τ_3 is constant. The results will be presented in eight graphs in ref. 8 for the β-values 90°, 75°, 60° and 45°. In the crack tip region the curves of constant τ_2 or τ_3 are almost geometrically similar for different values of τ, see section B4. Therefore a comparison for different values of β is made here for one value of τ_2 and τ_3 only. The results are shown in figs B1 and B2 respectively, the loading direction being vertical for all cases. The figures show that the effect of β on τ_3 is somewhat larger than the effect on τ_2, but in both cases the effect is considered to be fairly small.

Although plasticity of the material will invalidate the stress distribution it is expected that the effect of β on the stress distribution will remain small, in other words the stress and strain distribution will remain approximately symmetric around the direction perpendicular to the stress S. If the crack extension would depend only on the amount of plastic strain, whereas the strain distribution remains approximately symmetric, it is difficult to see why there should be persistently asymmetric crack growth, such as found in section 4.3. This aspect is reconsidered in section B6 of this appendix.

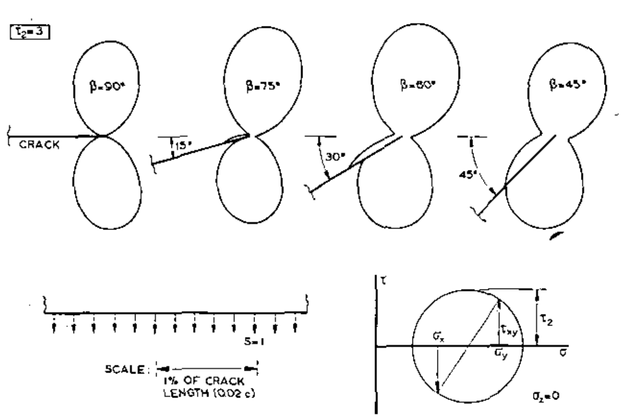

Fig. B1: Effect of the crack orientation on the shear stress distribution (curves of constant τ_2).

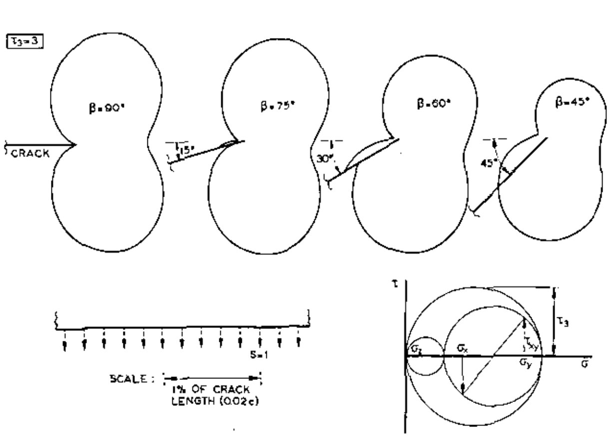

Fig. B2 Effect of the crack orientation on the shear stress distribution (curves of constant τ_3).

B3: *Some results for a finite tip radius*

At the tip of the crack the solutions given in the

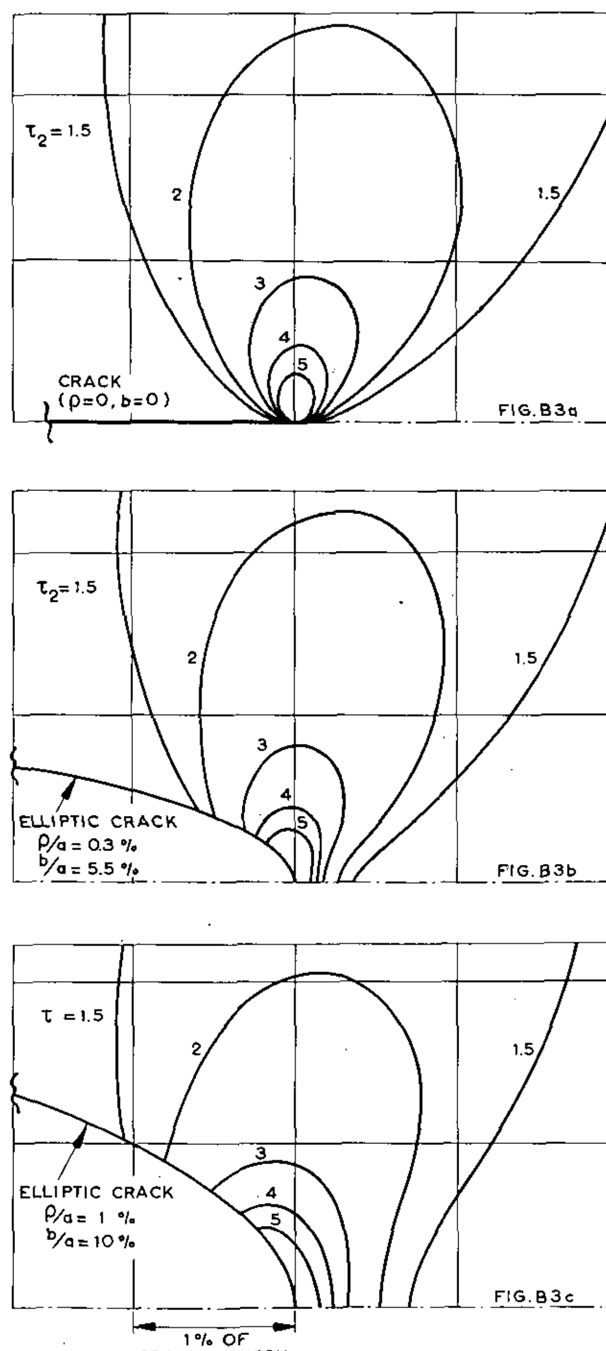

Fig. B3 The effect of the crack tip radius on the shear stress distribution around the tip of the crack ($\beta = 90°$, $S = 1$).

preceding are not valid for two reasons, viz. (1) the elastic strains are no longer small and (2) plastic deformation will occur. The latter reason will undoubtedly be the most important one. Due to plastic deformations the sharp tips of a crack will become somewhat rounded although the exact shape remains a matter of speculation. Assuming the crack to have a finite tip radius it is reasonable to approximate the crack by an ellipse. The solution of the previous section is applicable for elastic deformations since the stress singularity has vanished. It was thought to be instructive to see how much the elastic shear stress distribution is affected by the tip radius of the ellipse. Calculations were made for $\beta = 90°$ and three values of the tip radius ϱ, viz. $\varrho/a = 0$, 0.3% and 1% respectively ("a" is the semi major axis of the ellipse). The calculations were made for τ_2 only and the results are shown in fig. B3.

The figure shows that the effect of the size of the tip radius is the most pronounced in the proximity of the tip of the crack, as was to be expected. In this region the shape of the curves for constant τ_2-values has changed considerably. Despite these changes the area encircled by a curve of a certain value of τ_2 remains approximately the same. So one may say that for a crack, although the elastic theory is not applicable, it still gives a reasonable approximation of the size of the plastic zone.

Away from the tip of the crack the effect of the tip radius on the stress distribution decreases rapidly, which is also illustrated by fig. B3.

One might try to speculate on the value for the tip radius ϱ if the rounding is a consequence of local plastic deformation. Since micrographs of fatigue cracks always show the crack fully closed, unless a very high load is applied, it is thought that ϱ would have extremely small dimension. Probably the value $\varrho/a = 0.3\%$, which applies to fig. B3b, would have to be considered as high in most cases. Consequently one might feel that the rounding of the crack tip due to plastic deformation will have a small effect on the stress distribution.

B4: *Asymptotic solutions*

If stresses in the neighbourhood of the tip of the crack are considered, asympotic solutions, valid for the tip region only, may be acceptable. They can be obtained from the solutions given in section B1 by realizing that in the tip region ξ and η are very small, or ζ is very small. However, it is more expedient to start from a solution based on the work of Muskelishvili.

A solution was presented by Koiter (ref. 9) pertaining to a sheet loaded in both tension and shear*. Combination of his equations (4), (5), (11) and (12) gives:

$$\sigma_y + \sigma_x = 4 \text{ Re } \phi(z) \tag{B13}$$

$$\sigma_y - \sigma_x = (\sigma_2 - \sigma_1) - 2 \text{ Re } [\phi(z) - \phi(\bar{z})] - 4y \text{ Im } \overline{\phi'(z)} \tag{B14}$$

$$\tau_{xy} = \tau - \text{Im}[\phi(z) + \phi(\bar{z})] - 2y \text{ Re } \overline{\phi'(z)} \tag{B15}$$

$$\text{with } \phi(z) = \tfrac{1}{2}(\sigma_2 - i\tau)\left(1 - \frac{c^2}{z^2}\right)^{-\frac{1}{2}} - \tfrac{1}{4}(\sigma_2 - \sigma_1) + \tfrac{1}{2}i\tau \tag{B16}$$

where again $z = x + iy$ and c = the semi crack length. σ_1, σ_2 and τ are the stresses σ_x, σ_y and τ_{xy} at infinity. In order to obtain asymptotic solutions for the region near the tip of the crack at $x = c$, polar coordinates (r, θ) with the pole at the tip of the crack are introduced:

$$z = c + r(\cos\theta + i\sin\theta) \tag{B17}$$

If this substitution is made in the above equations the asymptotic solutions are obtained by considering the limiting case that r approaches zero. The case of a sheet loaded in tension as considered in section B2 is then obtained by further substitution of $\sigma_1 = \tfrac{1}{2}S(1 + \cos 2\beta)$, $\sigma_2 = \tfrac{1}{2}S(1 - \cos 2\beta)$ and $\tau = \tfrac{1}{2}S \sin 2\beta$. The asymptotic solutions are:

$$\sigma_x + \sigma_y = S\sqrt{\frac{c}{2r}}\left[(1 - \cos 2\beta)\cos\frac{\theta}{2} - \sin 2\beta \sin\frac{\theta}{2}\right] + S\cos 2\beta \tag{B18}$$

$$\sigma_y - \sigma_x = \tfrac{1}{2}S\sqrt{\frac{c}{2r}}\left[(1 - \cos 2\beta)\sin\theta\sin\frac{3\theta}{2} + \sin 2\beta\left(\cos\theta\sin\frac{3\theta}{2} + \sin\frac{\theta}{2}\right)\right] - S\cos 2\beta \tag{B19}$$

$$\tau_{xy} = \tfrac{1}{4}S\sqrt{\frac{c}{2r}}\left[(1 - \cos 2\beta)\sin\theta\cos\frac{3\theta}{2} + \sin 2\beta\left(\cos\theta\cos\frac{3\theta}{2} + \cos\frac{\theta}{2}\right)\right] \tag{B20}$$

* Ref. 9 essentially deals with an infinite row of collinear cracks, the sheet with a single crack being a special case.

Similar relations were recently published by Sih, Paris and Erdogan (ref. 10). The constant term $S \cos 2\beta$ in the equations (B18) and (B19) does not appear in their solution. This term is practically negligible for r much smaller than c. As an example fig. B4 shows a comparison between the exact solution with the preceding asymptotic solution, with and without the constant term $S \cos 2\beta$. The calculations were made for the shear stress τ_2 as defined in section B2, $\beta = 60°$ and $\tau_2/S = 1.5$. The

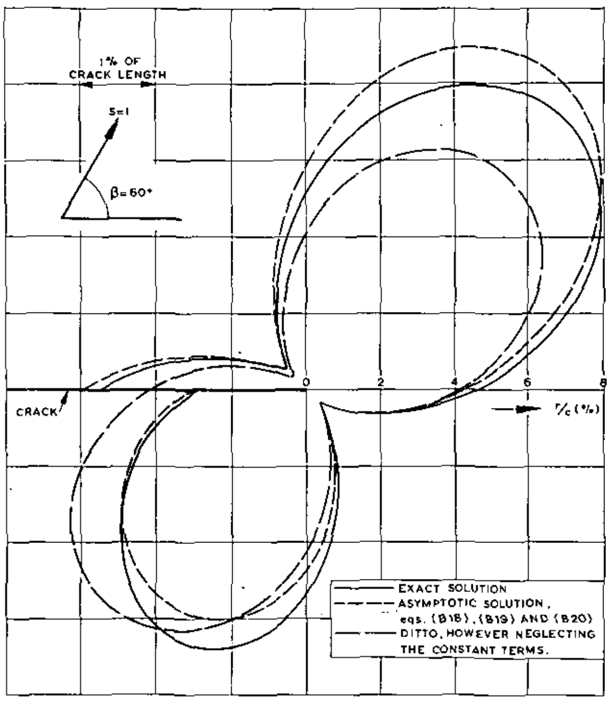

Fig. B4 The shear stress distribution for $\tau_2 = 1.5$ ($\beta = 60°$) according to the exact solution and two asymptotic solutions.

agreement between the exact solution and the approximate solution including the constant term $S \cos 2\beta$ is good, whereas the approximate solution without this constant term gives a somewhat more diverging result. However, for higher values of τ_2, i.e. smaller r-values, the differences between the solutions will tend to zero. So for the purpose of this study the use of the asymptotic solutions neglecting the constant term seems to be justified. Then along a radial line (θ = constant)

$$\text{stress} \propto r^{-1/2} \tag{B21}$$

Consequently curves of constant τ_2-values are geometrically similar, their size being proportional to τ_2^2. The same applies to other stresses. The solution for the case of a pure shear loading, see sketch, is obtained by substitution of $\sigma_2 = \sigma_1 = 0$ in eqs (B13) to (B16). The solution presumes the crack transmitting neither shear stress nor normal stress from one edge of the crack to the other one. This requires that the crack will not be closed. Since calculation of the edge displacements in the y-direction shows these displacements to be zero (see Koiter's equation no. 17, ref. 9), the presumption is theoretically correct.

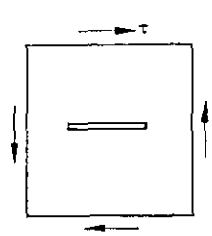

Asymptotic solutions, obtained in the same way as for the tension case, are:

$$\sigma_y + \sigma_x = -2\tau\sqrt{\frac{c}{2r}}\sin\frac{\theta}{2} \tag{B22}$$

$$\sigma_y - \sigma_x = \tau\sqrt{\frac{c}{2r}}\left(\sin\frac{\theta}{2} + \cos\theta\sin\frac{3\theta}{2}\right) \tag{B23}$$

$$\tau_{xy} = \tfrac{1}{2}\tau\sqrt{\frac{c}{2r}}\left(\cos\frac{\theta}{2} + \cos\theta\cos\frac{3\theta}{2}\right) \tag{B24}$$

A constant term does not appear in these relations.

B5: *The shear stress distributions for plane stress and plane strain and the size of the plastic zone*

All calculations in the previous sections were made for plane stress. This seems to be an obvious approach for a thin sheet, i.e. if the sheet thickness is small as compared with the size of the plastic zone at the tip of the crack. If the plastic zone is much smaller than the sheet thickness the material at the centre of the sheet around the tip of the crack will approximately be in a state of plane strain. The shear stress distribution for the two cases will be compared for an infinite sheet with a crack loaded in tension, the loading being perpendicular to the crack ($\beta = 90°$).

For plane strain the stress σ_z perpendicular to the sheet, is the third principal stress S_3 and

$$S_3 = \sigma_z = \nu(S_1 + S_2) \tag{B25}$$

where ν is the Poisson ratio. The solutions for σ_x, σ_y and τ_{xy} for plane strain are the same as for plane stress (ref. 7). Consequently the results for τ_2 are also the same. τ_3 according to eq. (B11) has to be replaced by the larger value of

$$\tau_3 = \frac{|S_1 - S_3|}{2} \quad \text{or} \quad \tau_3 = \frac{|S_2 - S_3|}{2} \tag{B26}$$

For the calculation the asympotic solutions given in eqs (B18), (B19) and (B20) are used ($\beta = 90°$), while neglecting the constant term of magnitude S in the former two equations. The results are:

Plane stress and plane strain: $$\tau_2 = \tfrac{1}{2}S\sqrt{\frac{c}{2r}}\sin\theta \tag{B27}$$

$$\text{Plane stress:} \quad \tau_3 = \tfrac{1}{2}S\sqrt{\frac{c}{2r}}\cos\frac{\theta}{2}\left(1 \pm \sin\frac{\theta}{2}\right) \tag{B28)*}$$

$$\text{Plane strain:} \quad \tau_3 = \tfrac{1}{2}S\sqrt{\frac{c}{2r}}\cos\frac{\theta}{2}\left(1 - 2\nu \pm \sin\frac{\theta}{2}\right) \tag{B29)*}$$

Curves for constant τ-values have been plotted in fig. B5 for $\tau_2 = \tau_3 = 2S$, the curves for other τ-values being geometrically similar (see the previous section).

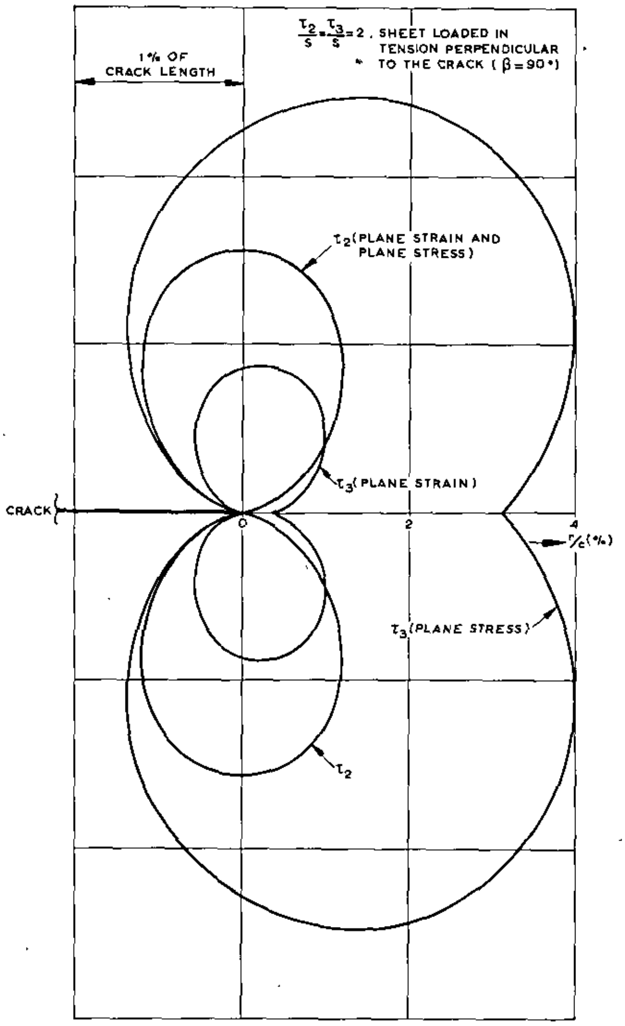

Fig. B5 The shear stress distribution for plane stress and for plane strain ($\nu = 0.33$) (asymptotic solution). Crack loaded in tension.

Fig. B5 shows that for plane stress τ_3 is always larger than τ_2 whereas for plane strain τ_2 highly dominates τ_3. An estimate of the size of the plastic zone can be obtained by assuming that plastic straining occurs if either τ_2 or τ_3 exceeds a critical value, τ_0 (Tresca yield criterion) and that the elastic solution remains valid outside the plastic zone. The latter assumption implies that the effect of the stress redistribution in the plastic zone on the stress distribution outside that zone is ignored. The boundary of the plastic zone is then defined by either $\tau_2 = \tau_0$ or $\tau_3 = \tau_0$. The size of the plastic zone is now characterized by p, such that the area πp^2 is equal to the area of the plastic zone, which leads to:

$$p = \left[\frac{1}{2\pi}\int_{-\pi}^{\pi} r_{\tau_0}{}^2 \, d\theta\right]^{\frac{1}{2}} \tag{B30}$$

where r_{τ_0} is the radius at which either τ_2 or τ_3 is equal to τ_0. Substitution of $\tau_2 = \tau_3 = \tau_0 = \frac{1}{2}S_0$, S_0 being the yield stress of the material, in eqs (B27) and (B28) gives the relation for r_{τ_0}. Integration of eq. (B30) then gives the following results

$$\text{Plane stress } (\tau_3 = \tau_0) \quad \frac{p}{c} = 0.60\left(\frac{S}{S_0}\right)^2 \tag{B31}$$

$$\text{Plane strain } (\tau_2 = \tau_0) \quad \frac{p}{c} = 0.31\left(\frac{S}{S_0}\right)^2 \tag{B32}$$

For the case of plane strain the relatively small area where $\tau_3 > \tau_2$ was neglected for simplicity. A comparison of the two relations shows that the plastic zone is smaller in the case of plane strain, which also follows from fig. B5.

B6: *The distribution of the shear stress on planes through the tip of the crack*

The model of the fatigue crack propagation proposed in the thesis requires dislocation movements on planes through the tip of the crack. The shear stress on such planes is the driving force behind the movements. The distribution of the shear stress on planes θ = constant, indicated as τ'_2, may be of interest. The notation for the stress components in polar coordinates is given in the sketch. As a conversion of eqs (B18), (B19) and (B20) one obtains:

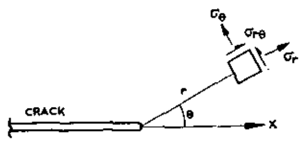

* Plus sign for $0 \leqslant \theta \leqslant \pi$, minus sign for $-\pi \leqslant \theta \leqslant 0$

$$\sigma_\theta = \frac{S}{8}\sqrt{\frac{c}{2r}}\Big[(1-\cos 2\beta)(3\cos\frac{\theta}{2}+\cos\frac{3\theta}{2}) - 3\sin 2\beta\,(\sin\frac{3\theta}{2}+\sin\frac{\theta}{2})\Big] + \tfrac{1}{2}S\cos 2\beta\,(1-\cos 2\theta) \qquad \text{(B33)}$$

$$\sigma_r = \frac{S}{8}\sqrt{\frac{c}{2r}}\Big[(1-\cos 2\beta)(5\cos\frac{\theta}{2}-\cos\frac{3\theta}{2}) + \sin 2\beta\,(3\sin\frac{3\theta}{2}-5\sin\frac{\theta}{2})\Big] + \tfrac{1}{2}S\cos 2\beta\,(1+\cos 2\theta) \qquad \text{(B34)}$$

$$\tau_{r\theta} = \frac{S}{8}\sqrt{\frac{c}{2r}}\Big[(1-\cos 2\beta)(\sin\frac{\theta}{2}+\sin\frac{3\theta}{2}) + \sin 2\beta\,(3\cos\frac{3\theta}{2}+\cos\frac{\theta}{2})\Big] - \tfrac{1}{2}S\cos 2\beta\sin 2\theta \qquad \text{(B35)}$$

From the definition of τ'_2 it follows that:

$$\tau'_2 = \tau_{r\theta} \qquad \text{(B36)}$$

In section B2 calculations were made on the influence of the crack orientation on the shear stress distribution in an infinite sheet loaded in tension. Similar calculations were made for τ'_2, again for $\beta = 90°$, $75°$, $60°$ and $45°$. The results are given in fig. B6. Contrary to figs B1 and B2 fig. B6 shows a more pronounced influence of the orientation of the crack. For increasing β there is a tendency towards an increasing shear stress (τ'_2) concentration in line with the crack. This feature is in accordance with intuitive feelings. So if τ'_2 were controlling the fatigue crack growth one might feel that in a sheet loaded in tension an oblique orientation of a crack ($\beta \neq 90°$) will be favoured. However, the orientation of available slip systems may be another controlling factor, see chapter 7.

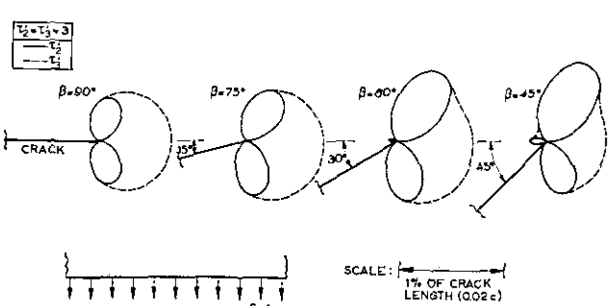

Fig. B6 Effect of the crack orientation on the distribution of the shear stress on planes through the tip of the crack (τ'_2 and τ'_3, plane stress).

For the study of the effect of β on the stress distribution calculations were also made for σ_θ, a stress component which might be important if crack extension occurred by tension rather than shear. The results obtained from eq. (B33) are shown in fig. B7, which reveals a negligible effect of β.

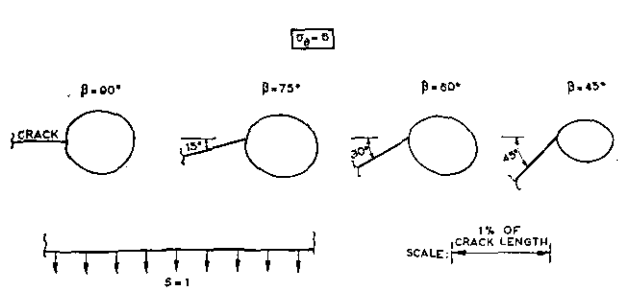

Fig. B7 Effect of the crack orientation on the distribution of the tensile stress σ_θ around the tip of the crack.

The shear stress τ'_2 on the planes θ = constant is the same for plane stress and plane strain. The planes θ = constant are perpendicular to the sheet. Planes will be considered now which are also passing through the tip of the crack, but making an oblique angle α with the plane of the sheet. For such planes it is easily shown from equilibrium conditions that the shear stress τ_α is:

$$\tau_\alpha = \Big[\Big(\frac{\sigma_\theta - \sigma_z}{2}\sin 2\alpha\Big)^2 + \Big(\tau_{r\theta}\sin\alpha\Big)^2\Big]^{\frac{1}{2}} \qquad \text{(B37)}$$

The maximum value of τ_α if α varies from 0 to 90° is indicated as τ'_3. The equation $d\tau_\alpha/d\alpha = 0$ yields three solutions: $\alpha = 0$ ($\tau_\alpha = 0$), $\alpha = 90°$ ($\tau_\alpha = \tau_2$) and an α value defined by

$$\cos 2\alpha = -\Big(\frac{\tau_{r\theta}}{\sigma_\theta - \sigma_z}\Big)^2 \qquad \text{(B38)}$$

If this equation yields a real solution the corresponding shear stress will be indicated by τ'_3 for which then applies $\tau'_3 > \tau'_2$. Combining eqs (B37) and (B38) gives:

$$\tau'_3 = \frac{(\sigma_\theta - \sigma_z)^2 + \tau_{r\theta}^2}{2(\sigma_\theta - \sigma_z)} \qquad \text{(B39)}$$

Calculated results for τ'_3 for plane stress ($\sigma_z = 0$) and plane strain ($\sigma_z = \nu[\sigma_r + \sigma_\theta]$) are shown in fig. B8 for $\beta = 90°$. For the calculations the constant terms in eqs (B33), (B34) and (B35) were neglected. For plane stress τ_3 results are obtained for $|\theta| \leqslant 90°$ and for plane strain for $|\theta| < 31.8°$ and $180° \geqslant |\theta| > 121.9°$. In the latter θ range the difference between τ'_2 and τ'_3 is very small and the corresponding τ'_3-curve was not drawn in fig. B8. In this figure values of α were indicated at some locations.

Fig. B8 illustrates a significant difference between the results for plane strain and plane stress. For plane strain τ'_2 is highly dominating τ'_3. For plane stress the reverse is true. Maximum values of τ'_3 for plane stress are found on planes near $\theta = 0°$, which are associated with α-values of 45° or slightly higher. If β varies from 90° to 45° calcu-

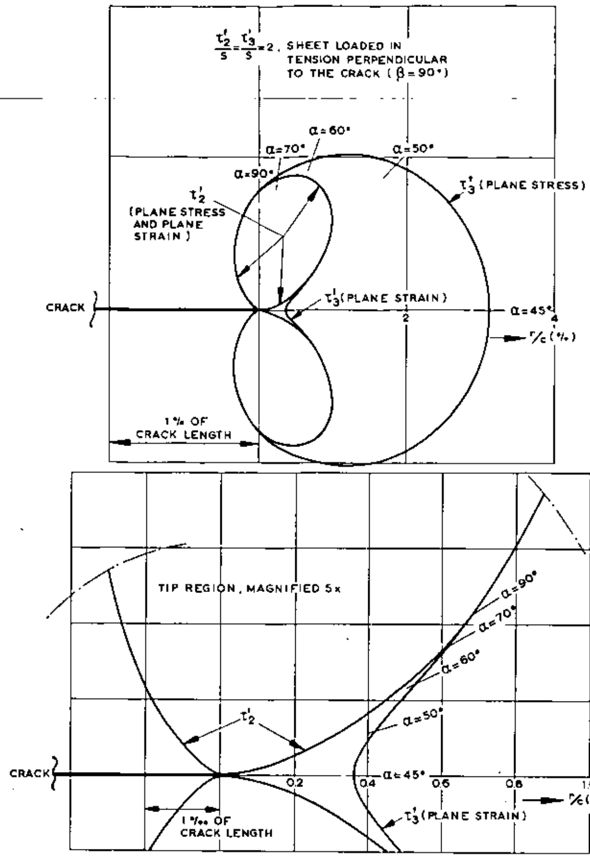

Fig. B8 The distribution of the shear stress on planes through the tip of the crack for plane stress and plane strain ($\nu = 0.33$) (asymptotic solution). Crack loaded in tension.

lations learned that τ'_2 remains dominating τ'_3 for plane strain. For plane stress the domination of τ'_3 over τ'_2 is decreasing. The latter is illustrated in fig. B6 which shows dotted lines for $\tau'_3 =$ constant.

B7: *The shear stress distribution around a crack in a sheet subjected to pure shear.*

The asymptotic solutions were already given in section B4, eqs (B22), (B23) and (B24). From these equations the maximum shear stresses τ_2 and τ_3 are easily derived.

$$\tau_2 = \tau\sqrt{\frac{c}{2r}}\left(1 - \tfrac{3}{4}\sin^2\theta\right)^{\frac{1}{2}} \qquad \text{(B40)}$$

$$\tau_3 = \tfrac{1}{2}\tau\sqrt{\frac{c}{2r}}\left[\left(1 - \tfrac{3}{4}\sin^2\theta\right)^{\frac{1}{2}} \pm (1 - 2\nu)\sin\frac{\theta}{2}\right] \qquad \text{(B41)*)}$$

Eq. (B40) applies to plane strain and plane stress. Eq. (B41) ($\nu = 0.33$) applies to plane strain and by dropping the term with ν also to plane stress. Curves for a constant value of τ_2 and τ_3 are shown in fig. B9.

* Plus sign for $0 \leqslant \theta \leqslant \pi$, minus sign for $-\pi \leqslant \theta \leqslant 0$.

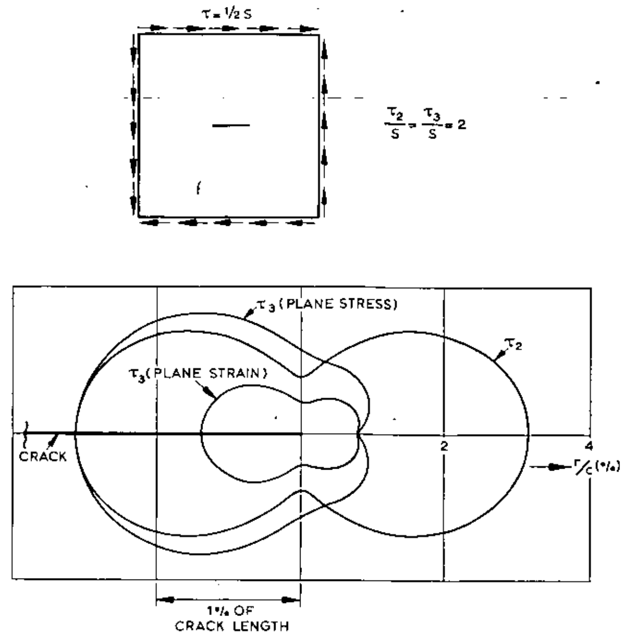

Fig. B9 Shear stress distribution for a sheet loaded in shear (asymptotic solution).

For calculating the shear stress on planes through the tip of the crack eqs (B22), (B23) and (B24) are expressed in terms of σ_r, σ_θ and $\tau_{r\theta}$ as defined before.

$$\sigma_r = \tfrac{1}{2}\tau\sqrt{\frac{c}{2r}}\sin\frac{\theta}{2}(3\cos\theta - 1) \qquad \text{(B42)}$$

$$\sigma_\theta = -\tfrac{3}{4}\tau\sqrt{\frac{c}{2r}}\sin\frac{\theta}{2}(\cos\theta + 1) \qquad \text{(B43)}$$

$$\tau_{r\theta} = \tfrac{1}{4}\tau\sqrt{\frac{c}{2r}}\left(\cos\frac{\theta}{2} + 3\cos\frac{3\theta}{2}\right) \qquad \text{(B44)}$$

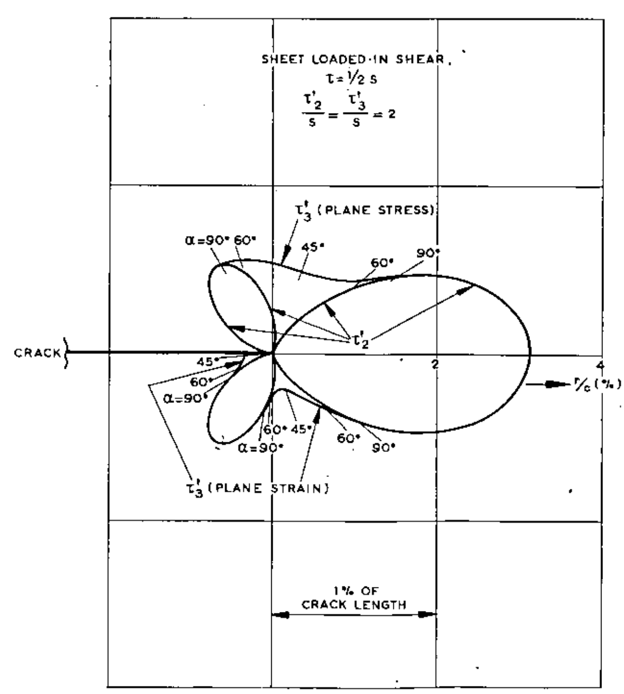

Fig. B10 The distribution of the shear stress on planes through the tip of the crack for plane stress and for plane strain ($\nu = 0.33$) (asymptotic solution). Sheet loaded in shear.

For calculating τ'_2, τ'_3 and α as defined in the previous section the above relations were substituted into eqs (B36), (B38) and (B39). Curves for a constant value of τ'_2 and τ'_3, with some α-values indicated, are presented in fig. B10.

Both figs B9 and B10 show the region of high stress to be elongated in the direction of the crack as might have been expected intuitively. The two figures still show considerable differences. In fig. B9 the highly stressed region is not only found ahead of the crack ($|\theta| < 90°$), but also in the "shadow" of the crack ($90° < |\theta| < 180°$). However, in fig. B9 the shear stress on planes through the tip of the crack has a pronounced maximum for $\theta = 0$, a secondary maximum occurring at $|\theta| \approx 125°$.

B8: *The shear stress distribution around a crack in a sheet loaded in compression*

For a sheet with a crack loaded in compression the following decomposition is considered:

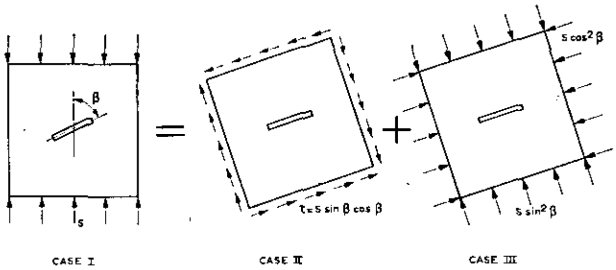

In case III the crack will be closed and will not introduce any stress raising effect. The solution for case II has been presented in the previous section. The objection against the decomposition is based on the fact that the crack is closed by the compression stress of case III. This implies that frictional loads acting on the inside of the crack have to be added to case II. Since the normal stress over the crack in case III is $S \sin^2\beta$ the frictional loading can be indicated by $\mu S \sin^2\beta$, μ being a coefficient of friction. Case II is then replaced by case II′ as sketched below. The shear stress loading on the inside of the crack is denoted as τ_i, the crack being for convenience drawn as a rectangular hole. Case II′ is split in cases IV and II″.

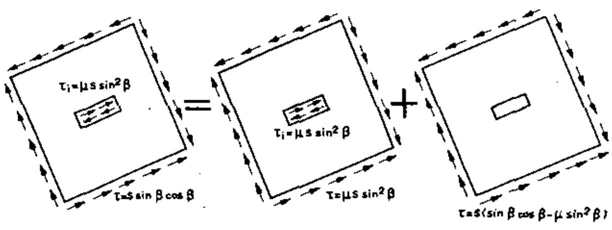

In case IV the shear stress, loading the inside of the hole is equal to the external shear stress and consequently the crack will have no stress raising effect. Case II″ is similar to case II, the only difference being a reduced external load. Neglecting the homogeneous stresses of cases III and IV it may be concluded that the shear stress distribution around the tips of the crack will be the same for case I and case II″. The restriction to be made is that in case I the crack will have a stress raising effect only if sliding in the crack occurs (without sliding the crack does not interrupt the continuity of the sheet). This requires that

$$S \sin\beta \cos\beta > \mu S \sin^2\beta$$

$$\text{or} \quad \operatorname{tg}\beta < \frac{1}{\mu} \tag{B45}$$

So, it should be expected that β has to be considerably smaller than 90°.

B9: *Concluding remarks*

All calculations in this appendix were made for a crack in an infinite sheet of linearly elastic and isotropic material. The infinite size of the sheet is not considered to be a serious limitation since for a specimen with a finite width and either a central crack or an edge crack the character of the stress singularity is the same ($r^{-1/2}$). The shape of the stress distributions in the proximity of crack tips also remains the same, whereas the size of equally stressed regions is only slightly affected as long as the crack is small in relation to the relevant dimensions of the specimen.

A more serious limitation may be set by the plasticity of the material. Although it obliterates the stress singularity it also invalidates the elastic solution. As long as the gross stress on the specimen is relatively low, the plastic zone is small and redistribution of stress may be negligible. The work of Dixon and Visser (ref. 11) on aluminium alloy specimens seems to give some substantiation for this view. One might assume that the strain distribution according to the elastic solution is approximately applicable to the major part of the plastic zone. Since fatigue crack growth is a consequence of plastic strain a correlation between the elastic stress distribution and the fatigue crack growth seems to be a realistic possibility. This is confirmed by the work of Paris et al. (ref. 12) who could correlate the rate of crack growth in aluminium alloy specimens with the so-called stress intensity factors, characteristic parameters for the elastic stress distribution, not further explained in this appendix (see also the study of Barrois (ref. 13).

Some information derived from the elastic solutions presented in this appendix will now be recapitulated.

(1) A formula was derived for estimating the size of the plastic zone, based on the Tresca yield criterion.

(2) For a sheet loaded in tension the effect of the angle β between the crack and the loading direction was studied. The effect on the size and the shape of the plastic zone is small. However, there is a more pronounced effect on the distribution of the shear stress (τ'_2) on slip planes passing through the tip of the crack. If β is decreasing from 90° to 45° there is a tendency for an increasing concentration of τ'_2 in line with the crack. Other circumstances being favourable a crack with an oblique orientation ($\beta \neq 90°$) may thus persist in growing in the oblique direction.

(3) For a sheet loaded in tension with a crack perpendicular to the loading direction there is a considerable difference between the stress distributions for plane strain and plane stress. For plane strain the maximum shear stress on slip planes through the tip of the crack is found on planes perpendicular to the sheet and making an angle with the crack ($|\theta| \neq 0$). For plane stress the maximum shear stress on slip planes through the tip of the crack is found on planes in line with the crack ($\theta \sim 0$) and making an angle $\alpha = \pm 45°$ with the sheet.

(4) A sheet loaded in compression shows the same type of shear stress distribution around the tip of the crack as a sheet subjected to pure shear. However, in the former case the stresses are much lower depending on the amount of shear stress transmitted along the edges of the crack by friction.

(5) Rounding of the tip of the crack by plastic deformation will probably have a minor influence on the trends summarized above.

It may be emphasized once more that all results, although being derived from quantitative calculations, only have a qualitative meaning for the fatigue problem in view of the limitations set by the idealized continuum approach.

Finally it may be pointed out that the shear stresses on planes through the tip of the crack (τ'_2 and τ'_3) changed the picture noticeably from the one obtained by considering maximum shear stresses (τ_2 and τ_3). To draw full advantage of the theory of elasticity a physical model for the phenomenon studied is obviously required.

B10: *List of references for Appendix B*

1 INGLIS, C. E., Stresses in a plate due to the presence of cracks and sharp corners. Trans. Inst. of Naval Architects, Vol. 55, part 1, p. 219 (1913).

2 MUSKHELISHVILI, N. I., Some basic problems of the mathematical theory of elasticity. Translated from the Russian by J. R. M. Radok Noordhoff, Groningen (1963).

3 STEVENSON, A. C., Complex potentials in two-dimensional elasticity. Proc. of the Royal Soc., Series A, Vol. 184, p. 129 (1945).

4 ROTHMAN, M. AND ROSS, D. S., Stresses in plates with cracks and notches. A theoretical and experimental investigation. Engineering, Febr. 11, 1955, p. 175.

5 COX, H. L., Stress concentration in relation to fatigue. Proc. International Conf. on Fatigue of Metals, London, 1956. The Inst. of Mech. Eng., London, p. 212 (1956).

6 DIXON, J. R., Computed values of the elastic stresses around a crack in an infinite plate under tension. NEL Report No. 12, East Kilbride (1961).

7 TIMOSHENKO, S. AND GOODIER, J. N., Theory of Elasticity, 2nd ed., Mc Graw Hill Book Co., Inc. (1951).

8 SCHIJVE, J., Some calculated stress distributions around the tip of a crack. NLR Report, to be published.

9 KOITER, W. T., An infinite row of collinear cracks in an infinite elastic sheet. Ingenieur-Archiv, Vol. 28, p. 168 (1959).

10 SIH, G. C., PARIS, P. C. AND ERDOGAN, F., Application of Muskelishvili's methods to the analysis of crack tip stress intensity factors for plane problems. Part II. Lehigh University, Interim Report, 7 Jan. 1961.

11 DIXON, J. R. AND VISSER, W., An investigation of the elastic-plastic strain distribution around cracks in various sheet materials. Proc. of the International Symp. on Photoelasticity, p. 231, Pergamon (1963).

12 PARIS, P. C., GOMEZ, M. P. AND ANDERSON, W. E., A rational analytic theory of fatigue. The Trend in Engineering, Vol. 13, p. 9 (1961).

13 BARROIS, W., Critical study on fatigue crack propagation. AGARD Report 412 (1962).